Witnessing Multipartite Entanglement

Universität Rostock — Traditio et Innovatio

Institut für Physik

Kumulative Dissertation

zur

Erlangung des akademischen Grades

doctor rerum naturalium (Dr. rer. nat.)

der

Mathematisch-Naturwissenschaftlichen Fakultät

der

Universität Rostock

vorgelegt von   Stefan Gerke, geb. am 09.01.1989 in Kappeln

Betreuer   Prof. Dr. Werner Vogel

Gutachter

Prof. Dr. Werner Vogel
Institut für Physik
Universität Rostock

Albert-Einstein-Straße 23
18059 Rostock

Univ.-Prof. Dr. Peter van Loock
Quanten-, Atom- und Neutronenphysik (QUANTUM)
Johannes Gutenberg-Universität
Institut für Physik

Staudingerweg 7
55128 Mainz

Selbstständigkeitserklärung

Hiermit erkläre ich an Eides statt, dass ich die hier vorliegende Dissertation selbstständig und ohne fremde Hilfe verfasst habe, bis auf die in der Bibliographie angegebenen Quellen keine weiteren Quellen benutzt habe und die den Quellen wörtlich oder inhaltlich entnommene Stellen als solche kenntlich gemacht habe.

Stefan Gerke
Wittingen, 3. Juni 2019

Witnessing Multipartite Entanglement

Dissertation by Stefan Gerke

Dated: June 3, 2019

*After sleeping through a hundred million centuries
we have finally opened our eyes on a sumptuous
planet, sparkling with color, bountiful with life.
Within decades we must close our eyes again.
Isn't it a noble, an enlightened way of spending
our brief time in the sun, to work at
understanding the universe and how we have
come to wake up in it?*
–Richard Dawkins

Dedicated to my family and my loved ones

Acknowledgment

I would like to thank Prof. Werner Vogel for giving me the opportunity to complete my PhD studies in his group and under his supervision. His knowledge in the field of quantum optics and his persistence motivated me to always take the extra step in my research. A huge thank you to Dr. Jan Sperling whose cosupervision developed into friendship in the last years. The insightful personal meetings and later internet meetings are fundamental to large parts of my work. To the entire group Theoretical Quantum Optics, former and current colleagues, Peter, Farid, Andrii, Dima, Eliza, Martin, Sergej, and Fabian, thank you. Special thanks to Benjamin, my "roomy" in the institute as well as on multiple project meetings, for inspiring conversations, coffee, and (not) painting on the wallpaper in Paris. The comradery in our group always felt very good and it was a pleasant experience working with you and spending some late afternoon sessions with discussions. A warm gratitude towards Mel, Oskar, and Karsten not only for coffee, but also for insightful discussions about experimental work. I would like to thank my experimental collaborators in the group of Prof. Claude Fabre and Prof. Nicolas Treps for very interesting discussions and being excellent hosts for work meetings.

Thank you Tobi for proofreading my thesis, but most importantly your friendship, having an open ear, and just being you. It is hard finding new words to thank my parents but I will try nonetheless: Thank you mom and dad for raising me, being there for me, and forging my curiosity that helped me in my research. To my siblings, all teasing is always well-meant. Thanks for all the fun we have had and will have. A special thank you to Sebastian for proofreading.

Last but by far not least, my dearest Monique, who had to endure me while writing my thesis, words cannot express the gratitude and love towards you. I am happy to be sharing our new adventure with our little treasure with you.

Abstract

Quantum entanglement is a nonclassical correlation of a quantum state acting on multiple Hilbert spaces. Entanglement is the cornerstone of many ideas concerning the fundamentals of nature and the basis for protocols of quantum technologies. This work presents new approaches to numerically test for entanglement, applicable to a broad range of quantum states in multipartite systems.

The main building blocks for my entanglement tests are a genetic algorithm, which is employed to find the optimal element in a family of entanglement tests, and the separability eigenvalue equations, which are applied to construct the family of tests. In applications to experimental data, this approach was able to show the complete entanglement structure of highly multimode states, which is, to the candidate's best knowledge, not possible with other entanglement tests. To extend the range of states accessible by the method, I developed an algorithm that is able to find the optimal solution of separability eigenvalue equations.

The work presented in this thesis is of an interdisciplinary nature. The separability problem, which is posed by entanglement tests, is of interest in the mathematical field of functional analysis. Finding solutions to the separability eigenvalue equations is equivalent to many related problems and the implementation of a genetic algorithm in combination with the introduced numerical solver for nonlinear equations may be of interest for computer sciences as well. Beyond its theoretical impact, we also applied our technique to experimental data to uncover challenging forms of multipartite entanglement.

Zusammenfassung

Quantenverschränkung ist eine nichtklassische Korrelation in einem Quantenzustand, welcher auf mehreren Hilberträume wirkt. Verschränkung ist der Grundstein vieler Ideen über die Grundlagen der Natur und die Basis von Protokollen in der Quantentechnologie. Diese Arbeit stellt neue numerischen Verschränkungstest vor, welcher auf eine Vielzahl von Quantenzuständen anwendbar ist.

Das Hauptwerkzeug meiner Verschränkungstests sind genetische Algorithmen, welche eingesetzt werden um das optimale Element in der Familie von Verschränkungstests zu finden, und die Separabilitätseigenwertgleichungen, welche angewendet werden um die Testfamilie zu konstruieren. In einer Anwendung auf experimentelle Daten konnte der Verschränkungstest für hochgradig multipartite Zustände die vollständige Struktur im Sinne der Verschränkung aufdecken. Das ist zum Wissen des Autors der erste Test, der dazu in der Lage ist. Um die Anzahl der Zustände zu erhöhen, die durch den Test zugänglich sind, habe ich einen Algorithmus entwickelt, der in der Lage ist eine optimale Lösung der Separabilitätseigenwertgleichungen zu finden.

Die vorgestellte Arbeit hat einen interdisziplinären Charakter. Das Separabilitätsproblem, auf welches durch den Verschränkungstest eingegangen wird, ist für das mathematische Gebiet der Funktionalanalysis von Interesse. Das Finden der Lösungen von Separabilitätseigenwertgleichungen ist äquivalent zu vielen verwandten Problemen und die Implemetierung eines genetischen Algorithmus in Kombination mit dem eingeführten Lösungsalgorithmus für nichtlineare Gleichungen könnte für die Informatik interessant sein. Jenseits des Einflusses in der Theorie, wurden unsere Methoden auf experimentelle Daten angewendet um anspruchsvolle Formen multipartiter Verschränkung aufzudecken.

Contents

Introduction

<div style="text-align: right">**1**</div>

Entanglement is a quantum correlation in a compound quantum system, which cannot be understood classically. It is oftentimes considered as a—if not the—defining property of quantum physics. In their pioneering work, Einstein, Podolsky, and Rosen [1] (EPR) brought up the idea of a previously unknown quantum correlation. Although at this point, rather than acknowledging the theoretical model that was later understood as entanglement, the authors recognized the observed phenomenon as an incompleteness to quantum theory. Schrödinger realized the importance of the discovery and introduced the term entanglement [2–4]. Furthermore, Schrödinger called entanglement the fundamental property of quantum physics.

Although raising fundamental questions in physics and even inspiring the DeBroglie-Bohm interpretation of quantum physics [5], it took many years for the theory introduced in EPR to be investigated. In his famous publication [6], Bell formulated inequalities based on the experimental state in the EPR paper. These inequalities are a mathematical formulation of locality and realism based on the claim that a measurement at one location should not affect the measurement at a different location. Bell showed that quantum states do not fulfill these inequalities, therefore proving the possibility of the existence of states proposed by Einstein, Podolsky, and Rosen true. A few years later the results of Bell could be experimentally verified [7, 8]. Until today, there are discussions whether Bell tests are indeed loophole-free, meaning there can be no other explanation except for entanglement for the violation of the Bell inequalities. Recent experiments try closing all remaining loopholes [9–11]. Eventually, entanglement was discovered as a prime resource for quantum information protocols in quantum cryptography [12, 13], quantum dense coding [14], and quantum teleportation [15]. Those tasks are not possible to perform with classical states, which shows entanglement is useful in applications [16].

Since many quantum technology protocols rely on the presence of entanglement between two parties (bipartite entanglement) or many parties (multipartite entanglement), the actual detection of entanglement has been a major concern in entanglement research. The multipartite scenario poses an entirely new challenge on the detection of entanglement as the degrees of freedom in the distribution of entanglement rise. This introduces new highly complex structures [17–19]. As showing the presence of entanglement in a compound quantum system purely by definition is highly impractical, in fact nearly impossible because of the required computational resources, entanglement criteria have been developed [20–22]. For bipartite entangled states, a sufficient criterion was introduced by Peres [23]. This criterion is prominently known as the partial transposition criterion and was generalized to positive-but-not-completely-positive maps (PNCP maps) [24], where it was shown to be necessary and sufficient for small systems. As these criteria work for discrete-variables states, related approaches were developed to address continuous-variable states [25, 26].

Entanglement verification by means of an operator was shown to be possible with so-called entanglement witness operators [20, 24, 27, 28]. Interestingly, the set of PNCP maps and the set of entanglement witness operators are isomorphic via the Choi-Jamiołkowski

isomorphism [29–31]. Entanglement witnesses are observables which gives them a crucial advantage over PNCP maps: It is possible to measure experimentally whether entanglement is present when employing entanglement witnesses. Early direct measurements of entanglement witnesses were performed shortly after the introduction of the theoretical notion [32–34]. The named examples of entanglement witnesses all show linear witnesses, referring to a linear operator as test operator. Nonlinear witness operators exist as well [35, 36], which add nonlinear terms to linear witnesses to better approximate the hull of the set of separable states. This class of operators is not covered in this thesis, as linear witnesses are sufficient to verify entanglement [24, 27].

Entanglement witnesses are a versatile approach to certify entanglement. In general, for any possible scenario, if entanglement is present, there exists at least one entanglement witness to verify this entanglement. Due to their usefulness, entanglement witnesses have been rigorously studied and special cases for various systems have been found. Entanglement witnesses for multipartite cluster states have been applied theoretically [37] as well as experimentally [32]. Furthermore, the approach was used to show entanglement in discrete-variable systems [38], such as trapped ions [38] and single-photon states [39], continuous-variable systems [40] and hybrid systems [41]. These entanglement witnesses all share a common disadvantage as they are specially tailored to the system at hand. For a more universal access, a construction scheme for entanglement witnesses should be followed. This is possible by employing the separability eigenvalue equations, which are formulated for bipartite entanglement [42] and also multipartite entanglement [43]. In recent years, the concept of device-independent entanglement witnessing was introduced [44–47]. The idea is, to find witness operators without a priori knowledge of the experimental setup. In this work, this concept is not followed, and knowledge about the measurement scheme is assumed.

An aspect in entanglement research that goes beyond the scope of this work is the topic of entanglement quantification. Quantification describes assigning a measure to the strength of entanglement, where an entanglement measure needs to fulfill certain properties [48, 49]. A universal entanglement measure has been found in the Schmidt numbers [50], which count the minimal numbers of superpositions necessary to describe a quantum state [16]. Applying this entanglement measure, a unified quantification of entanglement and nonclassicality is possible [51]. This relates entanglement to other nonclassical correlations [52] that go beyond entanglement and are not measurable by other means, such as quantum discord [53, 54]. General quantum correlations relate to the field of quantum thermodynamics as they allow for work to be extracted from the quantum system [55]. While the quantification of entanglement and other forms of quantum correlations are not directly adressed in this work, it can be shown in many scenarios, however, that there exists a direct or indirect connection to the notion of entanglement.

The goal of this thesis is to describe a universal entanglement test for arbitrary quantum systems. The cornerstones of the entanglement test are published in two Physical Review Letters [G1, G2], with [G1] having received an editor's suggestion and a viewpoint in Physics, and a Physical Review X [G3]. Note that throughout this work, references to work by the candidate are set apart and have the template [G#]. Basis for the developed scheme are the separability eigenvalue equations to construct entanglement witnesses. I developed a method that utilizes a genetic algorithm [56] to minimize a quantifier that describes the quality of an entanglement witness. This method was successfully implemented to show the complete entanglement structure of a ten mode Gaussian state [G1] as

well as to show entanglement in cases other tests would fail [G2]. For some special cases, the solution to this set of equations is known, yet generally solving separability eigenvalue equations is an NP-hard problem [57, 58]. To circumvent this problem, I developed an algorithm to numerically find a valid solution to the equations and use it to construct witnesses [G3]. As a next step, the correct entanglement witness operator fitting the problem at hand need to be found which will be achieved by means of numerical optimization. In combination with the genetic algorithm, this enable a construction of an approximation to the best entanglement witness. The close relation of the separability problem to fundamental mathematics problems and the usage of numerical methods—one specifically designed to the separability problem—shows the interdisciplinary nature of the thesis.

This thesis is structured as follows. In Chapter 2, the definition of entanglement is presented. Furthermore, this chapter will explain different notions of entanglement and how they are related to each other. Chapter 3 will give a brief overview of the theory of entanglement witnesses and explain the relation to separability eigenvalue equations. The numerical algorithm separability power iteration for approximating solutions to the separability eigenvalue equations is introduced in Chapter 4. Chapter 5 introduces general concept to finding statistically significant entanglement witnesses for experimental states, which can also be applied for theoretical analysis. An application to the presented methods and concepts to measured multipartite entangled states is shown in Chapter 6. The final Chapter 7 summarizes the results and gives an outlook to future development and application of the introduced framework.

Entanglement

For understanding the notion of entanglement, a few fundamentals have to be stated first. Entanglement is presented as a result of the absence of separability between parts of a compound system. Therefore, it has to be understood what parts of a system can exist, or in which ways a system might be split up. A clear definition of separability needs to be stated as well. As separability is not defined uniquely in multipartite quantum systems, entanglement can be understood ambiguously. This chapter will give an introduction of the partitioning of quantum systems and focus on the different notions of separability in multipartite systems and the coinciding entanglement.

2.1 Partitioning

Throughout this work, we will consider quantum states $\hat{\rho} : \mathcal{H} \to \mathcal{H}$ mapping the compound Hilbert space $\mathcal{H} = \bigotimes_{i=1}^{N} \mathcal{H}_i$, with $N \geq 2$, onto itself. To describe a quantum state, $\hat{\rho}$ needs to have the properties of a density operator, $\text{tr}(\hat{\rho}) = 1$ and $\hat{\rho}$ is Hermitian and positive definite. Such a state is called a multipartite state; in the case $N = 1$, no correlation and thus no entanglement can exist. The Hilbert spaces indices are arbitrary and fixed such that they can be adressed by the index set $\mathcal{S} = \{1, \ldots, N\}$ unambiguously. A partition $\mathcal{P}$ of the set $\mathcal{S}$ is a set of nonempty subsets of $\mathcal{S}$ in which every element of $\mathcal{S}$ is contained exactly once. Mathematically, a partition can be expressed as $\mathcal{P} = \mathcal{I}_1 {:} \cdots {:} \mathcal{I}_K$ with $K \leq N$ such that

- $\bigcup_{i=1}^{K} \mathcal{I}_i = \mathcal{S}$

- $\forall i \neq j : \mathcal{I}_i \cap \mathcal{I}_j = \emptyset$.

The number $K = \mathcal{P}$ is called length of the partition $\mathcal{P}$.

For quantum systems with $N > 2$, not one unique partition of the index set exists. Consider, for example, the set $\{1, 2, 3, 4\}$, which has a total of 15 different partitions, which are depicted in Fig. 2.1. In general, the number of partitions of a set of magnitude N is determined by the Bell-number B_N. The Bell-number is calculated by summing over the number of partitions for a fixed length, which is given by the Stirling number of the second kind $S_{N,K}$,

$$S_{N,K} = \frac{1}{K!} \sum_{j=0}^{K} (-1)^{K-j} \binom{K}{j} j^N,$$

$$B_N = \sum_{i=0}^{N} S_{N,i}. \tag{2.1}$$

A partition $\mathcal{P}'$ is called a *refinement* of partition $\mathcal{P}$ if every set in $\mathcal{P}'$ is a subset of the sets in $\mathcal{P}$. Then we can write $\mathcal{P}' \preceq \mathcal{P}$. In the example set $\{1, 2, 3, 4\}$, Fig. 2.1, the
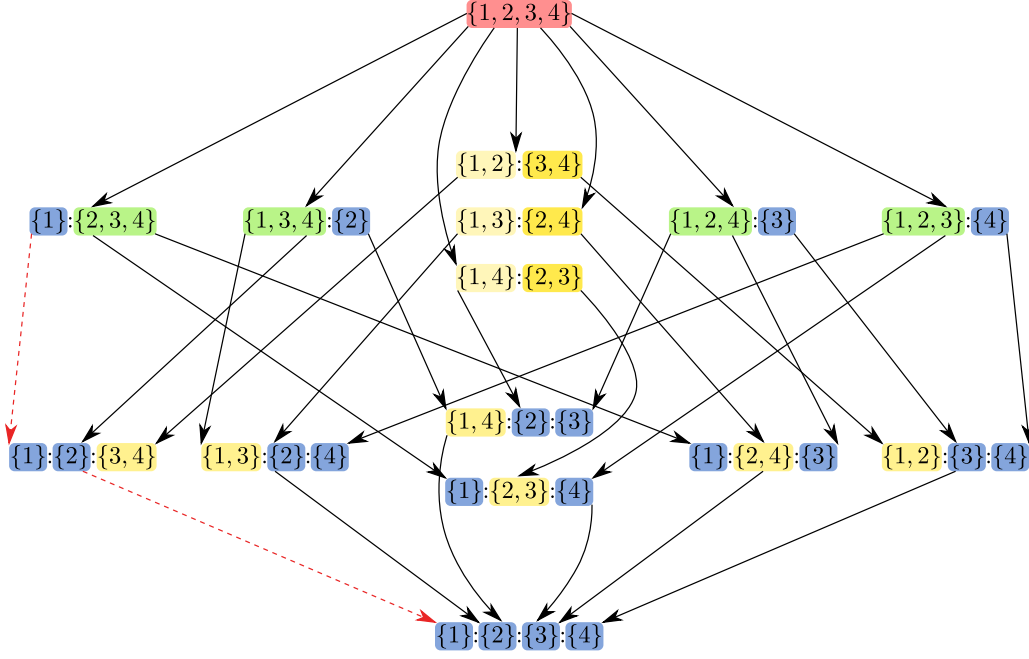
Figure 2.1: Partitioning of a set of cardinality four. The different color shades represent the cardinality of the set in the partition, red represents the full set of cardinality four, green represents subsets of length three, blue represents subsets of length one. Different shades of yellow represent subsets of length two and are shaded for better visibility. Refinements of a partition are represented by an arrow pointing from a partition to its refinement. A particular refinement path is highlighted in a red dashed line.

refinement of partition $\{1\}{:}\{2,3,4\}$ is shown along the red path. In fact, the refinements of all partitions of sets of length 4 are shown there. We can clearly see that refinement of different partitions may lead to the same partition. Continuing to find the refinement of a partition will always lead to the full partition $\{1\}{:}\cdots{:}\{N\}$ of the index set $\mathcal{S}$.

2.2 Separability and Entanglement

The concept of partitions of the index set of a compound Hilbert space has a direct consequence on the possible ways a quantum state can possibly be split. First, the definition of a separable state needs to be stated: A mixed quantum state $\hat{\sigma}$ on an N-partite Hilbert space $\mathcal{H}$ is called separable if and only if it can be written as

$$\hat{\sigma}_\chi = \int_{|s\rangle\langle s|\in\mathfrak{S}_\chi^*} \mathrm{d}P(s)\,|s\rangle\,\langle s|. \tag{2.2}$$

The function P is a classical probability distribution, thus $P \geq 0$ and $\int \mathrm{d}P = 1$ hold true. The set $\mathfrak{S}_\chi^*$ contains pure state projectors $|s\rangle\langle s|$ which need to be defined according to the scenario χ which is considered. Definition 2.2 is the most general definition of separability and allows for special cases of separability to be defined by adjusting the set of pure states.

One notable case of separability that has been investigated is *partition separability*. In this case, consider a partition $\mathcal{P} = \mathcal{I}_1{:}\ldots{:}\mathcal{I}_K$ of the index set of the Hilbert space.

Per definition [59], a multipartite quantum state $\hat{\sigma_{\mathcal{P}}}$ acting on a Hilbert space is called separable with respect to partition $\mathcal{P}$ if and only if it can be written as a convex mixture of pure states, separable in partition $\mathcal{P}$. Therefore, the set of pure states is

$$\mathfrak{S}^*_{\mathcal{P}} = \{|a_1,\ldots,a_K\rangle \langle a_1,\ldots,a_K| : \forall i : |a_i\rangle \in \mathcal{H}_{\mathcal{I}_i}, \mathcal{I}_i \in \mathcal{P}\}. \tag{2.3}$$

Here, $|a_i\rangle \in \mathcal{H}_{\mathcal{I}_i}$ is an arbitrary state in the product subsystem $\mathcal{H}_{\mathcal{I}_i} = \bigotimes_{j \in \mathcal{I}_i} \mathcal{H}_j$ and normalized, $\langle a_i|\, a_i\rangle = 1$. The state $|a_1,\ldots,a_K\rangle$ is a pure separable state in the product Hilbert space $\mathcal{H}$ and is defined as a tensor product

$$|a_1,\ldots,a_K\rangle = \bigotimes_{i=1}^{K} |a_i\rangle. \tag{2.4}$$

Similarly to the definition of partial entanglement, the term K-*separability* is defined. Instead of considering a single partition, any partition with a fixed length K, written as $|\mathcal{P}| = K$, is considered. Thus, a multipartite quantum state $\hat{\sigma}_K$ is defined as K-separable [60] if and only if it can be written as a convex mixture of pure states that are separable in at least one partition of length K. In this case, the set of pure states is

$$\mathfrak{S}^*_K = \{|a_1,\ldots,a_K\rangle \langle a_1,\ldots,a_K| : \forall i : |a_i\rangle \in \mathcal{H}_{\mathcal{I}_i}, \mathcal{I}_i \in \mathcal{P}, |\mathcal{P}| = K\}. \tag{2.5}$$

More general notions of separability may also be defined by different convex combinations of separable sets [61].

Entanglement, in general, is defined as the absence of separability. As separability is not defined uniquely, different classifications of entanglement arise: A quantum state $\hat{\rho}$ is called *entangled with respect to partition* $\mathcal{P}$, if it can not be written as in Eq. (2.2). If a state does not have a decomposition shown in Eq. (2.5), the state is called K-*entangled* for a given K.

An alternate definition of entanglement is based on the sets of states, separable in different notions. Consider the set of separable states with respect to a partition $\mathcal{P}$

$$\mathfrak{S}_{\mathcal{P}} = \left\{ \hat{\sigma} \in \mathcal{O} : \hat{\sigma} = \int_{|s\rangle\langle s| \in \mathfrak{S}^*_{\mathcal{P}}} \mathrm{d}P(s)\, |s\rangle \langle s| \right\} \tag{2.6}$$

and the set of K-separable states

$$\mathfrak{S}_K = \left\{ \hat{\sigma} \in \mathcal{O} : \hat{\sigma} = \int_{|s\rangle\langle s| \in \mathfrak{S}^*_K} \mathrm{d}P(s)\, |s\rangle \langle s| \right\}. \tag{2.7}$$

By construction, the set of K-separable states is the convex hull of the union of the sets of separable states for all partitions of length K, thus $\mathfrak{S}_K = \mathrm{Conv}\left(\bigcup_{|\mathcal{P}|=K} \mathfrak{S}_{\mathcal{P}}\right)$ holds true.

2.3 Inheritance of Separability and Entanglement

After introducing the various forms of separability, Eqs. (2.3) and (2.5), and the entanglement arising from absence of these separabilities, we are going to look at the relationship
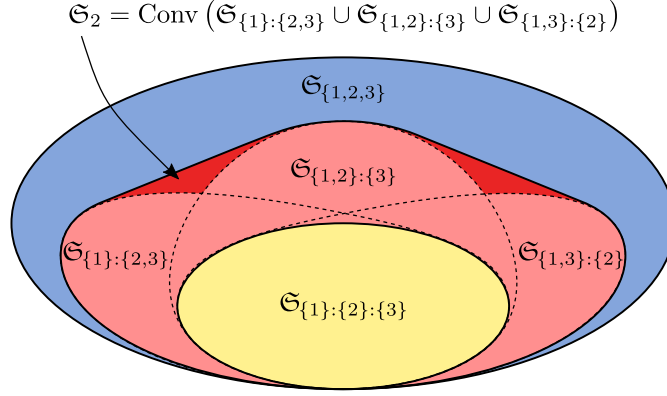
Figure 2.2: Separable sets for a three partite quantum system. For a three partite quantum state, a total of five partitions can be created from the index set. The sets represent sets of separable states with respect to the partition that is shown. Different colors represent different lengths of partitions (blue: $K = 1$, red: $K = 2$, yellow: $K = 3$). The dark red area shows the addition of the convex hull for all separable states for bipartitions.

between separability and entanglement of quantum states with respect to those definitions. An interesting property related to the inheritance of entanglement and separability of quantum states will be stated first and proved afterwards.

At first, we will look at separability and entanglement of a quantum state with respect to partitions that are included within a refinement graph such as Fig. 2.1. Should a quantum state be entangled with respect to a partition $\mathcal{P}$, then it is also entangled with respect to all partitions that are refinements of $\mathcal{P}$. Vice versa, if a quantum state is separable with respect to a partition then it is also separable with respect to all partitions that refine to this partition. Thus going top to bottom along the arrows in Fig. 2.1, entanglement is inherited, whereas going against the direction of the arrows, separability is inherited.

Applying this concept to the notion of K-separability, a few more inheritance properties can be concluded. Suppose a quantum state is K-entangled, then it is also $K + 1$-entangled, as well as entangled with respect to all partitions of length larger or equal to K. On the other hand, in general, no separability of a state can be implied by the presence of K-separability.

In the extreme cases, should a quantum state be 2-entangled, it is entangled for all (nontrivial) K and entangled with respect to all partitions. A quantum state, separable with respect to the full partition, is separable with respect to all partitions and K-separable for all K.

These statements follow directly from the definition of separability. For a visualization of the formulas, refer to Fig. 2.2 will be given, when applicable. Assuming separability of a quantum state $\hat{\rho}$ with respect to a certain partition $\mathcal{P}'$ of length K, then it can be expressed as

$$\hat{\rho} = \int_{\mathfrak{S}_{\mathcal{P}'}} \mathrm{d}P(a_1, \ldots, a_K) \, |a_1, \ldots, a_K\rangle \, \langle a_1, \ldots, a_K| \, . \tag{2.8}$$

If it can be shown, that separability of a state with respect to a partition $\mathcal{P}'$ implies the separability with respect to a partition $\mathcal{P}$ with $\mathcal{P} \succeq \mathcal{P}'$, it follows by induction for all

partitions which refine to $\mathcal{P}'$. Any partition $\mathcal{P} \succeq \mathcal{P}'$ has at most length $K{-}1$. Thus, a partition $\mathcal{P} = \mathcal{I}_1{:}\ldots{:}(\mathcal{I}_{K-1} \cup \mathcal{I}_K)$ is constructed from $\mathcal{P}' = \mathcal{I}_1{:}\ldots{:}\mathcal{I}_K$. Without loss of generality, any partition of length $K{-}1$ which refines to $\mathcal{P}'$ can be constructed this way by renaming the modes. Therefore, it follows that

$$\hat{\rho} = \int_{\mathfrak{S}_{\mathcal{P}}} \mathrm{d}P_1(a_1, \ldots, a_{K-1}) \, |a_1, \ldots, a_{K-1}\rangle \langle a_1, \ldots, a_{K-1}| , \tag{2.9}$$

where P_1 is a classical distribution of states from the compound Hilbert spaces indexed by the sets in $\mathcal{P}$. It can then be immediately concluded that $\hat{\rho}$ is separable with respect to $\mathcal{P}$. Since all states which are separable with respect to $\mathcal{P}'$ are also separable with respect to $\mathcal{P}$, the set of separable states for $\mathcal{P}'$ is contained in the set of states separable to $\mathcal{P}$, thus $\mathfrak{S}_{\mathcal{P}'} \subseteq \mathfrak{S}_{\mathcal{P}}$. This is shown in Fig. 2.2 as areas representing separable sets for larger partitions are completely included in areas representing separable sets for smaller partitions.

By definition, $\hat{\rho}$ is entangled with respect to a certain partition $\mathcal{P}$ if it is not within $\mathfrak{S}_{\mathcal{P}}$. Since $\mathcal{P} \succeq \mathcal{P}'$ implies $\mathfrak{S}_{\mathcal{P}} \supseteq \mathfrak{S}_{\mathcal{P}'}$, it follows, that if a quantum state is entangled with respect to $\mathcal{P}$, thus not contained in $\mathfrak{S}_{\mathcal{P}}$, it is also not contained in $\mathfrak{S}_{\mathcal{P}'}$ and thus entangled with respect to $\mathcal{P}'$.

The entanglement inheritance for K-entanglement follows from a similar argument. Suppose a quantum state is K-entangled, then it is not within $\mathfrak{S}_K = \mathrm{Conv}\left(\bigcup_{|\mathcal{P}|=K} \mathfrak{S}_{\mathcal{P}}\right)$. As any set of separable states for any partition $\mathcal{P}$ of length K is a subset of $\mathfrak{S}_K$, the state is not within either of the sets. Thus, a K-entangled state is entangled with respect to any partition of length K. This implies entanglement of this state with respect to any partition of length greater or equal to K. Furthermore, as $\mathfrak{S}_{\mathcal{P}} \supseteq \mathfrak{S}_{\mathcal{P}'}$ for partitions with $\mathcal{P} \succeq \mathcal{P}'$, the set of $K+1$-separable states is a subset of the set of K-separable states, $\mathfrak{S}_K \supseteq \mathfrak{S}_{K+1}$. Therefore, a state which is K-entangled is also $K+1$-entangled and, more precisely, l-entangled for $l \geq K+1$ For a visualization, see Fig. 2.2, where $\mathfrak{S}_2$ completely encloses all separable states with respect to bipartitions, which in turn completely include the separable set with respect to the single tripartition—and in more general cases would include all separable sets with respect to all tripartitions.

2.4 Summary

This chapter reviews the definition of entanglement in different notions. A certain notion of entanglement is always defined as the absence of separability of some kind. The different notions of separability arise from different set partitions and thus different elementary separable states, which are pure product states with the different parts from product Hilbert spaces designated by the partition. Furthermore, additional notions arise by combining the sets of different states. To be able to unambiguously talk about multipartite entanglement, it becomes necessary to clearly state the frame of reference.

Consider the example of threepartite pure states

$$|\psi_{\{1,2,3\}}\rangle = \frac{1}{\sqrt{2}} \left(|0,0,0\rangle + |1,1,1\rangle\right), \tag{2.10a}$$

$$|\psi_{\{1\}:\{2,3\}}\rangle = |0\rangle \otimes \frac{1}{\sqrt{2}} \left(|0,0\rangle + |1,1\rangle\right), \tag{2.10b}$$

$$|\psi_{\{1\}:\{2\}:\{3\}}\rangle = |0\rangle \otimes |0\rangle \otimes |0\rangle. \tag{2.10c}$$

These are exemplary states which are separable with respect to the partition in its index. Whereas the first state is fully entangled—entangled with respect to every partition—the last state is fully separable—separable with respect to every partition. The second state is separable with respect to a single bipartition, yet entangled with respect to the other two bipartitions.

Therefore, it becomes indispensable to clearly analyze the partitioning of index sets for the compound Hilbert space in which a state under investigation lies. For multipartite cases, the number of possible partitions grow exponentially according to the Bell number. A certain part of the entanglement analysis can be covered by the described inheritance properties. Yet, cases exist, in which entanglement may not be verified for a partition of small length and entanglement needs to be tested for succeeding partitions along the partition graph.

The different challenges for entanglement detection in multipartite systems that arise from the various definitions of separability are addressed in this work and can be overcome with the methods that are presented.

Entanglement Testing

<div style="text-align: right">3</div>

The question whether entanglement is present in a quantum state is an important one in the field of quantum optics, quantum information, and related fields. It does not simply suffice to consider the definitions of separability, Eq. (2.2), and check whether our quantum state under investigation suffices the criterion. This would require perfect knowledge of all separable pure states and all possible classical probability distributions of those states. Therefore, for viably and efficiently testing, entanglement criteria have been developed. This chapter gives a brief introduction to the broad topic of entanglement witnesses and describe a recent method how to construct witnesses.

3.1 Entanglement Witnesses

A common approach for testing entanglement introduces *entanglement witness* operators [27]. An entanglement witness operator $\hat{W}$ is an operator on the Hilbert space $\mathcal{H}$ that the state under investigation acts on. It has to fulfill two properties

$$\langle \hat{W} \rangle = \mathrm{tr}\left(\hat{W}\hat{\sigma}\right) \geq 0, \quad \forall \hat{\sigma} : \hat{\sigma} \in \mathfrak{S}, \tag{3.1}$$

$$\exists \hat{\rho} : \langle \hat{W} \rangle = \mathrm{tr}\left(\hat{W}\hat{\rho}\right) < 0. \tag{3.2}$$

Suppose an entanglement witness operator has been found, then entanglement is verified if it has a negative expectation value for the state under consideration. On the other hand, should the expectation value be non negative, the quantum state might be separable or entangled, cf. Fig. 3.1. To minimize the set of states that are entangled, yet not detected as entangled by a chosen witness, the concept of optimal entanglement witnesses is introduced. Consider two witness operators $\hat{W}_1$ and $\hat{W}_2$; $\hat{W}_2$ is a *finer* entanglement witness than $\hat{W}_1$, if

$$\{\hat{\rho} : \mathrm{tr}(\hat{W}_1\hat{\rho}) < 0\} \subseteq \{\hat{\rho} : \mathrm{tr}(\hat{W}_2\hat{\rho}) < 0\}. \tag{3.3}$$

A witness operator $\hat{W}_{\mathrm{opt}}$ is called *optimal* witness, if there is no finer witness [62].

The base for entanglement witnesses is the Hahn-Banach separation theorem; see, e.g., [63]. It states for two convex disjoint and nonempty subsets $A, B \subset \mathcal{V}$, with $\mathcal{V}$ being the set of all operators acting on $\mathcal{H}$, there exists a finite linear map $\varphi : \mathcal{V} \to \mathbb{C}$ and a $\lambda \in \mathbb{R}$, such that $\mathrm{Re}(\varphi(a)) < \lambda \leq \mathrm{Re}(\varphi(b))$, $\forall a \in A, b \in B$. In other words, there exists a hyperplane which is defined by the linear map φ that separates the convex subsets A and B. Of particular interest in the Hahn-Banach theorem is the separation of a convex set by a hyperplane. Note that the reference set of pure separable states is not explicitly named here. When talking about separability and entanglement, the reference set is implied to be equal. A set of separable states is convex and closed by definition; see Eq. (2.2). Therefore, a linear map φ must exist that defines a hyperplane between all separable states
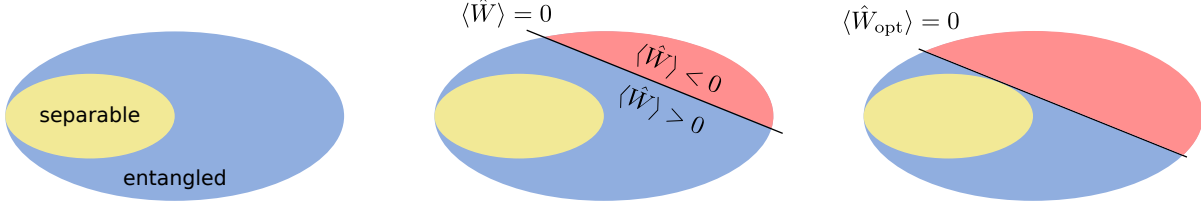
Figure 3.1: Witness operator separating some entangled states from set of separable states. Left: The set of all quantum states is split into the convex set of separable states (yellow) and inseparable states (blue). Middle: The witness operator defines a hyperplane for all states that satisfy $\langle \hat{W} \rangle = 0$. All separable states (yellow) and also some entangled states (blue) fulfill the property $\langle \hat{W} \rangle \geq 0$. States with $\langle \hat{W} \rangle < 0$ are detected as entangled (red). Right: An optimal witness operator maximizes the magnitude of the set of states that are detected as entangled for the direction defined by the witness operator.

and another convex set without any separable states. For now, it shall be ignored that there also will be entangled states—which do not define a convex set—on the same side of the hyperplane as the separable states. In particular, the linear map can be explicitly stated according to the Horodeckis, $\varphi : \hat{\rho} \mapsto \mathrm{tr}\left(\hat{W}\hat{\rho}\right)$. Then, the set B are the set of separable states, A is the set that does not contain any separable state at all and the real parameter $\lambda = 0$. To fulfill the properties stated for an entanglement witness, Eq. (3.1), if there is a state $\hat{\rho}$ which should be verify to be entangled, it suffices to let $A = \{\hat{\rho}\}$. Thus, entanglement witnesses in general define a hyperplane in operator space with the normal vector of the plane pointing toward the set of separable states. Optimal entanglement witnesses define a hyperplane tangent to the set of separable states, cf. Fig. 3.1.

3.2 Separability Eigenvalue Equations

A different but equivalent approach to finding a separating hyperplane between parts of the entangled states and the set of separable states are the separability eigenvalue equations [42, 43]. Suppose a Hermitian operator $\hat{L}$ and its optimal values with respect to all separable states $\mathfrak{S}$ is wanted; that is we have the optimization problem

$$\max \ \mathrm{tr}(\hat{L}\hat{\sigma}) \quad \text{or} \quad \min \ \mathrm{tr}(\hat{L}\hat{\sigma}) \tag{3.4}$$
$$\text{subject to } \hat{\sigma} \in \mathfrak{S}.$$

The separability eigenvalue equations are a solution to the optimization problem Eq. (3.4) in the case of separable states with respect to a given partition $\mathcal{P}$, setting $\mathfrak{S} = \mathfrak{S}_{\mathcal{P}}$. For an operator $\hat{L}$ acting on an N-fold Hilbert-space and a partition $\mathcal{P}$ of length K of the set $\mathcal{S}$, the equations take the form

$$\hat{L}_{a_1,\ldots,a_{j-1},a_{j+1},\ldots,a_K} |a_j\rangle = g_{\mathcal{P}} |a_j\rangle, \quad \forall j, \tag{3.5}$$

where the real number $g_{\mathcal{P}}$ is called separability eigenvalue for partition $\mathcal{P}$ and the product vector $|a_1,\ldots,a_K\rangle$ is called separability eigenvector. The operator $\hat{L}_{a_1,\ldots,a_{j-1},a_{j+1},\ldots,a_K}$ is defined by finding the mean value of $\hat{L}$ with respect to all but one parts of the separability
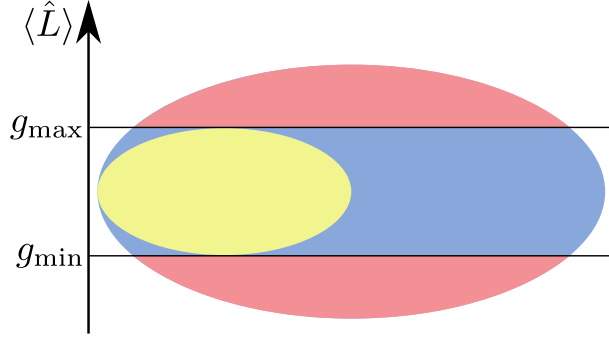
Figure 3.2: Boundaries of the set of separable states found by operator $\hat{L}$. The minimal and maximal separability eigenvalues determine the bounds of expectation values for separable states in the direction dictated by $\hat{L}$. The set of separable states (yellow) is always within the bounds, whereas there can also exist entangled states, that are within the bounds (blue). Any state not within these boundaries is necessarily entangled (red).

eigenvector:

$$\forall |x\rangle, |y\rangle \in \mathcal{H}_j : \quad \langle x|\hat{L}_{a_1,\ldots,a_{j-1},a_{j+1},\ldots,a_K}|y\rangle$$
$$= \langle a_1,\ldots,a_{j-1},x,a_{j+1},\ldots,a_K|\hat{L}|a_1,\ldots,a_{j-1},y,a_{j+1},\ldots,a_K\rangle.$$

For the detection of entanglement, either the minimal separability eigenvalue, $g_{\mathcal{P}}^{(\min)}$ or the maximal separability eigenvalue, $g_{\mathcal{P}}^{(\max)}$ are required. In the case of verification of K-entanglement, the set of separable states in Eq. (3.4) becomes $\mathfrak{S} = \mathfrak{S}_K$. The solution to the optimization problem can then be calculated from the individual separability eigenvalues for each partition of length K,

$$g_K^{(\max)} = \max\{g_{\mathcal{P}}^{(\max)} : |\mathcal{P}| = K\}, \tag{3.6}$$
$$g_K^{(\min)} = \min\{g_{\mathcal{P}}^{(\min)} : |\mathcal{P}| = K\}. \tag{3.7}$$

This statement follows directly from the definition of $\mathfrak{S}_K$. For a prove see [G2]. Henceforth, the nomenclature $g_{\max}$ and $g_{\min}$ for the optimal separability eigenvalues will be used whenever the specific notion is not required.

Having found the maximal and/or minimal separability eigenvalue, a criterion for entanglement can be formulated according to Eq. (3.4): A quantum state $\hat{\rho}$ is entangled, if there exists an operator $\hat{L}$, such that

$$\operatorname{tr}(\hat{L}\hat{\rho}) > g_{\max} \quad \text{or} \quad \operatorname{tr}(\hat{L}\hat{\rho}) < g_{\min}. \tag{3.8}$$

If one of the cases in Eq. (3.8) is fulfilled, then $\hat{\rho}$ exceeds the bounds for expectation values which $\hat{L}$ has. Thus, $\hat{\rho}$ is not a separable state and is necessarily entangled, see Fig. 3.2.

It is especially noteworthy that there is a connection between the separability eigenvalue equations and optimal entanglement witnesses. Considering optimal entanglement witnesses $\hat{W}_{\mathrm{opt}}$, then the relations

$$\hat{W}_{\mathrm{opt}} = g_{\max}\hat{1} - \hat{L} \quad \text{and} \quad \hat{W}_{\mathrm{opt}} = \hat{L} - g_{\min}\hat{1} \tag{3.9}$$

hold true. Thus, an optimal entanglement witness can be directly derived from any Hermitian operator by calculating its (maximal or minimal) separability eigenvalues.

The ability to construct arbitrary multipartite entanglement witness from Hermitian operators is a huge advantage of the separability eigenvalue equations. Instead of schemes that find witness operators that rely on a specific structure of a quantum state and proving the chosen operator is a witness, any operator that is designed in the fashion of Eq. (3.9) is a witness operator by construction. The problem of finding a witness operator has been shifted to finding either the minimal or the maximal separability eigenvalue. For special cases, the solution has been found [42, 43]. In general, an analytic solution to the separability eigenvalue equations can not be found and a different, i.e., numerical, approach needs to be taken to construct optimal witnesses.

3.3 Summary

This chapter reviews entanglement testing with entanglement witnesses. The concept of entanglement witnesses and their mathematical background in the Hahn-Banach separation theorem was presented. An analytic construction of these operators is possible by solving the separability eigenvalue equations for a testing operator. As witnessing is based on the geometry of the separable set—the set is always convex—the specific notion of entanglement to test is not important to the approach in itself. Only in the actual construction of the witness, the notion needs to be taken into account and the separability eigenvalue equations solved accordingly.

Separability eigenvalue equations are not only applicable to testing entanglement but many related problems follow the same algebraic structure. Entanglement quasiprobabilities, which are essentially the probability distributions in the definition of a separable state, can be constructed by finding all separability eigenvectors of a quantum state [64]. Entanglement quantification applies Schmidt number eigenvalue equations which couple the separability eigenvalue equations to a weight matrix [19, 65].

Because of the complex structure of multipartite entanglement, it is difficult to find the best-suited witness operator and solve the nonlinear eigenvalue equations for its construction. To address these challenges, I developed and applied numerical approaches, which are presented in the following parts.

Numerical Construction of Entanglement Witnesses

<div style="text-align: right">4</div>

In general, the separability eigenvalue equations cannot be solved analytically. The standard eigenvalue problem does not have an analytic solution for matrices of dimension larger than four. The same holds for the separability eigenvalue equations that reduce to the standard eigenvalue equation for a single partition, $K = 1$. Furthermore, there exists almost no diagonalization of an operator in the separability eigenvalues, which complicated the problem of finding solutions. Therefore, to find separability eigenvalues of Hermitian operators, an alternative approach must be used. This chapter describes an approach to finding the maximal separability eigenvalue of a multipartite operator which was introduced in [G3], the Separability Power Iteration (SPI). The SPI was devised by the candidate in collaboration with his supervisor and cosupervisor. Individual steps were proved mathematically to be able to guarantee convergence towards the maximal separability eigenvalue. Rigorous testing with different types of operators was carried out, and it was shown that the computation time is significantly lower than other means of finding the maximal separability eigenvalue.

4.1 Separability Power Iteration

The method introduced is a vast generalization of the power iteration [66], which is a well-known algorithm for finding the largest eigenvalue of a positive-definite and symmetric matrix. Similarly, the SPI finds the maximal separability eigenvalue for a positive-definite Hermitian operator. Thus, the SPI is able to solve a nonlinear system of equations. A regular eigenvector is, in general, not a separability eigenvector as it is not a product vector. The SPI approaches this issue by projecting an iterated vector of each step in the regular power iteration on product vectors to find the product vector which maximally projects onto the iterated vector an approximation to the separability eigenvector.

Figure 4.1 shows the flowchart of the SPI, a layout of the individual steps of the algorithm. This flowchart is descriptive to keep focus on the steps of the algorithm and not the mathematics involved. Each part of the algorithm is described in detail in Section 4.2. The run of the SPI differs for two types of operators. First for onepartite operators, the SPI reduces to the regular power iteration and second, multipartite operators require the modification of the regular power iteration, which are essentially given by the *forward iteration* and the *backward iteration*.

The forward iteration is based on the cascaded structure of the separability eigenvalue equations, cf. [43]. The cascaded structure claims for an N-partite pure operator $\hat{L} = |\Psi\rangle\langle\Psi|$ that its nonzero solutions to the separability eigenvalue equations are equal to the solutions of an $N - 1$-partite operator $\hat{L}' = \text{tr}_N \hat{L}$. Essentially, having found the
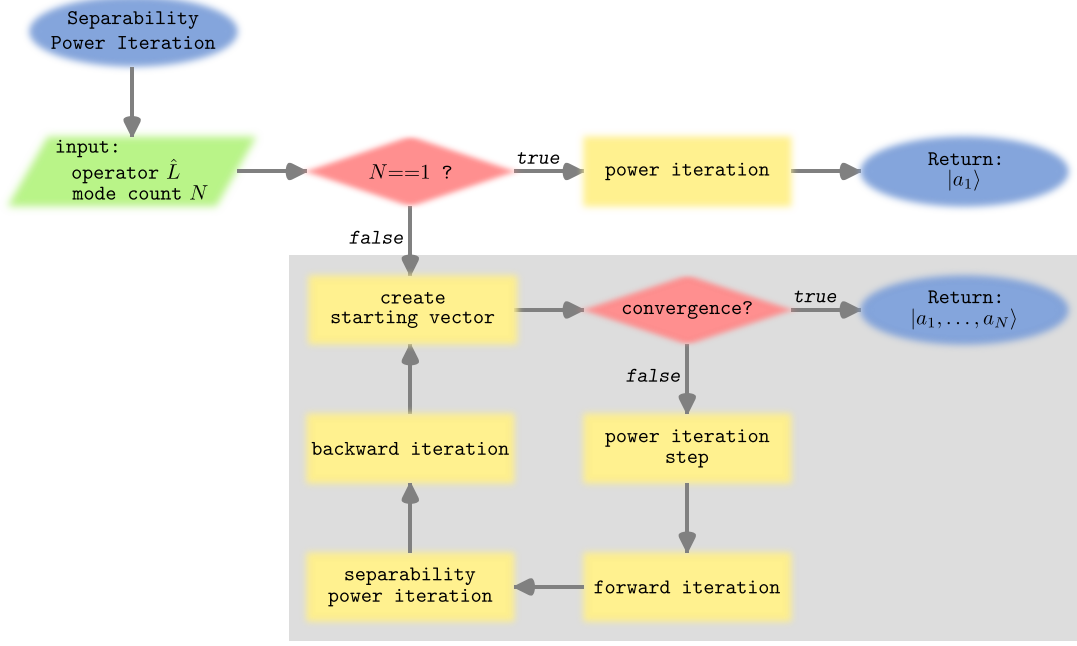
Figure 4.1: Flowchart of the Separability Power Iteration. The algorithm takes two input arguments shown in the green parallelogram. Blue ellipses are starting and end points to the algorithm. Yellow rectangles are program snippets which are run and red diamonds show branches.

separability eigenvector $|a_1, \ldots, a_{N-1}\rangle$ of $\hat{L}'$, the separability eigenvector $|s\rangle$ of $\hat{L}$ can be found as $|s\rangle = |a_1, \ldots, a_{N-1}\rangle \otimes |a_N\rangle$. This effectively enables the SPI to find the maximal separability eigenvalue of an N-partite operator in an $(N-1)$-partite Hilbert space. The backwards iteration is a trivial inference of the cascaded structure, as the N-th part $|a_N\rangle$ of the separability eigenvector of $\hat{L}$ fulfills the equation

$$\nu |a_N'\rangle = \langle a_1, \ldots, a_{N-1}, \cdot |\hat{L}|a_1, \ldots, a_N\rangle$$

for some $\nu \in \mathbb{C} \setminus \{0\}$. Both the forward iteration and the backward iteration are essential for finding the maximally projecting product vector onto the iterated vector by a single power iteration step.

In the `input` section of the SPI, the corresponding $\hat{L}$ and the number of parts in the partitions, N, for which the separability eigenvalue shall be calculated are entered. The code snippet `create starting vector` will generate a product vector $|a_1, \ldots, a_N\rangle$. For this, different approaches can be taken. To cover the entire space of possible solutions and to avoid iterating into a local maximum, multiple starting vectors should be used and the SPI run for each. Ideally these starting vectors cover the search space which the operator basis fulfills. As, in general, $N > 1$, the first branch will return `false` and generally, the `convergence` branch will also return `false`. Thus the next essential step is a `power iteration step`, which will apply operator $\hat{L}$ on the starting vector, $|\Psi\rangle = \hat{L}|a_1, \ldots, a_N\rangle$. Generally, $|\Psi\rangle$ is not a product vector anymore and cannot be an approximation to a separability eigenvector. The `forward iteration` part of the

program finds a onepartite operator constructed as

$$\hat{L}' = \text{tr}\left(|\Psi\rangle\langle\Psi|\right). \tag{4.1}$$

Again, the `separability power iteration` is called, yet for operator $\hat{L}'$ and $N' = N-1$. Should $N' = 1$ hold, the `power iteration` is called, which has a well analyzed behavior. Otherwise the SPI will start over by finding new starting vectors and the forward iteration step until $N' = 1$ and then run the power iteration. The power iteration will return the eigenvector—since a onepartite operator is entered, separability eigenvector and regular eigenvector are identical—corresponding to the maximal eigenvalue of $\hat{L}'$ which will be called $|a_1'\rangle$. The SPI will return to the `backward iteration`, where the returned vector will first be projected onto $|\Psi\rangle$ and then normalized,

$$|b\rangle = \langle a_1', \cdot \mid \Psi\rangle, \qquad |a_2'\rangle = \frac{1}{\sqrt{\langle b|b\rangle}}|b\rangle. \tag{4.2}$$

It follows the next iteration of the approximation to the $N' = 2$ case $|a_1', a_2'\rangle$. Forward iteration, power iteration and backward iteration are repeated until a convergence criteria has been met. Then the backward iteration for the $N' = 3$ case will be calculated. The scheme continues until the backward iteration finds a vector for N and then repeats until convergence.

4.2 Working Behavior

For a better understanding of the behavior of the SPI, an example will be considered, that has already been discussed in detail in [G3]. The task is to find the maximal separability eigenvalue of the swap operator shifted to make it positive definite

$$\hat{L} = 2\hat{1} - \hat{S}, \text{ with } \hat{S}|a_1, a_2\rangle = |a_2, a_1\rangle. \tag{4.3}$$

The analytic solution to the separability eigenvalue equations is $g_{\max} = 2$ for $|a_1\rangle \perp |a_2\rangle$.

Because of this structure, the separability eigenvector corresponding to the maximal
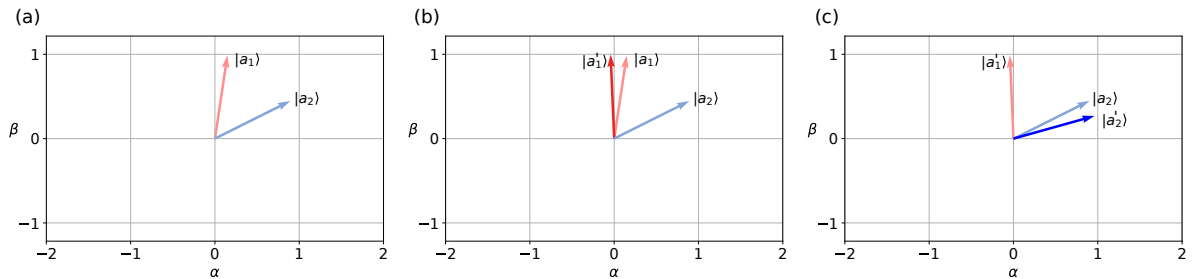
Figure 4.2: Parts of iterated approximation of the separability eigenvector for a shifted swap operator. The starting vectors are shown in (a). After the forward iteration, a new approximation, $|a_1'\rangle$, has been found in (b). The results of the backwards iteration are shown in (c) with a new approximation, $|a_2'\rangle$. After this one step, the angle between the iterated vectors is closer to $\pi/2$ and, therefore, the vectors closer to being orthogonal compared to the starting vectors.
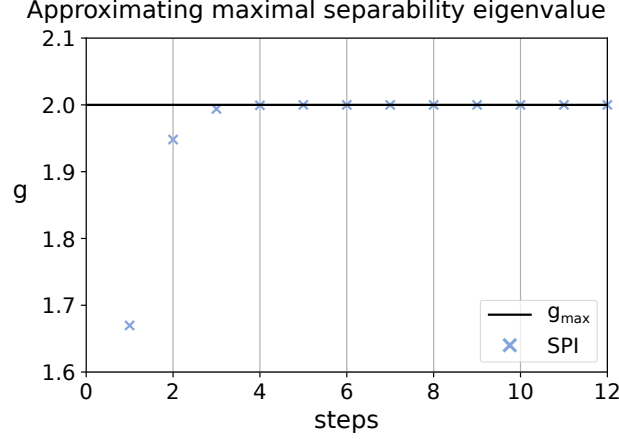
Figure 4.3: Approximations to the maximal separability eigenvalue of a shifted swap operator. The approximation g to the maximal separability eigenvalue converges towards the analytic value of $g_{\max} = 2$. Whereas the iterated values are already close to the analytic maximum after 4 steps, true convergence is only reached after 12 steps.

separability eigenvalue can be found in $\mathbb{R}^{2d}$, with d the dimension of one Hilbert space. Assuming $\mathcal{H} = \mathbb{R}^2$, the individual states which combine to this separability eigenvector can be plotted. The individual vectors $|a_i\rangle \in \mathcal{H}_i$ will be decomposed in qubit basis

$$|a_i\rangle = \alpha_i |0\rangle + \beta_i |1\rangle . \tag{4.4}$$

Figure 4.2 shows the evolution of two randomly picked real starting vectors in a single step of the SPI. The leftmost figure shows the starting vectors. After the forward iteration, the angle between the vectors is increased because one of the vectors, $|a_1\rangle$, was adjusted. The backwards iteration adjusts $|a_2\rangle$ again increasing the angle between the vectors. This process is repeated until the angle will be $\pi/2$, in which case $|a_1\rangle \perp |a_2\rangle$ holds true. At the same time, an approximation to the maximal separability eigenvalue of $\hat{L}$ is calculated as $\langle a_1, a_2 | \hat{L} | a_1, a_2 \rangle$. In each step, the approximated value grows, until in converges towards the global maximum, which is the maximal separability eigenvalue; see Fig. 4.3. Convergence is checked by vectors $|a_1\rangle$ and $|a_2\rangle$ fulfilling the separability eigenvalue equations, Eq. (3.5).

The presented figures represent the typical working behavior of the SPI. Separability eigenvectors are successively calculated by the partition of Hilbert spaces: A single part of the vector is iterated and the new solution applied to find a new iteration for the next part. The iterated approximations to the maximal separability eigenvalue will always generate a monotonically growing sequence.

4.3 Summary

This chapter introduces the SPI, a numerical solver for finding the maximal separability eigenvalue of a positive-definite Hermitian operator. Mathematical proofs regarding the working behavior and convergence guarantee that the SPI is a powerful tool in the construction of entanglement witnesses. There exist different approaches to finding the optimal expectation value of an operator with respect to separable states which are based

on semidefinite programming [67–71]. The SPI has an advantage over these methods as it is specifically constructed to the separability problem and semidefinite programming address general optimization tasks.

Furthermore, benchmarks show an improvement in calculation time by multiple orders of magnitude in comparison to an alternative approach. Even in complex compound Hilbert spaces of multiple qubits or higher dimensional cases in discrete variables, convergence is possible in reasonable time. The solid framework will be applicable to constructing witnesses even in complex systems, such as bound entangled states, as is shown in a proof of concept.

Regardless of the entanglement testing, the SPI can find application in related problems. Entanglement quantification, entanglement quasiprobabilities, and other fundamental problems are addressable by equations that are algebraically of the same structure as the separability eigenvalue equations. An SPI-like approach that takes the special structure of the involved equations into consideration can be envisioned.

Numerical Verification

In practice, it is not feasible to find suitable operators for entanglement verification analytically. This will happen for general quantum states and, more importantly, for experimentally generated states. Here, the operator space cannot be limited to a small subspace and the test operator needs to be found among all possible states. In these cases, a numerical approach is favorable. This chapter will focus on numerical treatment of entanglement detection and introduce a practical approach based on optimization problems to find suitable test operators. This approach will be applied to the entanglement detection in experimentally generated Gaussian states, which has been performed in [G1, G2].

5.1 Practical Entanglement Detection

Consider a random test operator $\hat{L}$, for which, without loss of generality, the minimal separability eigenvalue $g_{\min}^{\mathcal{P}}$ for the particular partition under consideration has been found. Entanglement witnesses define a hyperplane in the operator space, cf. Fig. 3.2. Let $\mathcal{E} := \{\hat{\rho} : \mathrm{tr}\left(\hat{L}\hat{\rho}\right) < g_{\min}^{\mathcal{P}}\}$ describe the set of entangled states which are detected as entangled by this hyperplane. The complementary set $\bar{\mathcal{E}}$ will contain all other states..

A particular entangled state $\hat{\varrho}$ might be within either $\mathcal{E}$ or $\bar{\mathcal{E}}$. In the case $\hat{\varrho} \in \mathcal{E}$ the test is successful and the entangled state has been detected as entangled by $\hat{L}$. Thus, we assume $\hat{\varrho} \in \bar{\mathcal{E}}$ and the state was not detected. In this case, the test needs to be modified, in other words, a different test operator $\hat{L}'$ must be used.

Experimental uncertainties further complicate this manner. Geometrically, an experimentally generated state is not a point in the operator space anymore, but rather an ellipsoid which extension is determined by experimental uncertainties

In this sense, a more rigorous description of the set $\mathcal{E}$ is needed. Entanglement detection needs to be classified by a quantifier Σ, the larger this quantifier for a certain state, the more reliably this quantum state can be detected as entangled. For entanglement witnesses, a suitable definition for Σ is

$$\Sigma = \left|\tilde{\Sigma}\right|, \tag{5.1}$$

with the signed significance

$$\tilde{\Sigma} = \frac{\mathrm{tr}\left(\hat{L}\hat{\rho}\right) - g_{\min}^{\mathcal{P}}}{\sigma(\hat{L})} \quad \text{or} \quad \tilde{\Sigma} = \frac{g_{\max}^{\mathcal{P}} - \mathrm{tr}\left(\hat{L}\hat{\rho}\right)}{\sigma(\hat{L})}, \tag{5.2}$$

where $\sigma(\hat{L})$ describes the uncertainty of the measurement of $\hat{L}$. That way, $\tilde{\Sigma}$ is an indicator for entanglement: $\tilde{\Sigma} < 0$ implies detected entanglement, whereas $\tilde{\Sigma} \geq 0$ renders an inconclusive test. In the case $\tilde{\Sigma} < 0$, the corresponding Σ quantifies the detection.
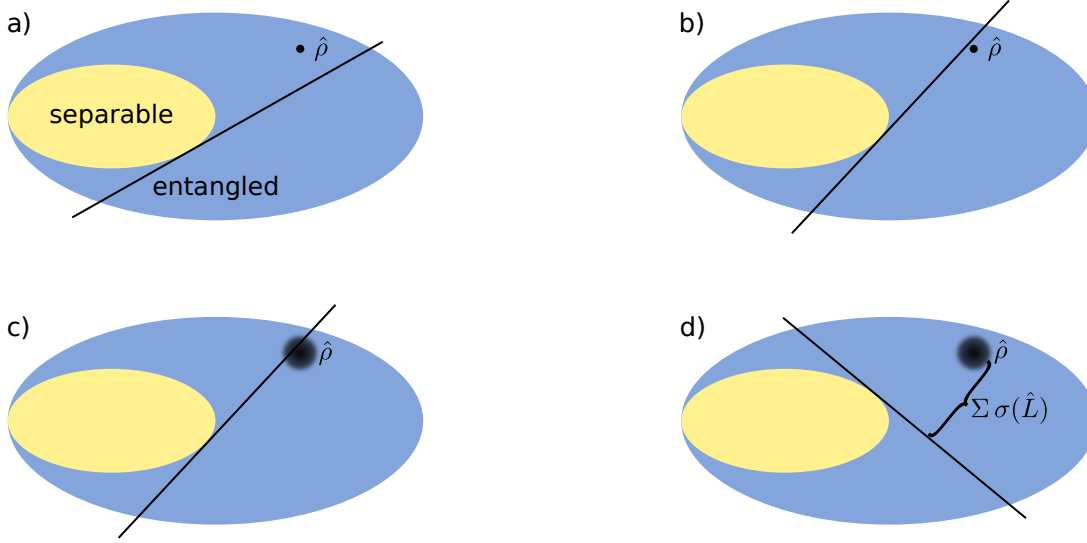
Figure 5.1: Witnessing of an entangled state $\hat{\rho}$. Part (a): The witness is unable to verify entanglement in $\hat{\rho}$. Part (b): The witness is able to verify entanglement in $\hat{\rho}$. Part (c): Experimental uncertainties (blurred area) of a quantum state require precaution. Part (d): Experimentally optimal witness for the particular state.

The optimization procedure is depicted in Fig. 5.1. For a given entangled state $\hat{\rho}$, witness operators, visualized by straight lines, are found that certify the state's entanglement. An optimization of $\tilde{\Sigma}$ takes different entanglement witnesses into account, each defining a hyperplane until $\tilde{\Sigma}$ is minimal; cf. Fig. 5.1 d).

5.2 Numerical Optimization: Genetic Algorithm

In order to find the best suitable entanglement witness operator, the global optimum of Eq. (5.2) needs to be found. The operator $\hat{L}$ for which the function is optimal will generate the best witness operator for the state. Generally, the signed significance cannot be explicitly expressed as a function of $\hat{L}$ since the separability eigenvalue is not a simple function of $\hat{L}$. Therefore, the optimization requires an algorithm that does not require explicit knowledge about the function. A further requirement is a global optimization rather than a local search.

The requested properties in an algorithm can be found in the *genetic algorithm*. A simple flowchart for this kind of algorithm is shown in Fig. 5.2. Genetic algorithms describe a class of algorithms that simulate the evolutionary trait survival of the fittest. Therefore, genetic algorithms follow a scheme rather than being expressed by pseudo code. The modules in yellow rectangles in Fig. 5.2 serve as placeholders for instructions in the genetic algorithm that can be chosen among a variety of possible approaches. A broad description of the working behavior of genetic algorithms will be given and individual steps shown in figures. For further details and analysis of possible implementation; see, e.g., [72].

Necessary input parameters are the *objective function* $f : \mathbb{C}^d \to \mathbb{R}$ whose optimal value f_{opt} is wanted and the dimension d of the parameter space the function resides in. As a first step, a number of random elements $X \in \mathbb{C}^d$ is selected and called *population*. In

analogy to natural selection—where only the best members in the population survive—a *selection* is performed on X. Since the optimization requires finding the minimum of f, the best elements in X are those with minimal fitness. A certain number of $x \in X$ is kept which fulfill a condition of their fitness, whereas those elements, that do not comply to the condition are deleted, cf. Fig. 5.3 (b). The set of members that are fulfilling the set condition are called *survivors*.

Among the survivors, *mating* is performed. Until every deleted element in the population has been replaced, two distinct survivors are selected based on a predetermined scheme and, by a given method, generate new population members called *children*, cf. Fig. 5.3. The last step is called *mutation*. Among the elements in X, a small subset is selected and randomly varied. All steps between and including the fitness evaluation and mutation are repeated until a criterion has been met and the algorithm concludes and returns the minimum value of the objective function.

5.3 Proof of Concept

As a prove of concept, the described method of finding the best entanglement witness for an entangled state will be applied to a Bell states. Therefore, the considered operator $\hat{\rho}$ will be a projector

$$\hat{\rho} = |\Psi\rangle\langle\Psi|, \quad \text{with} \quad |\Psi\rangle = \frac{1}{\sqrt{2}}\left(|0,0\rangle - |1,1\rangle\right). \tag{5.3}$$

For pure states, the best possible test operator $\hat{L}_{\mathrm{opt}}$ is the state itself. This statement will be numerically tested: The signed significance, Eq. (5.2), over operators $\hat{L}$ will be minimized using a genetic algorithm. In this case, the equation with the maximal separability eigenvalue will be used, as this separability eigenvalue can numerically be determined with
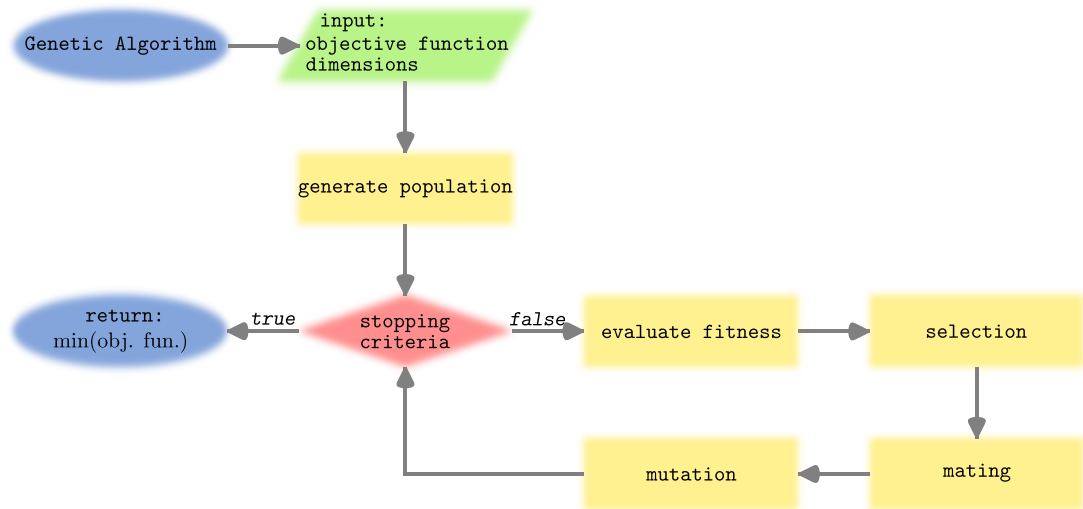

Figure 5.2: Flowchart of the genetic algorithm. Blue ellipses represent the entry and output points of the algorithm. The green parallelogram represents the input of the algorithm. The red diamond represents the while loop checking for the termination criterion. Yellow rectangles represent instructions that are the basis of the genetic algorithm.
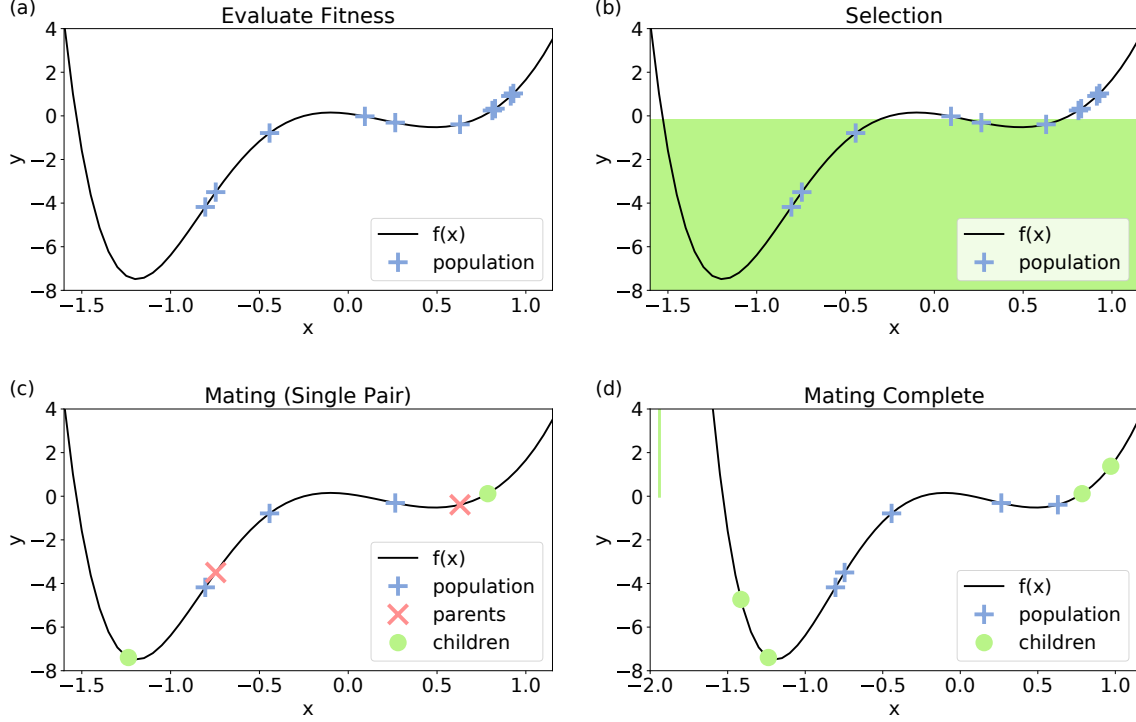
Figure 5.3:   Part (a): Evaluation of an exemplary fitness function for randomly chosen $x_i \in \mathbb{C}$ Part (b): Selection of elements. The green area in the selection figure displays values below the median of the fitness values. Part (c): Mating among a single pair of parents Part (d): Mating among all selected parents. The combination of two parents (red crosses) generates two children (green dots). Since a child was generated with $y \approx 52$, it cannot be displayed properly. Therefore, it is represented by a green line.

the SPI. Furthermore, it is assumed that $\sigma(\hat{L}) = 1$ as no experimental uncertainties are present. There is only a single nontrivial partition for which entanglement can be tested in the present bipartite case, thus the partition will not be explicitly stated.

The objective function to minimize is

$$\tilde{\Sigma} = g_{\max} - \mathrm{tr}\left(|\Psi\rangle\langle\Psi|\, \hat{L}\right). \tag{5.4}$$

Assuming $\hat{L}_{\mathrm{opt}} = |\Psi\rangle\langle\Psi|$ the goal of the optimization can be determined. For a Bell state, the maximal separability eigenvalue is $g_{\max} = 1/2$ and thus, the minimum for the signed significance is $\tilde{\Sigma}_{\mathrm{opt}} = -1/2$. This value will be used as a comparison for the numerical test. For a general test over all positive definite test operators, $\hat{L}$ can be decomposed as

$$\hat{L} = \lambda\hat{I} + \hat{M}\hat{M}^{\dagger}. \tag{5.5}$$

Here, $\hat{I}$ is the identity operator and $\hat{M}$ is a random operator acting on the compound Hilbert space the Bell state lies in.

The parameters for the implemented genetic algorithms are as follows: The population count is 250, survivors are selected as all members that have a fitness lower than the first quartile of all fitness values. Parents are selected by tournament selection and children generated by cross-over. The mutation probability is 10%. Figure 5.4 shows the minimal
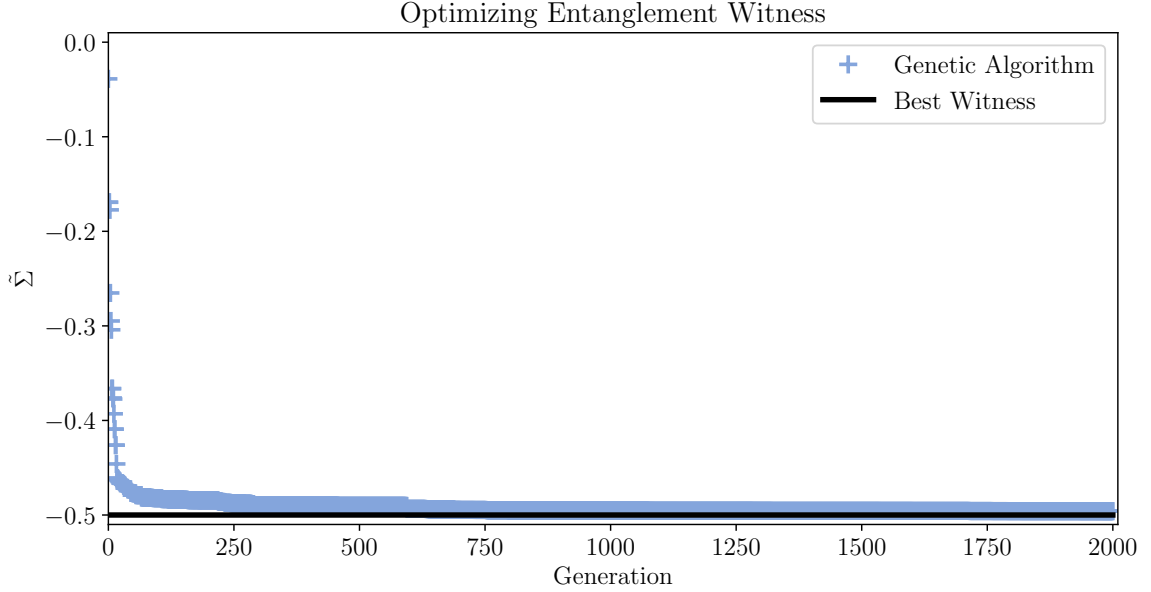
Figure 5.4: Optimization of constructed entanglement tests. During the run time of the genetic algorithm for optimizing the entanglement test quantifier, the value approaches the global minimum of $-1/2$. Note the rather large change in the first few generations while for longer run times the gain is lower.

values over all members of the population for each generation of the genetic algorithm. A comparison measure γ between the numerical best test operator $\hat{L}_N$ and the true best test operator (which is the state itself) $\hat{L}_{\text{opt}}$ is calculated with the Frobenius norm,

$$\gamma = \|\hat{L}_N - \hat{L}_{\text{opt}}\| = \text{tr}\left((\hat{L}_N - \hat{L}_{\text{opt}})(\hat{L}_N - \hat{L}_{\text{opt}})^{\dagger}\right) \approx 0.487 \cdot 10^{-3}. \tag{5.6}$$

The asymptotic approach of the fitness function of the genetic algorithm towards the optimal entanglement test quantifier in this example and the small difference between the true best test operator and the numerical solution, Eq. (5.6), are indicators for the functionality of the suggested approach.

5.4 Summary

In this chapter, a quantifier was introduced which takes its minimum for the best entanglement witness in regards to experimental data. A global optimization algorithm needs to be used to find this minimum. Such a minimizer is found in the genetic algorithm, an algorithm that simulates the natural evolution and finds a wide range in application from economics [73] to the design of space antennas [74].

By approximating the global minimum of the entanglement test quantifier, the best witness for a Bell state could be found. This serves as a proof of concept. In general, the proposed concept is applicable to arbitrary quantum states and serves as a background to numerical entanglement testing in highly complex quantum systems.

Application to Experiments

Gaussian states are a class of quantum states that are widely used in experiments. As they are continuous-variable states, the entanglement behavior can be controlled easier as opposed to discrete-variable states and states in multiple partitions can be generated, cf. [75–77]. Due to their large scale, Gaussian states are an interesting testing ground for entanglement tests as multiple partitions can be considered. This chapter focuses on the work in [G1, G2], where Gaussian states from experimental data were analyzed for entanglement. The data post processing, implementation of the entanglement test and analysis of results was performed by the candidate. The experiment and data extraction was performed by collaborators.

6.1 Gaussian Entanglement Tests

Gaussian states are quantum states that can be fully described by their covariance matrix. Consider a vector of quadrature operators

$$\hat{\xi} = (\hat{x}_1, \ldots, \hat{x}_N, \hat{p}_1, \ldots, \hat{p}_N)^T, \tag{6.1}$$

with the amplitude quadratures $\hat{x}_i$ and phase quadratures $\hat{p}_i$, acting on each individual Hilbert space in an N-fold compound Hilbert space $\mathcal{H}$. Then the covariance matrix $\boldsymbol{C}$, which contains all second moments of a state, can be written as $\boldsymbol{C}_{ij} = \langle \hat{\xi}_i \hat{\xi}_j + \hat{\xi}_j \hat{\xi}_i \rangle / 2 - \langle \hat{\xi}_i \rangle \langle \hat{\xi}_j \rangle$. As local displacements do not affect the entanglement of a quantum state, the covariance matrix is sufficient to describe the entanglement in Gaussian states.

In [G1], the most general entanglement test operator for Gaussian states was introduced as

$$\hat{L} = \sum_{i,j=1}^{2N} \boldsymbol{M}_{i,j} \hat{\xi}_i \hat{\xi}_j, \tag{6.2}$$

with a $2N \times 2N$ symmetric and positive definite matrix $\boldsymbol{M}$. It was shown in the supplemental material of [G1] that the minimal separability eigenvalue of this operator for a partition $\mathcal{P} = \mathcal{I}_1 : \ldots : \mathcal{I}_K$ is

$$g_{\mathcal{P}}^{\min} = \sum_{j=1}^{K} \sum_{k=1}^{|\mathcal{I}_j|} \lambda_k^{\mathcal{I}_j}, \tag{6.3}$$

where $|\mathcal{I}_j|$ is the cardinality of the subset $\mathcal{I}_j$ of the index set $\{1, \ldots, N\}$. The values $\lambda_k^{\mathcal{I}_j}$ are the symplectic eigenvalues of the sub matrix of $\boldsymbol{M}$ which has the row index and column index in $\mathcal{I}_j$. A symplectic decomposition is always possible for positive and positive definite matrices such as $\boldsymbol{M}$; see, e.g., [78]. According to Eq. (3.6), the minimal

separability eigenvalue for testing K-entanglement is, cf. [G2],

$$g_K^{\min} = \min_K \{g_{\mathcal{P}}^{\min} : |\mathcal{P}| = K\}. \tag{6.4}$$

6.2 Application to Data

An entanglement test for Gaussian states was performed on experimental data from the group of C. Fabre and N. Treps which was measured in their synchronously pumped optical parametric oscillator setup [77]. The most prominent examples that were tested are a six mode and a ten mode state. In total, the number of possible partitions of the index sets of the underlying compound Hilbert space can be calculated by the Bell-numbers, Eq. (2.1), and is $B_6 = 203$ and $B_{10} = 115\,975$, respectively. Referencing with Fig. 2.1, the index set of the modes have a rich structure in refinements. For both states, entanglement was tested for every possible partition. Additionally, the six mode state was also tested for all possible K-entanglement.

A numerical implementation based on Eq. (5.2) which defines a testing criterion based on a testing operator and its minimum separability eigenvalue was implemented. In the case of Gaussian states, this criterion can be rewritten in terms of the coefficient matrix $\boldsymbol{M}$ in Eq. (6.2) and the covariance matrix $\boldsymbol{C}$ of the Gaussian state since $\mathrm{tr}\left(\hat{\rho}\hat{L}\right) = \mathrm{Tr}\left(\boldsymbol{CM}\right)$. As there is no maximal separability eigenvalue for Gaussian type test operator (or rather they take the value ∞), the testing criterion for the minimal separability eigenvalue is considered,

$$\tilde{\Sigma} = \frac{\mathrm{Tr}\left(\boldsymbol{CM}\right) - g_{\chi}^{\min}}{\sigma(\boldsymbol{C})}. \tag{6.5}$$

The index χ of the separability eigenvalue either designates the partition $\mathcal{P}$ tested for entanglement or the value K for testing K-entanglement. This is precisely the signed significance which was introduced in [G1].

Using a genetic algorithm the entanglement test quantifier in Eq. (6.5) was minimized to find the best possible entanglement test. The results are shown in Fig. 6.1. For both states, entanglement was verified in every possible partition. Furthermore, $K > 2$-
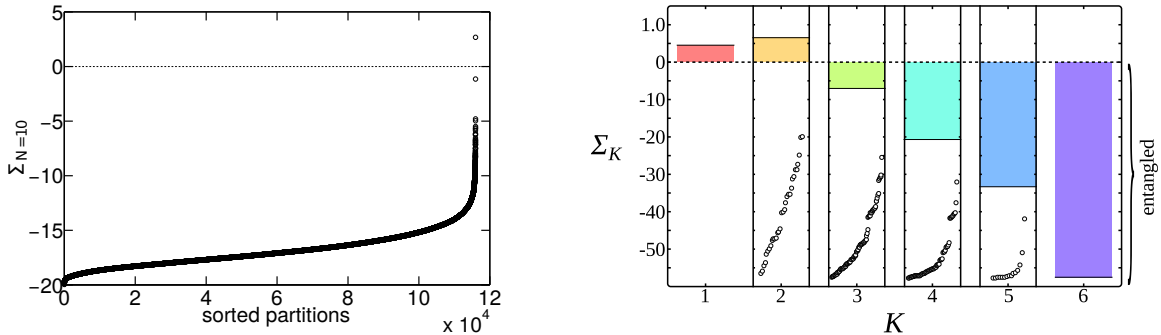

Figure 6.1: Results of entanglement test on Gaussian states. The left plot shows the results of the entanglement test on a ten mode state for every partition, cf. [G1]. The right plot shows the results of the entanglement test on a six mode state for every partition and K-entanglement, cf. [G2].

entanglement was verified in the six mode state. The latter phenomenon is a plausible cause in which a quantum state lies outside every set of separable states for individual partitions; yet when combining the partitions convexly, the state is within the resulting set.

Following the inheritance of separability and entanglement, entanglement in all possible partitions could have been verified by simply testing for bipartite entanglement for every bipartition. Similarly, if the six mode state was truly 2-entangled, every other form of tested entanglement would already have been verified. Yet, the results show that entanglement is not always present in every possible notion. Should an entanglement test fail for a partition, no conclusion can be found for the refined partitions. Therefore a test in the proposed fashion is favorable, as it can address all possible partitions easily.

6.3 Summary

This chapter describes testing of multipartite Gaussian entanglement using the newly introduced numerical approach. The presented results are the first test of entanglement with respect to every possible partition among the $115\,975$ partitions of a ten mode state. A generalization for testing K-entanglement enables to witness interesting properties of quantum states which imply the usefulness of such fine-grained methods. As a positive test on 2-entanglement sufficiently implies entanglement in every other notion, a negative test is unable to make any statement about the entanglement structure at all. The newly devised method on the other hand allows for addressing other notions as well and, therefore, the entanglement structure of such a state can still be uncovered.

The testing approach is not only a theoretical model but is readily applicable to experimental data, as shown in this chapter. Entanglement is verified with up to 60 standard deviations in the six mode example and with up to 20 standard deviations for the ten mode state. Calculation time may be further reduced if the interest lies in claiming entanglement and not finding the best possible entanglement test by aborting the genetic algorithm early. This calculation time can be further reduced for very low experimental uncertainties as this will scale the testing quantifier.

Conclusion

<div style="text-align:right">7</div>

7.1 Summary

In this work, numerical methods for witnessing multipartite entanglement were presented, which rely on a newly introduced algorithm (the SPI) and the application of a genetic algorithm. These techniques enable the practical detection of entanglement in highly complex multimode systems and are readily applicable to experimental data.

Different notions of entanglement have been explained, which result from the definition of entanglement as the absence of forms of multipartite separability. As separability needs to be defined with respect to a certain notion (different partitions, combination of separable sets), entanglement needs to be considered in a similar fashion. The different notions of entanglement and separability were put into relation and the concept of inheritance was explained.

In general, the definitions of entanglement can not be applied directly to test for its presence or absence. Therefore, entanglement criteria were introduced; the most prominently used are based on entanglement witnesses. The separability eigenvalue equations, propose a method which enables the analytic and numerical construction of entanglement witnesses. The numerical construction is achieved with the newly devised Separability Power Iteration.

Due to the witnesses defining a hyperplane in the operator space, there exist entangled states which are not detected by a specific (linear) witness. Therefore, multiple witnesses need to be constructed to detect entanglement in more states. Further considering experimental uncertainties in a measured quantum state, an entanglement testing quantifier was introduced whose minimization leads to the best possible entanglement witness in terms of experimental uncertainties for a given measured state. This testing quantifier has proven successful in uncovering entanglement in highly multimode quantum states and could address every single notion of entanglement in the considered states.

7.2 Discussion

The presented work combines numerical methods and the analytic construction of entanglement witness operators by means of the separability eigenvalue equations to introduce new methods for testing bipartite and, most importantly, multipartite entanglement. In principle, minimizing the introduced entanglement testing quantifier generates the best entanglement witness for a given experimental quantum state. This quantifier solely depends on a testing operator and its (maximal or minimal) separability eigenvalue. Thus, the verification of entanglement is shifted to finding a suitable testing operator. It was shown that a genetic algorithm is able to perform the required minimization and entanglement could be verified for highly multimode states. In this case, the minimal separability eigenvalue was known analytically. In the general case, this is not possible. Yet, with the introduced Separability Power Iteration, a numerical solution for the maximal sepa-

rability eigenvalue of a testing operator can be found. On paper, this would mean, that minimizing the entanglement testing quantifier can verify entanglement in any entangled quantum state.

Yet in practice, this is not quite possible. The convergence of the SPI to the maximal separability eigenvalue is largely dependent on the chosen starting vector. For a randomly chosen starting vector, the SPI would generally converge to a local maximum. To guarantee convergence to the global maximum, the starting vectors are chosen as basis elements of the operator basis of the underlying Hilbert space. This set of starting vectors grows exponentially in the number of modes and, therefore, the SPI converges slower for large systems. In combination with having to run the SPI for multiple testing operators in every generation of the genetic algorithm, this will increase the computation time to an impracticable amount. For small quantum systems, this general approach is viable on the other hand and performs well as shown in the Bell-state example.

The work in this thesis shows an interdisciplinary nature. The underlying concept of entanglement is based in physics. The numerical analysis and global minimization required methods from computer science in which parallel processes needed to be carefully evaluated. The rigorous mathematical proof of the SPI is placed in numerical mathematics. It has been shown that the introduced method is applicable to experimental data, thus not just making it a theoretical notion but very much a method applicable for experimentalists.

7.3 Outlook

In its implementation, the SPI serves a wider usage than finding the maximal separability eigenvalue and can be used to find solutions to related problems. Let us name a few examples: In mathematics a related problem is posed by finding positive polynomials [79]. In quantum optics several problems are of the same algebraic structure as the separability eigenvalue equations [19, 80–82]. Algorithms similar to the SPI in structure are applicable to finding solutions to these problems.

A publication considering more general description and further extension of the content of Chapter 2 is in preparation at the time of writing the thesis. The publication will cover different concepts and notion of entanglement and will give an overview about different classes of entangled states.

Entanglement tests for experimental states based on the suggested approaches have been performed on Gaussian states only at the point of writing this thesis, cf. Chapter 6. The combination of the SPI and a genetic algorithm presented here should be applied to experimental data as well. For this, a complete reconstruction of a density operator is necessary which is plausible for small quantum systems. A reconstruction using a measured Wigner function of a photon-subtracted Gaussian state is being considered at the point of writing the thesis. This will be the first implementation of the proposed coupling of the SPI with a genetic algorithm to experimental data and is a straightforward extension to the small scale Bell state example in this thesis.

All derivations for the numerical approach are independent of the actual Hilbert space structure. This has been done on purpose to keep the method as widely accessible as possible. An application is, in principle, possible to any given density operator of a quantum state.

Bibliography

Candidate's Publications

This part of the bibliography contains my publications in refereed journals during my PhD studies. Throughout the work, they are referenced in the style [G#] to set them apart from external references.

[G1] S. Gerke, J. Sperling, W. Vogel, Y. Cai, J. Roslund, N. Treps, and C. Fabre, *Full Multipartite Entanglement of Frequency-Comb Gaussian States*, Physical Review Letters **114**, 050501 (2015).

   The candidate's work consisted of preprocessing the covariance matrix by adjusting the data to a form suitable for the entanglement test. A general derivation of the separability eigenvalue for Gaussian type operators was performed with the cosupervisor. Furthermore, the genetic algorithm was implemented and the resulting data prepared and analysed.

[G2] S. Gerke, J. Sperling, W. Vogel, Y. Cai, J. Roslund, N. Treps, and C. Fabre, *Multipartite Entanglement of a Two-Separable State*, Physical Review Letters **117**, 110502 (2016).

   The candidate's work consisted of preprocessing the covariance matrix by adjusting the data to a form suitable for the entanglement test. Furthermore, the genetic algorithm was implemented and the resulting data prepared and analysed. The highlighted case of a six mode state, which two-separable yet entangled in every other notion was selected specifically among the tested data. This led to an interesting phenomenom that was discussed by the cadidate.

[G3] S. Gerke, W. Vogel, and J. Sperling, *Numerical Construction of Multipartite Entanglement Witnesses*, Physical Review X **8**, 031047 (2018).

   The candidate deviced the introduced algorithm in collaboration with his supervisor and cosupervisor. The full implementation was done by the candidate, including error analysis and optimization in regards to runtime and accuracy. Example states to show the usability of the algorithm were selected by the candidate. The candidate implemented a benchmark to showcase the speed of the algorithm.

Literature

[1]   A. Einstein, B. Podolsky, and N. Rosen, *Can Quantum-Mechanical Description of Physical Reality Be Considered Complete?*, Physical Review **47**, 777 (1935).

[2]   E. Schrödinger, *Die Gegenwärtige Situation in der Quantenmechanik*, Naturwissenschaften **23**, 807 (1935).

[3]   E. Schrödinger, *Die Gegenwärtige Situation in der Quantenmechanik*, Naturwissenschaften **23**, 823 (1935).

[4]   E. Schrödinger, *Die Gegenwärtige Situation in der Quantenmechanik*, Naturwissenschaften **23**, 844 (1935).

[5]   D. Bohm, *A Suggested Interpretation of the Quantum Theory in Terms of "Hidden" Variables. I*, Physical Review **85**, 166 (1952).

[6]   J. S. Bell, *On the Einstein Podolsky Rosen Paradox*, Physics **1**, 195 (1964).

[7]   S. J. Freedman and J. F. Clauser, *Experimental Test of Local Hidden-Variable Theories*, Physical Review Letters **28**, 938 (1972).

[8]   A. Aspect, P. Grangier, and G. Roger, *Experimental Realization of Einstein-Podolsky-Rosen-Bohm Gedankenexperiment: A New Violation of Bell's Inequalities*, Physical Review Letters **49**, 91 (1982).

[9]   B. Hensen, H. Bernien, A. E. Dréau, A. Reiserer, N. Kalb, M. S. Blok, J. Ruitenberg, R. F. L. Vermeulen, R. N. Schouten, C. Abellán, W. Amaya, V. Pruneri, M. W. Mitchell, M. Markham, D. J. Twitchen, D. Elkouss, S. Wehner, T. H. Taminiau, and R. Hanson, *Loophole-Free Bell Inequality Violation Using Electron Spins Separated by 1.3 Kilometres*, Nature **526**, 682 (2015).

[10] L. K. Shalm, E. Meyer-Scott, B. G. Christensen, P. Bierhorst, M. A. Wayne, M. J. Stevens, T. Gerrits, S. Glancy, D. R. Hamel, M. S. Allman, K. J. Coakley, S. D. Dyer, C. Hodge, A. E. Lita, V. B. Verma, C. Lambrocco, E. Tortorici, A. L. Migdall, Y. Zhang, D. R. Kumor, W. H. Farr, F. Marsili, M. D. Shaw, J. A. Stern, C. Abellán, W. Amaya, V. Pruneri, T. Jennewein, M. W. Mitchell, P. G. Kwiat, J. C. Bienfang, R. P. Mirin, E. Knill, and S. W. Nam, *Strong Loophole-Free Test of Local Realism*, Physical Review Letters **115**, 250402 (2015).

[11] M. Giustina, M. A. M. Versteegh, S. Wengerowsky, J. Handsteiner, A. Hochrainer, K. Phelan, F. Steinlechner, J. Kofler, J.-Å. Larsson, C. Abellán, W. Amaya, V. Pruneri, M. W. Mitchell, J. Beyer, T. Gerrits, A. E. Lita, L. K. Shalm, S. W. Nam, T. Scheidl, R. Ursin, B. Wittmann, and A. Zeilinger, *Significant-Loophole-Free Test of Bell's Theorem with Entangled Photons*, Physical Review Letters **115**, 250401 (2015).

[12] C. H. Bennett and G. Brassard, *Quantum Cryptography: Public Key Distribution and Coin Tossing*, in *Proceedings of the IEEE International Conference on Computers, Systems and Signal Processing, Bangalore, India, 1984* (IEEE Press, New York, 1984).

[13] A. K. Ekert, *Quantum Cryptography Based on Bell's Theorem*, Physical Review Letters **67**, 661 (1991).

[14] C. H. Bennett and S. J. Wiesner, *Communication Via One- and Two-Particle Operators on Einstein-Podolsky-Rosen States*, Physical Review Letters **69**, 2881 (1992).

[15] C. H. Bennett, G. Brassard, C. Crépeau, R. Jozsa, A. Peres, and W. K. Wootters, *Teleporting an Unknown Quantum State Via Dual Classical and Einstein-Podolsky-Rosen Channels*, Physical Review Letters **70**, 1895 (1993).

[16] M. A. Nielsen and I. L. Chuang, *Quantum Computation and Quantum Information* (Cambridge University Press, Cambridge, England, 2000).

[17] M. Huber and J. I. de Vicente, *Structure of Multidimensional Entanglement in Multipartite Systems*, Physical Review Letters **110**, 030501 (2013).

[18] F. Levi and F. Mintert, *Hierarchies of Multipartite Entanglement*, Physical Review Letters **110**, 150402 (2013).

[19] F. Shahandeh, J. Sperling, and W. Vogel, *Structural Quantification of Entanglement*, Physical Review Letters **113**, 260502 (2014).

[20] B. M. Terhal, *Bell Inequalities and the Separability Criterion*, Physics Letters A **271**, 319 (2000).

[21] R. Horodecki, P. Horodecki, M. Horodecki, and K. Horodecki, *Quantum Entanglement*, Review of Modern Physics **81**, 865 (2009).

[22] O. Gühne and G. Tóth, *Entanglement Detection*, Physics Reports **474**, 1 (2009).

[23] A. Peres, *Separability Criterion for Density Matrices*, Physical Review Letters **77**, 1413 (1996).

[24] M. Horodecki, P. Horodecki, and R. Horodecki, *Separability of Mixed States: Necessary and Sufficient Conditions*, Physics Letters A **223**, 1 (1996).

[25] L.-M. Duan, G. Giedke, J. I. Cirac, and P. Zoller, *Inseparability Criterion for Continuous Variable Systems*, Physical Review Letters **84**, 2722 (2000).

[26] R. Simon, *Peres-Horodecki Separability Criterion for Continuous Variable Systems*, Physical Review Letters **84**, 2726 (2000).

[27] M. Horodecki, P. Horodecki, and R. Horodecki, *Separability of n-Particle Mixed States: Necessary and Sufficient Conditions in Terms of Linear Maps*, Physics Letters A **283**, 1 (2001).

[28] G. Tóth, *Entanglement Witnesses in Spin Models*, Physical Review A **71**, 010301 (2005).

[29] A. Jamiołkowski, *Linear Transformations Which Preserve Trace and Positive Semidefiniteness of Operators*, Reports on Mathematical Physics **3**, 275 (1972).

[30] M.-D. Choi, *Positive Linear Maps on C*-Algebras*, Canadian Journal of Mathematics **24**, 520 (1972).

[31] M.-D. Choi, *Completely Positive Linear Maps on Complex Matrices*, Linear Algebra and its Applications **10**, 285 (1975).

[32] O. Gühne, P. Hyllus, D. Bruss, A. Ekert, M. Lewenstein, C. Macchiavello, and A. Sanpera, *Experimental Detection of Entanglement via Witness Operators and Local Measurements*, Journal of Modern Optics **50**, 1079 (2003).

[33] M. Bourennane, M. Eibl, C. Kurtsiefer, S. Gaertner, H. Weinfurter, O. Gühne, P. Hyllus, D. Bruß, M. Lewenstein, and A. Sanpera, *Experimental Detection of Multipartite Entanglement Using Witness Operators*, Physical Review Letters **92**, 087902 (2004).

[34] G. Tóth and O. Gühne, *Detecting Genuine Multipartite Entanglement with Two Local Measurements*, Physical Review Letters **94**, 060501 (2005).

[35] O. Gühne and N. Lütkenhaus, *Nonlinear Entanglement Witnesses*, Physical Review Letters **96**, 170502 (2006).

[36] P. Hyllus and J. Eisert, *Optimal Entanglement Witnesses for Continuous-Variable Systems*, New Journal of Physics **8**, 51 (2006).

[37] G. Tóth and O. Gühne, *Entanglement Detection in the Stabilizer Formalism*, Physical Review A **72**, 022340 (2005).

[38] H. Häffner, Hänsel, W., Roos, C. F., J. Benhelm, D. Chek-al-kar, M. Chwalla, T. Körber, U. D. Rapol, M. Riebe, P. O. Schmidt, C. Becher, O. Gühne, W. Dür, and R. Blatt, *Scalable Multiparticle Entanglement of Trapped Ions*, Nature **438**, 643 (2005).

[39] O. Morin, J.-D. Bancal, M. Ho, P. Sekatski, V. D'Auria, N. Gisin, J. Laurat, and N. Sangouard, *Witnessing Trustworthy Single-Photon Entanglement with Local Homodyne Measurements*, Physical Review Letters **110**, 130401 (2013).

[40] P. van Loock and S. L. Braunstein, *Multipartite Entanglement for Continuous Variables: A Quantum Teleportation Network*, Physical Review Letters **84**, 3482 (2000).

[41] M. Borrelli, M. Rossi, C. Macchiavello, and S. Maniscalco, *Witnessing Entanglement in Hybrid Systems*, Physical Review A **90**, 020301 (2014).

[42] J. Sperling and W. Vogel, *Necessary and Sufficient Conditions for Bipartite Entanglement*, Physical Review A **79**, 022318 (2009).

[43] J. Sperling and W. Vogel, *Multipartite Entanglement Witnesses*, Physical Review Letters **111**, 110503 (2013).

[44] S. Pironio, A. Acín, N. Brunner, N. Gisin, S. Massar, and V. Scarani, *Device-Independent Quantum Key Distribution Secure Against Collective Attacks*, New Journal of Physics **11**, 045021 (2009).

[45] R. Gallego, N. Brunner, C. Hadley, and A. Acín, *Device-Independent Tests of Classical and Quantum Dimensions*, Physical Review Letters **105**, 230501 (2010).

[46] O. Nieto-Silleras, S. Pironio, and J. Silman, *Using Complete Measurement Statistics for Optimal Device-Independent Randomness Evaluation*, New Journal of Physics **16**, 013035 (2014).

[47] N. Brunner, D. Cavalcanti, S. Pironio, V. Scarani, and S. Wehner, *Bell Nonlocality*, Review of Modern Physics **86**, 419 (2014).

[48] V. Vedral, M. B. Plenio, M. A. Rippin, and P. L. Knight, *Quantifying Entanglement*, Physical Review Letters **78**, 2275 (1997).

[49] J. Eisert and M. B. Plenio, *A Comparison of Entanglement Measures*, Journal of Modern Optics **46**, 145 (1999).

[50] J. Sperling and W. Vogel, *The Schmidt Number as a Universal Entanglement Measure*, Physica Scripta **83**, 045002 (2011).

[51] W. Vogel and J. Sperling, *Unified Quantification of Nonclassicality and Entanglement*, Physical Review A **89**, 052302 (2014).

[52] E. Agudelo, J. Sperling, and W. Vogel, *Quasiprobabilities for Multipartite Quantum Correlations of Light*, Physical Review A **87**, 033811 (2013).

[53] H. Ollivier and W. H. Zurek, *Quantum Discord: A Measure of the Quantumness of Correlations*, Physical Review Letters **88**, 017901 (2001).

[54] L. Henderson and V. Vedral, *Classical, Quantum and Total Correlations*, Journal of Physics A: Mathematical and General **34**, 6899 (2001).

[55] M. Perarnau-Llobet, K. V. Hovhannisyan, M. Huber, P. Skrzypczyk, N. Brunner, and A. Acín, *Extractable Work from Correlations*, Physical Review X **5**, 041011 (2015).

[56] J. H. Holland, *Adaptation in Natural and Artificial Systems: An Introductory Analysis with Applications to Biology, Control and Artificial Intelligence* (The University of Michigan Press, Ann Arbor, Michigan, 1975).

[57] L. Gurvits, *Classical Deterministic Complexity of Edmonds' Problem and Quantum Entanglement*, in STOC '03 Proceedings of the thirty-fifth annual acm symposium on theory of computing, San Diego, CA, USA, 2003 (ACM, 2003).

[58] L. M. Ioannou, *Computational Complexity of the Quantum Separability Problem*, Quantum Information & Computation **7**, 335 (2007).

[59] R. F. Werner, *Quantum States With Einstein-Podolsky-Rosen Correlations Admitting a Hidden-Variable Model*, Physical Review A **40**, 4277 (1989).

[60] M. Seevinck and G. Svetlichny, *Bell-Type Inequalities for Partial Separability in n-Particle Systems and Quantum Mechanical Violations*, Physical Review Letters **89**, 060401 (2002).

[61] B. C. Hiesmayr, M. Huber, and P. Krammer, *Two Computable Sets of Multipartite Entanglement Measures*, Physical Review A **79**, 062308 (2009).

[62] M. Lewenstein, B. Kraus, J. I. Cirac, and P. Horodecki, *Optimization of Entanglement Witnesses*, Physical Review A **62**, 052310 (2000).

[63] H. H. Schaefer and M. P. Wolff, *Topological Vector Spaces*, Second Edition (Springer Science & Business Media, New York, New York, 1999).

[64] J. Sperling and W. Vogel, *Entanglement Quasiprobabilities of Squeezed Light*, New Journal of Physics **14**, 055026 (2012).

[65] F. Shahandeh, J. Sperling, and W. Vogel, *Operational Gaussian Schmidt-Number Witnesses*, Physical Review A **88**, 062323 (2013).

[66] G. H. Golub and C. F. Van Loan, *Matrix Computations*, Third (The Johns Hopkins University Press, 1996).

[67] L. Vandenberghe and S. Boyd, *Semidefinite Programming*, SIAM Review **38**, 49 (1996).

[68] E. M. Rains, *A Semidefinite Program for Distillable Entanglement*, IEEE Transactions on Information Theory **47**, 2921 (2001).

[69] K. Audenaert and B. De Moor, *Optimizing Completely Positive Maps Using Semidefinite Programming*, Physical Review A **65**, 030302 (2002).

[70] F. G. S. L. Brandão and R. O. Vianna, *Robust Semidefinite Programming Approach to the Separability Problem*, Physical Review A **70**, 062309 (2004).

[71] A. C. Doherty, P. A. Parrilo, and F. M. Spedalieri, *Detecting Multipartite Entanglement*, Physical Review A **71**, 032333 (2005).

[72] R. L. Haupt and S. E. Haupt, *Practical Genetic Algorithms*, Second Edition (John Wiley & Sons, Hoboken, New Jersey, 2004).

[73] J. Sadeghi, S. T. A. Niaki, M. R. Malekian, and S. Sadeghi, *Optimising Multi-Item Economic Production Quantity Model with Trapezoidal Fuzzy Demand and Backordering: Two Tuned Meta-Heuristics*, European Journal of Industrial Engineering **10**, 170 (2016).

[74] G. Hornby, A. Globus, D. Linden, and J. Lohn, *Automated Antenna Design with Evolutionary Algorithms*, in *Collection of technical papers - space 2006 conference, San Jose, California, USA, 2006* (American Institute of Aeronautics and Astronautics, 2006).

[75] S. Yokoyama, R. Ukai, S. C. Armstrong, C. Sornphiphatphong, T. Kaji, S. Suzuki, J.-i. Yoshikawa, H. Yonezawa, N. C. Menicucci, and A. Furusawa, *Ultra-Large-Scale Continuous-Variable Cluster States Multiplexed in the Time Domain*, Nature Photonics **7**, 982 (2013).

[76] M. Chen, N. C. Menicucci, and O. Pfister, *Experimental Realization of Multipartite Entanglement of 60 Modes of a Quantum Optical Frequency Comb*, Physical Review Letters **112**, 120505 (2014).

[77] J. Roslund, R. M. de Araújo, S. Jiang, C. Fabre, and N. Treps, *Wavelength-Multiplexed Quantum Networks With Ultrafast Frequency Combs*, Nature Photonics **8**, 109 (2014).

[78] R. Simon, S. Chaturvedi, and V. Srinivasan, *Congruences and Canonical Forms for a Positive Matrix: Application to the Schweinler–Wigner Extremum Principle*, Journal of Mathematical Physics **40**, 3632 (1999).

[79] N. K. Bose, *Multivariate Polynomial Positivity Test Efficiency Improvement*, Proceedings of the IEEE **67**, 1443 (1979).

[80] A. Reusch, J. Sperling, and W. Vogel, *Entanglement Witnesses for Indistinguishable Particles*, Physical Review A **91**, 042324 (2015).

[81] J. Sperling and I. A. Walmsley, *Entanglement in Macroscopic Systems*, Physical Review A **95**, 062116 (2017).

[82] J. Sperling and I. A. Walmsley, *Separable and Inseparable Quantum Trajectories*, Physical Review Letters **119**, 170401 (2017).

Appendix

Candidate's Publications

Full Multipartite Entanglement of Frequency-Comb Gaussian States

S. Gerke,[1,*] J. Sperling,[1] W. Vogel,[1] Y. Cai,[2] J. Roslund,[2] N. Treps,[2] and C. Fabre[2]

[1]*Arbeitsgruppe Theoretische Quantenoptik, Institut für Physik, Universität Rostock, D-18051 Rostock, Germany*
[2]*Laboratoire Kastler Brossel, Sorbonne Universités—UPMC, École Normale Supérieure,*
Collège de France, CNRS, 4 place Jussieu, 75252 Paris, France

An analysis is conducted of the multipartite entanglement for Gaussian states generated by the parametric down-conversion of a femtosecond frequency comb. Using a recently introduced method for constructing optimal entanglement criteria, a family of tests is formulated for mode decompositions that extends beyond the traditional bipartition analyses. A numerical optimization over this family is performed to achieve maximal significance of entanglement verification. For experimentally prepared 4-, 6-, and 10-mode states, full entanglement is certified for all of the 14, 202, and 115 974 possible nontrivial partitions, respectively.

Introduction.—One of the most fundamental concepts in quantum physics is entanglement [1–3]. This property plays a central role in a host of quantum technologies, including metrology, imaging, communication, and quantum information processing [4–6]. Protocols in each of these domains rely upon the existence of nonclassical correlations among a multitude of subsystems within a multimode state [7–9]. As such, reliable, readily implementable, and versatile means of characterizing entanglement are essential for assessing the utility of certain states as well as understanding the fundamental physics underlying quantum interactions.

One method for identifying entanglement is formulated in terms of positive—but not completely positive—maps. The most prominent example of such a map is the partial transposition (PT) [10]. For bipartite Gaussian states, which are completely characterized by the covariance matrix, it has been shown that the PT criterion is necessary and sufficient to identify entanglement [11,12]. In the multipartite case, however, the PT criteria can only diagnose entanglement among bipartitions. Moreover, bound entangled Gaussian states are known to exist whose entanglement cannot be detected with the PT criterion. Such states have been formulated in theory and also realized in experiments [13,14]. Additionally, a number of moment-based entanglement probes have been successfully deployed to characterize entanglement, e.g., Refs. [15–24].

These criteria have been enormously successful at experimentally diagnosing entanglement among various beams [25,26] or among different parties of a multimode beam [27,28]. Alternatively, several studies have acquired the covariance matrix for a multidimensional state, which enables implementation of the PT criterion as a means for examining the nonclassical correlations among multiple beams [29,30]. In each of these situations, however, the employed methods restrict multipartite dynamics to the set of all possible bipartite state divisions.

Another well-established method for identifying entanglement is formulated in terms of entanglement witnesses [31,32]. In particular, the *separability eigenvalue equations* have recently been introduced as a method for constructing optimal witnesses [33,34]. The solutions of these coupled equations yield powerful entanglement assessments not only for bipartite divisions but also for high-order multipartite divisions of discrete and continuous variable quantum systems.

This Letter formulates entanglement conditions for multimode Gaussian states and subsequently demonstrates their application on an experimentally realized quantum ultrafast frequency comb. This quantum state, which is generated by the parametric down-conversion of a classical frequency comb, was recently shown to exhibit bipartite entanglement among its underlying frequency bands [35]. The covariance matrix for this high-dimensional quantum object has been measured, which renders it a unique test bed for exploring novel multipartite entanglement metrics. Importantly, we will show in this Letter that the criteria developed from the separability eigenvalue equations are able to examine nonclassical aspects of the frequency comb not feasible with strictly bipartite methods. Within this class of criteria, the significance of the verified entanglement is optimized with a genetic algorithm, which allows us to fully verify the entanglement present in highly complex multiparty quantum systems. For the 10-mode system considered here, entanglement is certified for each of the 115 974 possible nontrivial mode partitions.

Gaussian states and mode decompositions.—Gaussian states are described by a Gaussian characteristic function on a multimode phase space (for an introduction, see, e.g., Ref. [36]). The amplitude and phase quadratures of individual modes are denoted by $\hat{x}_k$ and $\hat{p}_k$, respectively, and a vector of quadratures is defined as

$$\hat{\xi} = (\hat{x}_1, \ldots, \hat{x}_N, \hat{p}_1, \ldots, \hat{p}_N)^{\mathrm{T}}. \qquad (1)$$

The covariance matrix C is then specified by its entries

$$C^{ij} = \frac{1}{2}\langle \hat{\xi}_i \hat{\xi}_j + \hat{\xi}_j \hat{\xi}_i \rangle - \langle \hat{\xi}_i \rangle \langle \hat{\xi}_j \rangle. \qquad (2)$$

First-order moments are irrelevant for entanglement since local unitary displacement operations may be applied to yield $\langle \hat{\xi} \rangle = 0$. Thus, without loss of generality, we can assume that all of the information for a Gaussian state is contained in its second-order moments.

The initial set of N orthonormal modes, on which the multimode quantum state is defined, can be decomposed into many different partitions, each one distributing the N modes in K different and complementary subsystems $\mathcal{I}_1 : \ldots : \mathcal{I}_K$, with K being any integer between 1 and N. A quantum state is considered entangled with respect to a given mode partitioning if one is not able to write it as a statistical mixture of product density matrices $\hat{\varrho}_1 \otimes \ldots \otimes \hat{\varrho}_K$, where $\hat{\varrho}_j$ describes a quantum state in subsystem $\mathcal{I}_j$ for $j = 1, \ldots, K$. The case $K = 2$ consists of $2^{N-1} - 1$ mode bipartitions, which are the only ones addressed by the PT criterion. However, even if entanglement does not exist among certain bipartitions, it may be present in higher-order partitions, i.e., $K > 2$. Considering that the total number of state partitions is given by the Bell number and increases rapidly as a function of N [37], the PT criterion addresses only a very small subset of the rich variety of possible partitionings.

Optimal entanglement tests.—The multipartite entanglement of a quantum state $\hat{\rho}$ may be probed with the use of a general Hermitian operator $\hat{L}$ [33]. In particular, the state under question is entangled with respect to a given K partition if and only if it may be shown that

$$\text{tr}(\hat{L}\hat{\rho}) < g^{\min}_{\mathcal{I}_1 : \ldots : \mathcal{I}_K}, \qquad (3)$$

where $g^{\min}_{\mathcal{I}_1 : \ldots : \mathcal{I}_K}$ is the minimum expectation value of $\hat{L}$ among all separable states of the K partition. It was established in Ref. [33] that this minimization problem can be solved with a set of coupled eigenvalue equations, denoted as separability eigenvalue equations. The resulting minimal separability eigenvalue is identical to $g^{\min}_{\mathcal{I}_1 : \ldots : \mathcal{I}_K}$.

The most general form of the operator $\hat{L}$ for continuous variable Gaussian states is given as $\hat{L} = \sum_{i,j}(M^{ji}_{xx}\hat{x}_i \hat{x}_j + M^{ji}_{px}\hat{p}_i \hat{x}_j + M^{ji}_{xp}\hat{x}_i \hat{p}_j + M^{ji}_{pp}\hat{p}_i \hat{p}_j)$, in which the coefficients of M are freely adjustable. Accordingly, attention may be restricted to the state's covariance matrix. Correlations between the amplitude and phase quadratures are negligible for the presently studied states, which allows the test operator $\hat{L}$ to be cast as

$$\hat{L} = \text{Tr}(M\hat{\xi}\hat{\xi}^{\text{T}}), \quad \text{with}$$

$$M = \begin{pmatrix} M_{xx} & 0 \\ 0 & M_{pp} \end{pmatrix} = M^{\text{T}} > 0, \qquad (4)$$

where M_{xx} and M_{pp} are coefficient matrices of the same dimensionality as the corresponding state covariance matrix, and the indices xx and pp refer to amplitude-amplitude and phase-phase correlations, respectively. The expectation value of this test operator readily follows and is written as [38]

$$\langle \hat{L} \rangle = \text{tr}(\hat{L}\hat{\rho}) = \text{Tr}(MC). \qquad (5)$$

Likewise, the minimal separability eigenvalue $g^{\min}_{\mathcal{I}_1 : \ldots : \mathcal{I}_K}$ for operators of this form has been derived in Ref. [33] and reads as

$$g^{\min}_{\mathcal{I}_1 : \ldots : \mathcal{I}_K} = \sum_{k=1}^{K} \text{Tr}_{\mathcal{I}_k}[M^{1/2}_{pp,\mathcal{I}_k} M_{xx,\mathcal{I}_k} M^{1/2}_{pp,\mathcal{I}_k}]^{1/2}, \qquad (6)$$

where $M_{\mathcal{I}_K}$ are the submatrices of M that contain only the rows and columns of the modes within $\mathcal{I}_K$. The solution for general Gaussian test operators is given in Ref. [39].

A partition's entanglement is characterized in terms of its statistical significance Σ, which compares the difference between the expectation value $\langle \hat{L} \rangle$ and its separable bound $g^{\min}_{\mathcal{I}_1 : \ldots : \mathcal{I}_K}$ to the experimental standard deviation $\sigma(L)$:

$$\Sigma = \frac{\langle \hat{L} \rangle - g^{\min}_{\mathcal{I}_1 : \ldots : \mathcal{I}_K}}{\sigma(L)}, \qquad (7)$$

which is the considered entanglement metric. The experimental error $\sigma(L)$ is determined through error propagation of $\langle \hat{L} \rangle$ and yields

$$\sigma(L) = \sqrt{\sum_{i,j=1}^{N}([M^{ij}_{xx}]^2[\sigma(C^{ji}_{xx})]^2 + [M^{ij}_{pp}]^2[\sigma(C^{ji}_{pp})]^2)}, \qquad (8)$$

where $\sigma(C^{ji}_{xx})$ and $\sigma(C^{ji}_{pp})$ are the measured errors corresponding to the covariance elements C^{ji}_{xx} and C^{ji}_{pp}, respectively. A partition is considered to be entangled if $\Sigma < 0$, and the statistical significance of its nonseparability is assessed with $|\Sigma|$. The coefficient matrix M may be freely tuned in order to maximize the significance of each partition, $\Sigma \to \Sigma_{\min} < 0$. This optimization is achieved with a *genetic algorithm* (see Refs. [39,40] for details).

Experimental realization.—Femtosecond frequency combs contain upwards of $\sim 10^5$ individual frequency components, and the simultaneous down-conversion of all of these frequencies in a nonlinear crystal inserted in an optical cavity initiates a network of frequency correlations that extends across the width of the resultant comb [43]. The laser source utilized to create the entangled comb is a titanium:sapphire mode-locked oscillator that delivers ~ 6 nm FWHM pulses (~ 140 fs) centered at 795 nm with a repetition rate of 76 MHz. This pulse train is frequency doubled, which serves to pump a below-threshold optical

TABLE I. The highest supermode squeezing (sqz.) and anti-squeezing levels of the considered 4-, 6-, and 10-mode quantum comb states. All of the noise levels are specified in decibels (dB).

4 modes		6 modes		10 modes	
Sqz.	Anti-sqz.	Sqz.	Anti-sqz.	Sqz.	Anti-sqz.
−5.1 dB	7.1 dB	−2.6 dB	3.0 dB	−3.7 dB	5.8 dB

parametric oscillator (OPO) containing a 2 mm BIBO crystal [44]. The state exiting the OPO is analyzed with homodyne detection, in which the spectral composition of the local oscillator (LO) is modified with an ultrafast pulse shaper capable of independent amplitude and phase modulation [45].

The LO spectrum is partitioned in either 4, 6, or 10 bands of equal energy. By scanning the relative phase between the down-converted comb and the LO, the x and p quadrature noises are measured from the state projected onto the spectral composition of the LO mode. The quadrature noises are then recorded for each spectral region as well as all possible pairs of regions. Upon doing so, a covariance matrix is assembled that furnishes a good approximation of the full quantum state. Cross correlations of the form $\langle \hat{x}\hat{p} + \hat{p}\hat{x} \rangle$ are observed to be negligible, which enables the covariance matrix to be expressed in a block diagonal form, i.e., one block for the x quadrature and another for the p quadrature [44]; cf. Eq. (4). From the data contained in the covariance matrix, it is possible to extract special modes, called *supermodes*, that are the eigenmodes of the parametric interaction [46] and are uncorrelated with each other. They turn out to be significantly squeezed [35], as shown in Table I. The existence of squeezed supermodes that span the entire frequency spectrum is at the origin of the entanglement that exists between the frequency bands.

Data analysis.—The genetic algorithm is implemented for every possible partition of the states $\hat{\rho}_N$ where $N = 4, 6,$ and 10. The mode decompositions $\mathcal{I}_1 : \ldots : \mathcal{I}_K$ are realized with the map $P\colon \{1, \ldots, N\} \mapsto \{1, \ldots, K\}$, where P maps $P(j) = k$, if and only if $j \in \mathcal{I}_k$. Consequently, the K partitions of the original N-member set can be arranged in matrix form, which is adapted from the Bell triangle (also referred to as Aitken's array or the Peirce triangle). The mode labels range from the highest frequency spectral components 1 to the lowest frequency components N, in ascending order. For example, the mode partitioning, along with the relevant spectral components, for $N = 4$ is depicted in Fig. 1.

Because of a measurement time ranging between ∼10 and 30 minutes per matrix, slowly varying drifts may render the covariance matrix slightly unphysical. In order to counter these effects, white noise is added to the experimentally measured covariance matrices so that the minimal symplectic eigenvalue of the noisy matrix becomes positive; cf. [39]. It is important to emphasize that such a local
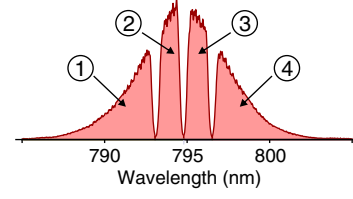
$$\begin{pmatrix}
\{1,2,3,4\} & \{1,2,3\}{:}\{4\} & & \\
\{1,2,4\}{:}\{3\} & \{1,2\}{:}\{3,4\} & \{1,2\}{:}\{3\}{:}\{4\} & \\
\{1,3,4\}{:}\{2\} & \{1,3\}{:}\{2,4\} & \{1,3\}{:}\{2\}{:}\{4\} & \\
\{1,4\}{:}\{2,3\} & \{1\}{:}\{2,3,4\} & \{1\}{:}\{2,3\}{:}\{4\} & \\
\{1,4\}{:}\{2\}{:}\{3\} & \{1\}{:}\{2,4\}{:}\{3\} & \{1\}{:}\{2\}{:}\{3,4\} & \{1\}{:}\{2\}{:}\{3\}{:}\{4\}
\end{pmatrix}$$

FIG. 1 (color online). Structure of 4-mode state. The spectral components (top panel) and partitionings (bottom panel) are shown.

noise convolution is a separable operation, and therefore is unable to induce entanglement from an originally separable state. Without this procedure, negative Σ values might occur, which are due to a violation of positivity of the covariance matrix instead of being authentic entanglement evidence. This extra noise is taken into account when obtaining Σ.

Results.—The results of our methodology for the 4-mode states are detailed in the matrix $\Sigma_{N=4}$ shown below. The significances Σ are calculated according to Eq. (7), and a particular element in the displayed matrix corresponds to the mode partition shown at the same position of the matrix in Fig. 1,

$$\Sigma_{N=4} = \begin{pmatrix}
0.01 & -21.06 & & \\
-11.21 & -24.34 & -24.59 & \\
-13.17 & -23.52 & -23.97 & \\
-4.66 & -20.93 & -21.63 & \\
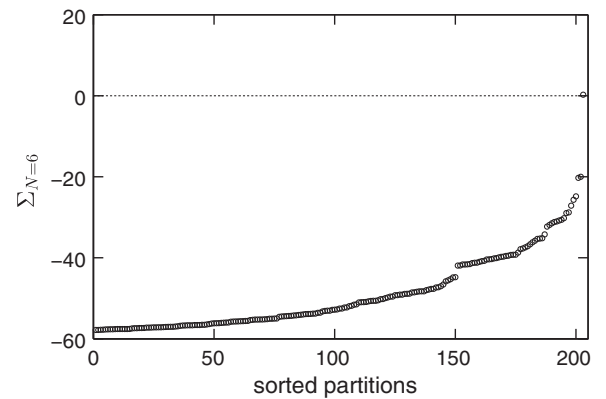-13.16 & -24.03 & -24.32 & -24.61
\end{pmatrix}.$$

FIG. 2. Significance of all partitions for the 6-mode states where the partitions are ordered according to the significance of the detected entanglement. All of the values are negative except for a single positive value, which represents the trivial partition, $K = 1$, and cannot be entangled.
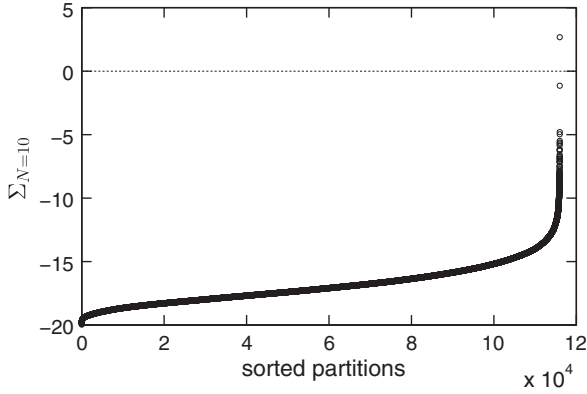
FIG. 3.   The verified entanglement for all 115 974 nontrivial partitions—sorted by significance Σ—for the 10-mode frequency-comb Gaussian state.

The first entry in the matrix is the trivial partition with only one party, $\mathcal{I}_1 = \{1, ..., N\}$, and, therefore, must not exhibit entanglement. The following 14 partitions, however, are each entangled to a significant degree ($|\Sigma| \gtrsim 4$, corresponding to a confidence level of 99.99%). The partition displaying the highest entanglement significance is not a bipartition, but rather coincides with the total division of the state into N independent structures. During the down-conversion process, the initial onset of any quantum correlation among the frequency bands invalidates the full separability of the state. Thus, this partition is the first to become entangled during down-conversion and therefore exhibits the most significant entanglement. Conversely, the least significantly entangled partition corresponds to detaching the spectral wings (elements $\{1, 4\}$) from the spectral center (elements $\{2, 3\}$). This partition indicates an asymmetric distribution of entanglement with respect to the central frequency of the comb. In general, symmetric quantum correlations in the comb are stronger since the preponderance of the down-conversion events originate from the pump spectral center. Asymmetric frequency correlations originate from down-conversion events displaced from the pump central frequency, which therefore occur with lower probability. Since the partition $\{1, 4\}:\{2, 3\}$ demands the highest degree of asymmetric correlations, it possesses a lowered entanglement significance. Nevertheless, the fact that all of the nontrivial partitions are entangled implies that each resolvable frequency band is entangled with every other band (i.e., the full entanglement of the comb). Importantly, this characteristic of the quantum comb would go unnoticed without the use of entanglement criteria capable of probing higher-order state partitions, i.e., $K > 2$.

In the case of 6 modes, 203 unique mode partitions are possible, and the resultant entanglement metric Σ is displayed in Fig. 2. The results for the entire set of unique partitions of the 10-mode scenario are likewise depicted in Fig. 3; cf. also Ref. [39]. All of the partitions in both

TABLE II.   The lowest and highest significances of all K partitions, $\mathcal{I}_1 : ... : \mathcal{I}_K$, for the 10-mode state are given.

K	Partition	Σ
1	$\{1, 2, 3, 4, 5, 6, 7, 8, 9, 10\}$	$+2.7$
2	$\{1, 10\}:\{2, 3, 4, 5, 6, 7, 8, 9\}$	-1.1
2	$\{1, 2, 3, 4, 5\}:\{6, 7, 8, 9, 10\}$	-17.6
3	$\{1, 10\}:\{2, 3, 8, 9\}:\{4, 5, 6, 7\}$	-5.5
3	$\{1, 2, 3, 4, 5\}:\{6, 9, 10\}:\{7, 8\}$	-18.9
4	$\{1, 10\}:\{2, 9\}:\{3\}:\{4, 5, 6, 7, 8\}$	-8.0
4	$\{1, 2, 3, 4\}:\{5\}:\{6, 9, 10\}:\{7, 8\}$	-20.0
5	$\{1, 10\}:\{2\}:\{3\}:\{4, 5, 6, 7, 8\}:\{9\}$	-9.4
5	$\{1, 6\}:\{2, 5\}:\{3, 4\}:\{7, 10\}:\{8, 9\}$	-19.8
6	$\{1, 10\}:\{2\}:\{3\}:\{4, 5, 6, 7\}:\{8\}:\{9\}$	-11.6
6	$\{1, 7\}:\{2, 5\}:\{3\}:\{4, 10\}:\{6\}:\{8, 9\}$	-19.9
7	$\{1, 10\}:\{2\}:\{3\}:\{4\}:\{5, 6, 7\}:\{8\}:\{9\}$	-14.3
7	$\{1, 5\}:\{2, 4\}:\{3\}:\{6, 9\}:\{7\}:\{8\}:\{10\}$	-19.8
8	$\{1, 10\}:\{2\}:\{3\}:\{4, 7\}:\{5\}:\{6\}:\{8\}:\{9\}$	-15.8
8	$\{1, 5\}:\{2\}:\{3\}:\{4\}:\{6\}:\{7, 10\}:\{8\}:\{9\}$	-19.7
9	$\{1, 10\}:\{2\}:\{3\}:\{4\}:\{5\}:\{6\}:\{7\}:\{8\}:\{9\}$	-16.8
9	$\{1\}:\{2, 5\}:\{3\}:\{4\}:\{6\}:\{7\}:\{8\}:\{9\}:\{10\}$	-19.7
10	$\{1\}:\{2\}:\{3\}:\{4\}:\{5\}:\{6\}:\{7\}:\{8\}:\{9\}:\{10\}$	-19.3

the 6- and 10-mode combs are demonstrated to be entangled except for the trivial partition.

Specific K partitions and their corresponding entanglement metrics Σ are shown in Table II for the 10-mode comb state. Within the $K = 2$ subgroup, the most significantly entangled partition results from bisecting the spectrum at its center, whereas the least significantly entangled structure originates from disconnecting the two extreme spectral zones from the remaining spectrum. This result is consistent with previous observations [35] as well as the results shown above for the 4-mode state. Additionally, 41 863 partitions ($\sim$36%) of the 10-mode state reveal an entanglement more significant than that detected for any of the 511 possible state bipartitions. Hence, a richer understanding of the quantum phenomena implicit in the multimode state is afforded only upon examination of these higher-order state partitions. As before, the complete dissolution of the frequency comb structure into ten discrete bins is among the most significantly entangled partitions.

It is worth noting that the number of analyzed frequency bands is currently limited by the optical resolution of the pulse shaper. A new generation of the setup should allow for observing at least 30 frequency modes, as predicted by theory in the present experimental conditions.

Conclusions.—We implemented covariance-based, high-order entanglement criteria on the multimode squeezed states contained within an ultrafast frequency comb. A genetic algorithm was exploited to maximize the statistical significance of the determined entanglement. Upon doing so, the criterion identifies entanglement in all of the 14, 202, and 115 974 nontrivial partitions of the 4-, 6-, and 10-mode scenarios, respectively. Consequently, the quantum comb exhibits full multipartite entanglement, i.e.,

entanglement for all partitionings. Importantly, the currently employed criterion was able to identify entanglement not recognizable with traditional separability metrics. The present approach allows for the identification of partially and fully entangled states for applications in quantum communication or cluster state computation.

---

[*]stefan.gerke@uni-rostock.de

[1] A. Einstein, N. Rosen, and B. Podolsky, Phys. Rev. **47**, 777 (1935).

[2] E. Schrödinger, Proc. Cambridge Philos. Soc. **31**, 555 (1935).

[3] E. Schrödinger, Proc. Cambridge Philos. Soc. **32**, 446 (1936).

[4] M. A. Nielsen and I. L. Chuang, *Quantum Computation and Quantum Information* (Cambridge University Press, Cambridge, England, 2000).

[5] R. Horodecki, P. Horodecki, M. Horodecki, and K. Horodecki, Rev. Mod. Phys. **81**, 865 (2009).

[6] O. Gühne and G. Tóth, Phys. Rep. **474**, 1 (2009).

[7] M. Huber and J. I. de Vicente, Phys. Rev. Lett. **110**, 030501 (2013).

[8] F. Levi and F. Mintert, Phys. Rev. Lett. **110**, 150402 (2013).

[9] G. Giedke and B. Kraus, Phys. Rev. A **89**, 012335 (2014).

[10] A. Peres, Phys. Rev. Lett. **77**, 1413 (1996).

[11] R. Simon, Phys. Rev. Lett. **84**, 2726 (2000).

[12] L.-M. Duan, G. Giedke, J. I. Cirac, and P. Zoller, Phys. Rev. Lett. **84**, 2722 (2000).

[13] R. F. Werner and M. M. Wolf, Phys. Rev. Lett. **86**, 3658 (2001).

[14] J. DiGuglielmo, A. Samblowski, B. Hage, C. Pineda, J. Eisert, and R. Schnabel, Phys. Rev. Lett. **107**, 240503 (2011).

[15] P. van Loock and A. Furusawa, Phys. Rev. A **67**, 052315 (2003).

[16] G. S. Agarwal and A. Biswas, New J. Phys. **7**, 211 (2005).

[17] E. Shchukin and W. Vogel, Phys. Rev. Lett. **95**, 230502 (2005).

[18] A. Serafini, Phys. Rev. Lett. **96**, 110402 (2006).

[19] P. Hyllus and J. Eisert, New J. Phys. **8**, 51 (2006).

[20] E. Shchukin and W. Vogel, Phys. Rev. A **74**, 030302(R) (2006).

[21] M. Hillery and M. S. Zubairy, Phys. Rev. Lett. **96**, 050503 (2006).

[22] O. Gühne, P. Hyllus, O. Gittsovich, and J. Eisert, Phys. Rev. Lett. **99**, 130504 (2007).

[23] A. Miranowicz, M. Piani, P. Horodecki, and R. Horodecki, Phys. Rev. A **80**, 052303 (2009).

[24] F. Shahandeh, J. Sperling, and W. Vogel, Phys. Rev. A **88**, 062323 (2013).

[25] X. Su, A. Tan, X. Jia, J. Zhang, C. Xie, and K. Peng, Phys. Rev. Lett. **98**, 070502 (2007).

[26] M. Yukawa, R. Ukai, P. van Loock, and A. Furusawa, Phys. Rev. A **78**, 012301 (2008).

[27] M. Pysher, Y. Miwa, R. Shahrokhshahi, R. Bloomer, and O. Pfister, Phys. Rev. Lett. **107**, 030505 (2011).

[28] S. Armstrong, J.-F. Morizur, J. Janousek, B. Hage, N. Treps, P. K. Lam, and H.-A. Bachor, Nat. Commun. **3**, 1026 (2012).

[29] A. S. Coelho, F. A. S. Barbosa, K. N. Cassemiro, A. S. Villar, M. Martinelli, and P. Nussenzveig, Science **326**, 823 (2009).

[30] C. E. Vollmer, D. Schulze, T. Eberle, V. Händchen, J. Fiurášek, and R. Schnabel, Phys. Rev. Lett. **111**, 230505 (2013).

[31] M. Horodecki, P. Horodecki, and R. Horodecki, Phys. Lett. A **223**, 1 (1996).

[32] M. Horodecki, P. Horodecki, and R. Horodecki, Phys. Lett. A **283**, 1 (2001).

[33] J. Sperling and W. Vogel, Phys. Rev. Lett. **111**, 110503 (2013).

[34] J. Sperling and W. Vogel, Phys. Rev. A **79**, 022318 (2009).

[35] J. Roslund, R. Medeiros de Arájo, S. Jiang, C. Fabre, and N. Treps, Nat. Photonics **8**, 109 (2014).

[36] G. Adesso and F. Illuminati, J. Phys. A **40**, 7821 (2007).

[37] D. Berend and T. Tassa, Probab. Math. Stat. **30**, 185 (2010).

[38] Note that we use the notion "tr" for the quantum mechanical trace, e.g., tr$(\hat{L})$, whereas "Tr" corresponds to the trace of a matrix, Tr(M) for $M \in \mathbb{C}^{d \times d}$.

[39] See Supplemental Material at http://link.aps.org/supplemental/10.1103/PhysRevLett.114.050501, which includes Refs. [33,40–42], for analytical solutions, numerical implementation, and data processing.

[40] R. L. Haupt and S. E. Haupt, *Practical Genetic Algorithms*, 2nd ed. (John Wiley & Sons, Hoboken, NJ, 2004).

[41] L. Huaixin and Z. Youngde, Int. J. Theor. Phys. **39**, 447 (2000).

[42] R. Simon, S. Chaturvedi, and V. Srinivasan, J. Math. Phys. (N.Y.) **40**, 3632 (1999).

[43] G. J. de Valcárcel, G. Patera, N. Treps, and C. Fabre, Phys. Rev. A **74**, 061801(R) (2006).

[44] R. Medeiros de Araújo, J. Roslund, Y. Cai, G. Ferrini, C. Fabre, and N. Treps, Phys. Rev. A **89**, 053828 (2014).

[45] A. M. Weiner, Rev. Sci. Instrum. **71**, 1929 (2000).

[46] G. Patera, G. De Valcárcel, N. Treps, and C. Fabre, Eur. Phys. J. D **56**, 123 (2010).

Supplemental Material
Full multipartite entanglement of frequency-comb Gaussian states

S. Gerke,[1, *] J. Sperling,[1] W. Vogel,[1] Y. Cai,[2] J. Roslund,[2] N. Treps,[2] and C. Fabre[2]

[1]*Arbeitsgruppe Theoretische Quantenoptik, Institut für Physik, Universität Rostock, D-18051 Rostock, Germany*
[2]*Laboratoire Kastler Brossel, Université Pierre et Marie Curie,*
Paris 6, ENS, CNRS; 4 place Jussieu, 75252 Paris, France
(Dated: December 15, 2014)

Section I derives the general solution for the separability eigenvalue equations for second order moment tests. Section II contains a brief overview over the functionality of a Genetic Algortithm. Section III lists the experimental data of the states under examination and how it was treated. Section IV lists the possible partitions for a 6-mode state. The appendix A includes the experimentally obtained covariances.

I. SOLUTION OF SEPARABILITY EIGENVALUE EQUATIONS

Before we solve the separability eigenvalue problem [1], let us recall some well-known facts. First, we start with the general form of the given operator Hermitian operator $\hat{L}$, $[\hat{\xi} = (\hat{x}_1, \ldots, \hat{x}_N, \hat{p}_1, \ldots, \hat{p}_N)]$

$$\hat{L} = \text{Tr}\left(M\hat{\xi}\hat{\xi}^{\text{T}}\right), \text{ with } 0 < M = \begin{pmatrix} M_{xx} & M_{px}^{\text{T}} \\ M_{px} & M_{pp} \end{pmatrix} = M^{\text{T}} \in \mathbb{R}^{2N \times 2N}. \tag{1}$$

The Williamson's Theorem states, that there exists a symplectic transformation, $S \in \text{Sp}(\mathbb{R}^{2N})$, and a positive diagonal matrix, $D = \text{diag}(d_1, \ldots, d_N)$, such that

$$M = S^{\text{T}} \begin{pmatrix} D & 0 \\ 0 & D \end{pmatrix} S, \tag{2}$$

see also [2, 3]. From elementary quantum mechanics of the harmonic oscillator, it follows that the minimal eigenvalue $\lambda^{\min}$ of $\hat{L}$ in the diagonalized representation is

$$\lambda^{\min} = \text{Tr } D, \text{ for the Gaussian wave function } \psi(x) \propto \exp\left[-\frac{1}{2}x^{\text{T}}x\right]. \tag{3}$$

Second, let us assume the covariances of two states, $C_i = \langle\hat{\xi}\hat{\xi}^{\text{T}}\rangle_i - \langle\hat{\xi}\rangle_i\langle\hat{\xi}\rangle_i^{\text{T}}$ for $i = 1, 2$, with displacements $\langle\hat{\xi}\rangle_1 = 0$ and $\langle\hat{\xi}\rangle_2 \neq 0$. Thus, we have for $C_1 = C_2$

$$\langle\hat{L}\rangle_2 = \text{Tr}(M\langle\xi\hat{\xi}^{\text{T}}\rangle_2) = \text{Tr}(M\langle\xi\hat{\xi}^{\text{T}}\rangle_1) + \underbrace{\langle\hat{\xi}\rangle_2^{\text{T}} M\langle\hat{\xi}\rangle_2}_{>0} > \langle\hat{L}\rangle_1. \tag{4}$$

Therefore, the minimal expectation value for equal covariances is obtained for a zero displacement.

Finally, we can study the minimal solutions of the separability eigenvalue equations for a partition $\mathcal{I}_1 : \cdots : \mathcal{I}_K$,

$$\hat{L}_{a_1, \ldots, a_{j-1}, a_{j+1}, \ldots, a_K}|a_j\rangle = g_{\mathcal{I}_1 : \cdots : \mathcal{I}_K}|a_j\rangle \text{ for } j = 1, \ldots, K \text{ and for all } |x\rangle, |y\rangle \in \mathcal{H}_j : \tag{5}$$

$$\langle x|\hat{L}_{a_1, \ldots, a_{j-1}, a_{j+1}, \ldots, a_K}|y\rangle = \langle a_1, \ldots, a_{j-1}, x, a_{j+1}, \ldots, a_K|\hat{L}|a_1, \ldots, a_{j-1}, y, a_{j+1}, \ldots, a_K\rangle.$$

Let us decompose the matrix M into the submatrices $M^{k,l}$ that contain the rows(columns) of M which belong to the index set $\mathcal{I}_{k(l)}$, respectively. In the same way, we may decompose $\hat{\xi} = (\hat{\xi}_1, \ldots, \hat{\xi}_K)^{\text{T}}$. Hence, the partially reduced operator for the jth subsystem reads as

$$\hat{L}_{a_1, \ldots, a_{j-1}, a_{j+1}, \ldots, a_K} = \sum_{k,l \neq j} \text{Tr}(M^{k,l}\langle\hat{\xi}_l\hat{\xi}_k^{\text{T}}\rangle) + \sum_{k \neq j} \left[\text{Tr}(M^{k,j}\hat{\xi}_j\langle\hat{\xi}_k\rangle^{\text{T}}) + \text{Tr}(M^{j,k}\langle\hat{\xi}_k\rangle\hat{\xi}_j^{\text{T}})\right] + \text{Tr}(M^{j,j}\hat{\xi}_j\hat{\xi}_j^{\text{T}}). \tag{6}$$

---

*Electronic address: stefan.gerke@uni-rostock.de

Due to separability we have $\langle \hat{\xi}_l \hat{\xi}_k^{\mathrm{T}} \rangle = \langle a_l | \hat{\xi}_l | a_l \rangle \langle a_k | \hat{\xi}_k | a_k \rangle$ for $k \neq l$, and due to a zero displacement for minimal expectation values, $\langle \hat{\xi}_k \rangle = 0$ for all k. Thus, the previous expression simplifies to:

$$\hat{L}_{a_1, \ldots, a_{j-1}, a_{j+1}, \ldots, a_K} = \sum_{k \neq j} \mathrm{Tr}(M^{k,k} \langle \hat{\xi}_k \hat{\xi}_k^{\mathrm{T}} \rangle) + \mathrm{Tr}(M^{j,j} \hat{\xi}_j \hat{\xi}_j^{\mathrm{T}}), \tag{7}$$

where the first sum is a constant in the subsystem $\mathcal{I}_j$. Up to this constant, this operator has the form as (1). We may redefine $M^{j,j} = M_{\mathcal{I}_j}$, which has the (locally) diagonalized form with $D_{\mathcal{I}_j}$ [see Eq. (2)]. Finally, this yields the minimal separability eigenvalue as

$$g_{\mathcal{I}_1:\cdots:\mathcal{I}_K}^{\min} = \sum_{k=1}^{K} \mathrm{Tr}\, D_{\mathcal{I}_k}. \tag{8}$$

The explicit solution for $M_{px} = 0$ can be also found in [1].

II. GENETIC ALGORITHM

A genetic algorithm can be categorized as a (meta-)heuristic algorithm. They efficiently scan the entire domain to explore local minima, and they converge to an approximate global minimum for sufficiently long calculation times. genetic algorithms can be implemented in different varieties, but all of them follow the same routine of:

1. Initialization; 2. Selection; 3. Mating; 4. Crossover; 5. Mutation.

One possible implementation for the minimization problem, $\Sigma \to \min$ with respect to the elements of M, will be briefly outlined here.

For a genetic algorithm, the number of parameters N_{var} and an objective function to optimize $F : \mathbb{R}^{N_{\mathrm{var}}} \to \mathbb{R}$ are given. Initially, a set of N_{pop} randomly generated vectors, the *population*, is created. The vectors are called *chromosomes* and the entries in each vector are called *alleles*. The initial range for every allel will be an interval $[x_{\min}, x_{\max}] \in \mathbb{R}$. So in total, the initial population can be described as a matrix $X \in [x_{\min}, x_{\max}]^{N_{\mathrm{pop}} \times N_{\mathrm{var}}}$. After every iteration step of the genetic algorithm, the generation count is increased, until either the maximum number of generations is reached or a termination criterion has been met. In every generation, the population will be altered by the following four steps:

1. **Selection.** Selection describes the process of choosing which chromosomes will be kept for mating and which not. The chromosomes that are kept are determined by evaluating the objective function. Chromosomes that result in a lower value are deemed better and the best fourth of all chromosomes are kept as so-called *survivors*.

2. **Mating.** To refill the pool of chromosomes (three quarters have already been discarded), *parents* have to be selected for mating. *Tournament selection* was used to determine which chromosomes are picked for mating. Thus a fourth of all survivors are randomly chosen and the best of those is selected as either *mother* or *father*. The set of parents is picked large enough to refill the entire population.

3. **Crossover.** Each pair of parents produces two offspring. In the algorithm used, two random alleles $\alpha_1 < \alpha_2$ were chosen as crossover points. For a certain mother (father) chromosome m (p respectively), the two offspring are created in the following way: A parameter $\beta \in [0, 2]$ is chosen randomly. The alleles j for child one $c^{(1)}$ with $j < \alpha_1$ and $\alpha_2 < j$ are copied from m. Analogously child two $c^{(2)}$ is created from the alleles of the father. The alleles between the crossover points are determined via the equations $c_j^{(1)} = m_j - \beta(m_j - p_j)$ and $c_j^{(2)} = p_j + \beta(m_j - p_j)$ for the two offspring. By allowing β to become greater than 1, the range of the parent chromosomes can be left by the offspring to scan a larger domain.

4. **Mutation.** After the reproduction, 10% of all alleles are selected for mutation. An allele is mutated by adding a normally distributed random number ($\mathcal{N}(0, 5)$) to it. The chromosome with the best fitness is exempt from mutation due to *elitism*. Elitism guarantees, that the chromosome with best fitness remains unchanged. Thus a possible global optimum will not be discarded.

For a more detailed description on the genetic algorithm; see, e.g., [? ?]. There is no proof showing that the genetic algorithm converges. For testing the algorithm, several multimode Gaussian states with known entanglement characteristic are created, and random errors have been assigned. It is important to note that the significances $|\Sigma|$ that are obtained for the measurement give a lower bound, i.e.: If the test shows entanglement, $\Sigma < 0$, then entanglement exists with at least the significance of $|\Sigma|$.

III. NOISE ADDITION

It is important to examine the physicality of the states described by the measured covariance matrices. The states are considered physical when all their symplectic eigenvalues are non negative. In matrix formulation this reads as

$$C + \frac{\mathrm{i}}{2}J \geq 0, \text{ with } J = \begin{pmatrix} 0 & I_N \\ -I_N & 0 \end{pmatrix} \tag{9}$$

and I_N being the $N \times N$ identity matrix. The prefactor $1/2$ in Eq. (9) is the vacuum variance of amplitude and phase quadratures of the radiation field. For every state the minimal symplectic eigenvalue, $\lambda_{\min}$, was calculated (see Table I). It shows, that the states are slightly nonphysical. Therefore white noise is added to the covariance matrices in the form

$$C_{\mathrm{noise}} = C + 1.001|\lambda_{\min}|I_{2N}. \tag{10}$$

The prefactor 1.001 was chosen, so that the resulting minimal symplectic eigenvalue of C_{noise} is positive definite. Adding such uncorrelated noise makes the covariance matrices physical, which is important for the following methods, and it is a separable operation – i.e. it cannot generate entanglement from a separable state.

TABLE I: Minimal and maximal symplectic eigenvalue for the states $\hat{\rho}_N$.

N = 4		N = 6		N = 10	
min	max	min	max	min	max
-0.0541	2.6596	-0.3209	1.4612	-0.0244	2.0858

IV. SIX-MODE PARTITIONS

The matrix (11) (on page 4) lists all possible 203 partitions of the set $\{1, 2, 3, 4, 5, 6\}$. The significances $\Sigma_{N=6}$ for the entanglement of the states $\hat{\rho}_6$ of the corresponding partition tests are:

$$\Sigma_{N=6} = \left(\begin{smallmatrix}
0.25897 & -49.22 & & & & -27.146 & -56.08 & -56.025 & & & -31.043 & -57.184 & -57.346 \\
-20.01 & -51.5 & -51.958 & & & -30.629 & -56.661 & -57.124 & & & -30.235 & -55.384 & -56.549 \\
-20.274 & -50.193 & -50.901 & & & -28.794 & -54.402 & -55.641 & & & -31.48 & -55.051 & -57.167 \\
-24.833 & -50.653 & -52.52 & & & -28.957 & -53.541 & -55.791 & & & -31.894 & -55.987 & -56.661 \\
-25.677 & -51.852 & -52.551 & -52.844 & & -30.801 & -55.26 & -56.151 & -56.723 & & -39.259 & -50.619 & -57.053 \\
-36.185 & -47.016 & -53.869 & & & -35.256 & -47.675 & -53.868 & & & -39.538 & -49.6 & -56.616 \\
-37.698 & -47.279 & -53.899 & & & -34.237 & -45.569 & -52.744 & & & -40.321 & -50.617 & -56.797 \\
-38.722 & -48.524 & -54.375 & -55.142 & & -36.677 & -48.403 & -54.249 & -54.491 & & -41.226 & -49.105 & -57.643 \\
-40.158 & -47.331 & -55.188 & & & -35.34 & -44.789 & -53.058 & & & -39.704 & -46.59 & -56.55 \\
-39.487 & -45.282 & -54.122 & & & -31.177 & -40.086 & -50.22 & & & -41.664 & -48.845 & -56.92 \\
-41.311 & -47.658 & -55.056 & -55.665 & & -35.785 & -44.86 & -52.272 & -53.057 & & -39.778 & -49.793 & -55.611 \\
-39.914 & -48.571 & -53.979 & -55.241 & & -37.425 & -48.272 & -53.129 & -54.323 & & -39.234 & -48.277 & -54.987 \\
-40.388 & -48.003 & -53.78 & -55.007 & & -35.173 & -45.825 & -51.585 & -52.82 & & -39.305 & -48.908 & -53.801 \\
-40.998 & -48.893 & -53.595 & -55.324 & & -37.144 & -47.856 & -52.266 & -54.056 & & & & \\
-41.652 & -49.247 & -54.57 & -55.26 & -55.712 & -37.887 & -48.297 & -53.243 & -54.203 & -54.447 & -40.432 & -49.968 & -55.583
\end{smallmatrix}\right.$$

$$\left.\begin{smallmatrix}
-57.608 & & & & & & \\
-56.715 & & & & & & \\
-57.161 & & & & & & \\
-57.183 & & -32.299 & -55.974 & -57.231 & -57.596 & -57.682 \\
-57.242 & & & & & & \\
-57.028 & & & & & & \\
-57.565 & & -40.843 & -50.956 & -57.326 & -57.747 & -57.703 \\
-57.587 & & & & & & \\
-56.61 & & & & & & \\
-57.596 & & -41.895 & -49.11 & -57.344 & -57.65 & -57.81 \\
-56.613 & & -41.211 & -50.971 & -56.136 & -57.437 & -57.595 \\
-56.167 & & -40.747 & -49.573 & -55.719 & -56.985 & -57.081 \\
-55.742 & & -41.557 & -50.486 & -55.24 & -57.391 & -57.384 \\
-56.455 & -56.66 & -41.61 & -50.763 & -56.234 & -57.046 & -57.598 & -41.931 & -51.031 & -56.358 & -57.233 & -57.78 & -57.813
\end{smallmatrix}\right)$$

Please note that the results of the 10-mode analysis cannot be presented here. The significances for all 115975 partitions would dramatically enlarge the supplement. Some selected results are given in the Letter.

$$
\left(
\begin{array}{ccccccc}
\{1, 2, 3, 4, 5\}{:}\{6\} & \{1, 2, 3, 4, 5\}{:}\{6\} & \{1, 2, 3, 4, 5\}{:}\{6\} & \{1, 2, 3, 4, 6\}{:}\{5\} & \{1, 2, 3, 4, 6\}{:}\{5\} & \{1, 2, 3, 4\}{:}\{5, 6\} & \{1, 2, 3, 4\}{:}\{5\}{:}\{6\} \\
\{1, 2, 3, 5, 6\}{:}\{4\} & \{1, 2, 3, 5\}{:}\{4, 6\} & \{1, 2, 3, 5\}{:}\{4\}{:}\{6\} & \{1, 2, 3, 6\}{:}\{4, 5\} & \{1, 2, 3, 6\}{:}\{4, 5\} & \{1, 2, 3\}{:}\{4, 5, 6\} & \{1, 2, 3\}{:}\{4, 5\}{:}\{6\} \\
\{1, 2, 4, 5, 6\}{:}\{3\} & \{1, 2, 4, 5\}{:}\{3, 6\} & \{1, 2, 4, 5\}{:}\{3\}{:}\{6\} & \{1, 2, 4, 6\}{:}\{3, 5\} & \{1, 2, 4, 6\}{:}\{3, 5\} & \{1, 2, 4\}{:}\{3, 5, 6\} & \{1, 2, 4\}{:}\{3, 5\}{:}\{6\} \\
\{1, 2, 5, 6\}{:}\{3, 4\} & \{1, 2, 5\}{:}\{3, 4, 6\} & \{1, 2, 5\}{:}\{3, 4\}{:}\{6\} & \{1, 2, 6\}{:}\{3, 4, 5\} & \{1, 2, 6\}{:}\{3, 4, 5\} & \{1, 2\}{:}\{3, 4, 5, 6\} & \{1, 2\}{:}\{3, 4, 5\}{:}\{6\} \\
\{1, 2, 5, 6\}{:}\{3\}{:}\{4\} & \{1, 2, 5\}{:}\{3, 6\}{:}\{4\} & \{1, 2, 5\}{:}\{3\}{:}\{4\}{:}\{6\} & \{1, 2, 6\}{:}\{3, 5\}{:}\{4\} & \{1, 2, 6\}{:}\{3, 5\}{:}\{4\} & \{1, 2\}{:}\{3, 5, 6\}{:}\{4\} & \{1, 2\}{:}\{3, 5\}{:}\{4\}{:}\{6\} \\
\{1, 3, 4, 5, 6\}{:}\{2\} & \{1, 3, 4, 5\}{:}\{2, 6\} & & \{1, 3, 4, 6\}{:}\{2, 5\} & \{1, 3, 4, 6\}{:}\{2, 5\} & \{1, 3, 4\}{:}\{2, 5, 6\} & \{1, 3, 4\}{:}\{2, 5\}{:}\{6\} \\
\{1, 3, 5, 6\}{:}\{2, 4\} & \{1, 3, 5\}{:}\{2, 4, 6\} & & \{1, 3, 6\}{:}\{2, 4, 5\} & \{1, 3, 6\}{:}\{2, 4, 5\} & \{1, 3\}{:}\{2, 4, 5, 6\} & \{1, 3\}{:}\{2, 4, 5\}{:}\{6\} \\
\{1, 3, 5, 6\}{:}\{2\}{:}\{4\} & \{1, 3, 5\}{:}\{2, 6\}{:}\{4\} & & \{1, 3, 6\}{:}\{2, 5\}{:}\{4\} & \{1, 3, 6\}{:}\{2, 5\}{:}\{4\} & \{1, 3\}{:}\{2, 5, 6\}{:}\{4\} & \{1, 3\}{:}\{2, 5\}{:}\{4\}{:}\{6\} \\
\{1, 4, 5, 6\}{:}\{2, 3\} & \{1, 4, 5\}{:}\{2, 6\}{:}\{3\} & & \{1, 4, 6\}{:}\{2, 3, 5\} & \{1, 4, 6\}{:}\{2, 3, 5\} & \{1, 4\}{:}\{2, 3, 5, 6\} & \{1, 4\}{:}\{2, 3, 5\}{:}\{6\} \\
\{1, 5, 6\}{:}\{2, 3, 4\} & \{1, 5\}{:}\{2, 3, 6\}{:}\{4\} & & \{1, 6\}{:}\{2, 3, 4, 5\} & \{1, 6\}{:}\{2, 3, 4, 5\} & \{1\}{:}\{2, 3, 4, 5, 6\} & \{1\}{:}\{2, 3, 4, 5\}{:}\{6\} \\
\{1, 5, 6\}{:}\{2, 3\}{:}\{4\} & \{1, 4, 5\}{:}\{2, 6\}{:}\{3\} & \{1, 2, 3\}{:}\{4\}{:}\{5, 6\} & \{1, 6\}{:}\{2, 3, 5\}{:}\{4\} & \{1, 6\}{:}\{2, 3, 5\}{:}\{4\} & \{1, 2, 3\}{:}\{4\}{:}\{5\}{:}\{6\} & \{1\}{:}\{2, 3, 5\}{:}\{4\}{:}\{6\} \\
\{1, 4, 5, 6\}{:}\{2\}{:}\{3\} & \{1, 5\}{:}\{2, 4, 6\}{:}\{3\} & \{1, 2, 4\}{:}\{3\}{:}\{5, 6\} & \{1, 4, 6\}{:}\{2, 5\}{:}\{3\} & \{1, 4, 6\}{:}\{2, 5\}{:}\{3\} & \{1, 4\}{:}\{2, 6\}{:}\{3\}{:}\{5\} & \{1, 4\}{:}\{2, 5\}{:}\{3\}{:}\{6\} \\
\{1, 5, 6\}{:}\{2, 4\}{:}\{3\} & \{1, 5\}{:}\{2, 6\}{:}\{3, 4\} & \{1, 2\}{:}\{3, 4\}{:}\{5, 6\} & \{1, 6\}{:}\{2, 4, 5\}{:}\{3\} & \{1, 6\}{:}\{2, 4, 5\}{:}\{3\} & \{1, 6\}{:}\{2, 4\}{:}\{3\}{:}\{5\} & \{1\}{:}\{2, 4, 5\}{:}\{3\}{:}\{6\} \\
\{1, 5, 6\}{:}\{2\}{:}\{3, 4\} & \{1, 5\}{:}\{2, 6\}{:}\{3\}{:}\{4\} & \{1, 2\}{:}\{3\}{:}\{4\}{:}\{5, 6\} & \{1, 6\}{:}\{2, 5\}{:}\{3, 4\} & \{1, 6\}{:}\{2, 5\}{:}\{3, 4\} & \{1, 6\}{:}\{2, 5\}{:}\{3, 4\} & \{1\}{:}\{2, 5\}{:}\{3, 4\}{:}\{6\} \\
\{1, 5, 6\}{:}\{2\}{:}\{3\}{:}\{4\} & \{1, 5\}{:}\{2, 6\}{:}\{3\}{:}\{4\} & \{1, 5\}{:}\{2\}{:}\{3\}{:}\{4\}{:}\{6\} & \{1, 6\}{:}\{2, 5, 6\}{:}\{3\}{:}\{4\} & \{1, 6\}{:}\{2, 5, 6\}{:}\{3\}{:}\{4\} & \{1, 6\}{:}\{2, 6\}{:}\{3\}{:}\{4, 5\} & \{1\}{:}\{2, 5\}{:}\{3\}{:}\{4, 5\}
\end{array}
\right)
\tag{11}
$$

{1}:{2, 5}:{3}:{4}:{6}

{1, 2}:{3}:{4}:{5, 6}   {1, 2}:{3}:{4}:{5}:{6}

{1, 3}:{2}:{4}:{5, 6}   {1, 3}:{2}:{4}:{5}:{6}

{1}:{2, 3}:{4}:{5, 6}   {1}:{2, 3}:{4}:{5}:{6}
{1, 4}:{2}:{3}:{5, 6}   {1, 4}:{2}:{3}:{5}:{6}
{1}:{2, 4}:{3}:{5, 6}   {1}:{2, 4}:{3}:{5}:{6}
{1}:{2}:{3, 4}:{5, 6}   {1}:{2}:{3, 4}:{5}:{6}
{1}:{2}:{3}:{4, 5, 6}   {1}:{2}:{3}:{4, 5}:{6}
{1, 6}:{2}:{3}:{4, 5, 6}   {1}:{2, 6}:{3}:{4}:{5}   {1}:{2}:{3, 6}:{4}:{5}   {1}:{2}:{3}:{4, 6}:{5}   {1}:{2}:{3}:{4}:{5, 6}   {1}:{2}:{3}:{4}:{5}:{6}

Appendix A: Measured Covariances

The measured covariance matrices, $\overline{C}_N$, with their respective uncertainties $\sigma(C_N)$ are listed below. The index refers to the the N-mode state, $\hat{\rho}_N$. Note that the prefactor $1/2$ results from the fact that the experimental normalization of vacuum variances is 1, whereas the theoretical part uses the normalization $1/2$. As in the other cases, we have no xp correlations for the 10-mode state.

$$\overline{C}_4 = \frac{1}{2}\begin{pmatrix} 2.19842 & 0.32184 & -0.35217 & -1.69661 & 0 & 0 & 0 & 0 \\ 0.32184 & 0.81876 & -0.32120 & -0.37926 & 0 & 0 & 0 & 0 \\ -0.35217 & -0.32120 & 0.92120 & 0.08637 & 0 & 0 & 0 & 0 \\ -1.69661 & -0.37926 & 0.08637 & 2.12837 & 0 & 0 & 0 & 0 \\ 0 & 0 & 0 & 0 & 2.19842 & 0.71066 & 0.72878 & 1.82769 \\ 0 & 0 & 0 & 0 & 0.71066 & 1.84564 & 1.14879 & 0.86775 \\ 0 & 0 & 0 & 0 & 0.72878 & 1.14879 & 2.08678 & 0.69736 \\ 0 & 0 & 0 & 0 & 1.82769 & 0.86775 & 0.69736 & 2.12838 \end{pmatrix} \tag{A1}$$

$$\sigma(C_4) = \frac{1}{2}\begin{pmatrix} 0.00653 & 0.02082 & 0.01787 & 0.01293 & 0 & 0 & 0 & 0 \\ 0.02082 & 0.01644 & 0.03695 & 0.03798 & 0 & 0 & 0 & 0 \\ 0.01787 & 0.03695 & 0.01722 & 0.02690 & 0 & 0 & 0 & 0 \\ 0.01293 & 0.03798 & 0.02690 & 0.01098 & 0 & 0 & 0 & 0 \\ 0 & 0 & 0 & 0 & 0.00915 & 0.02018 & 0.05534 & 0.08577 \\ 0 & 0 & 0 & 0 & 0.02018 & 0.02045 & 0.04201 & 0.04170 \\ 0 & 0 & 0 & 0 & 0.05534 & 0.04201 & 0.02931 & 0.03910 \\ 0 & 0 & 0 & 0 & 0.08577 & 0.04170 & 0.03910 & 0.00910 \end{pmatrix} \tag{A2}$$

$$\overline{C}_6 = \frac{1}{2}\begin{pmatrix} 1.16513 & 0.05675 & 0.00579 & -0.01204 & -0.09467 & -0.49452 & 0 & 0 & 0 & 0 & 0 & 0 \\ 0.05675 & 1.06805 & -0.00971 & -0.07579 & -0.15284 & -0.22850 & 0 & 0 & 0 & 0 & 0 & 0 \\ 0.00579 & -0.00971 & 0.91696 & -0.07267 & -0.09668 & -0.09837 & 0 & 0 & 0 & 0 & 0 & 0 \\ -0.01204 & -0.07579 & -0.07267 & 0.88268 & -0.05307 & -0.04094 & 0 & 0 & 0 & 0 & 0 & 0 \\ -0.09467 & -0.15284 & -0.09668 & -0.05307 & 0.95316 & 0.00177 & 0 & 0 & 0 & 0 & 0 & 0 \\ -0.49452 & -0.22850 & -0.09837 & -0.04094 & 0.00177 & 1.17781 & 0 & 0 & 0 & 0 & 0 & 0 \\ 0 & 0 & 0 & 0 & 0 & 0 & 1.16513 & 0.05675 & 0.04688 & 0.07030 & 0.12291 & 0.51779 \\ 0 & 0 & 0 & 0 & 0 & 0 & 0.05675 & 1.06805 & 0.10608 & 0.15140 & 0.21075 & 0.25904 \\ 0 & 0 & 0 & 0 & 0 & 0 & 0.04688 & 0.10608 & 1.18896 & 0.17003 & 0.17817 & 0.15185 \\ 0 & 0 & 0 & 0 & 0 & 0 & 0.07030 & 0.15140 & 0.17003 & 1.21135 & 0.15567 & 0.12267 \\ 0 & 0 & 0 & 0 & 0 & 0 & 0.12291 & 0.21075 & 0.17817 & 0.15567 & 1.17537 & 0.10738 \\ 0 & 0 & 0 & 0 & 0 & 0 & 0.51779 & 0.25904 & 0.15185 & 0.12267 & 0.10738 & 1.17781 \end{pmatrix} \tag{A3}$$

$$\sigma(C_6) = \frac{1}{2}\begin{pmatrix} 0.00332 & 0.00418 & 0.00605 & 0.00621 & 0.00724 & 0.01286 & 0 & 0 & 0 & 0 & 0 & 0 \\ 0.00418 & 0.00372 & 0.01039 & 0.01014 & 0.01319 & 0.00923 & 0 & 0 & 0 & 0 & 0 & 0 \\ 0.00605 & 0.01039 & 0.01087 & 0.01404 & 0.01166 & 0.00983 & 0 & 0 & 0 & 0 & 0 & 0 \\ 0.00621 & 0.01014 & 0.01404 & 0.00677 & 0.01441 & 0.00769 & 0 & 0 & 0 & 0 & 0 & 0 \\ 0.00724 & 0.01319 & 0.01166 & 0.01441 & 0.00635 & 0.00533 & 0 & 0 & 0 & 0 & 0 & 0 \\ 0.01286 & 0.00923 & 0.00983 & 0.00769 & 0.00533 & 0.00239 & 0 & 0 & 0 & 0 & 0 & 0 \\ 0 & 0 & 0 & 0 & 0 & 0 & 0.00485 & 0.00452 & 0.00602 & 0.00810 & 0.01237 & 0.02170 \\ 0 & 0 & 0 & 0 & 0 & 0 & 0.00452 & 0.00445 & 0.00867 & 0.01081 & 0.00999 & 0.01336 \\ 0 & 0 & 0 & 0 & 0 & 0 & 0.00602 & 0.00867 & 0.00818 & 0.01490 & 0.01218 & 0.00916 \\ 0 & 0 & 0 & 0 & 0 & 0 & 0.00810 & 0.01081 & 0.01490 & 0.00513 & 0.01091 & 0.00639 \\ 0 & 0 & 0 & 0 & 0 & 0 & 0.01237 & 0.00999 & 0.01218 & 0.01091 & 0.00657 & 0.00249 \\ 0 & 0 & 0 & 0 & 0 & 0 & 0.02170 & 0.01336 & 0.00916 & 0.00639 & 0.00249 & 0.00458 \end{pmatrix} \tag{A4}$$

$$\overline{C}_{10}^{xx} = \frac{1}{2}\begin{pmatrix} 1.65932 & 0.25017 & 0.08597 & 0.07579 & -0.03109 & -0.04817 & -0.07758 & -0.10678 & -0.41698 & -1.23296 \\ 0.25017 & 1.32597 & 0.18910 & 0.15109 & 0.05993 & -0.05633 & -0.17443 & -0.32828 & -0.59014 & -0.50723 \\ 0.08597 & 0.18910 & 1.22338 & 0.06505 & -0.00904 & -0.07993 & -0.20804 & -0.33675 & -0.43723 & -0.20332 \\ 0.07579 & 0.15109 & 0.06505 & 1.07701 & -0.02156 & -0.12138 & -0.20826 & -0.23675 & -0.25183 & -0.06551 \\ -0.03109 & 0.05993 & -0.00904 & -0.02156 & 0.92137 & -0.12627 & -0.14409 & -0.11292 & -0.09416 & 0.00915 \\ -0.04817 & -0.05633 & -0.07993 & -0.12138 & -0.12627 & 0.89173 & -0.06863 & 0.01984 & 0.02195 & 0.04463 \\ -0.07758 & -0.17443 & -0.20804 & -0.20826 & -0.14409 & -0.06863 & 1.02241 & 0.12361 & 0.09729 & 0.20589 \\ -0.10678 & -0.32828 & -0.33675 & -0.23675 & -0.11292 & 0.01984 & 0.12361 & 1.14469 & 0.28954 & 0.21799 \\ -0.41698 & -0.59014 & -0.43723 & -0.25183 & -0.09416 & 0.02195 & 0.09729 & 0.28954 & 1.35997 & 0.40409 \\ -1.23296 & -0.50723 & -0.20332 & -0.06551 & 0.00915 & 0.04463 & 0.20589 & 0.21799 & 0.40409 & 1.87529 \end{pmatrix} \tag{A5}$$

$$\overline{C}_{10}^{pp} = \frac{1}{2}\begin{pmatrix} 1.65894 & 0.24940 & 0.08575 & -0.01855 & 0.04390 & 0.00277 & 0.00861 & 0.09152 & 0.38982 & 1.19130 \\ 0.24940 & 1.32543 & 0.18988 & 0.05109 & 0.13493 & 0.11509 & 0.13734 & 0.27613 & 0.49756 & 0.53130 \\ 0.08575 & 0.18988 & 1.22285 & 0.17189 & 0.21092 & 0.27981 & 0.32466 & 0.36670 & 0.38884 & 0.25673 \\ -0.01855 & 0.05109 & 0.17189 & 1.30849 & 0.34432 & 0.37889 & 0.37201 & 0.33036 & 0.25970 & 0.12181 \\ 0.04390 & 0.13493 & 0.21092 & 0.34432 & 1.38456 & 0.46614 & 0.42485 & 0.31058 & 0.21631 & 0.10056 \\ 0.00277 & 0.11509 & 0.27981 & 0.37889 & 0.46614 & 1.42516 & 0.41797 & 0.30161 & 0.18960 & 0.10394 \\ 0.00861 & 0.13734 & 0.32466 & 0.37201 & 0.42485 & 0.41797 & 1.34370 & 0.26795 & 0.20547 & 0.07949 \\ 0.09152 & 0.27613 & 0.36670 & 0.33036 & 0.31058 & 0.30161 & 0.26795 & 1.30337 & 0.21818 & 0.14984 \\ 0.38982 & 0.49756 & 0.38884 & 0.25970 & 0.21631 & 0.18960 & 0.20547 & 0.21818 & 1.35896 & 0.40546 \\ 1.19130 & 0.53130 & 0.25673 & 0.12181 & 0.10056 & 0.10394 & 0.07949 & 0.14984 & 0.40546 & 1.87499 \end{pmatrix} \tag{A6}$$

$$\sigma(C_{10}^{xx}) = \frac{1}{2} \begin{pmatrix} 0.06227 & 0.06696 & 0.07717 & 0.06789 & 0.05367 & 0.04573 & 0.04380 & 0.04000 & 0.04399 & 0.04282 \\ 0.06696 & 0.05169 & 0.04672 & 0.05820 & 0.03515 & 0.04005 & 0.03493 & 0.03484 & 0.03742 & 0.04779 \\ 0.07717 & 0.04672 & 0.04306 & 0.03165 & 0.03779 & 0.03846 & 0.03649 & 0.02842 & 0.03704 & 0.04862 \\ 0.06789 & 0.05820 & 0.03165 & 0.01329 & 0.02617 & 0.02075 & 0.01992 & 0.02348 & 0.03414 & 0.03951 \\ 0.05367 & 0.03515 & 0.03779 & 0.02617 & 0.01794 & 0.02525 & 0.02393 & 0.02584 & 0.03852 & 0.04134 \\ 0.04573 & 0.04005 & 0.03846 & 0.02075 & 0.02525 & 0.02411 & 0.02925 & 0.02626 & 0.03713 & 0.04289 \\ 0.04380 & 0.03493 & 0.03649 & 0.01992 & 0.02393 & 0.02925 & 0.01559 & 0.02102 & 0.03395 & 0.08205 \\ 0.04000 & 0.03484 & 0.02842 & 0.02348 & 0.02584 & 0.02626 & 0.02102 & 0.01335 & 0.06343 & 0.06364 \\ 0.04399 & 0.03742 & 0.03704 & 0.03414 & 0.03852 & 0.03713 & 0.03395 & 0.06343 & 0.04800 & 0.06472 \\ 0.04282 & 0.04779 & 0.04862 & 0.03951 & 0.04134 & 0.04289 & 0.08205 & 0.06364 & 0.06472 & 0.05289 \end{pmatrix} \tag{A7}$$

$$\sigma(C_{10}^{pp}) = \frac{1}{2} \begin{pmatrix} 0.06214 & 0.06643 & 0.07772 & 0.06788 & 0.04768 & 0.04391 & 0.04259 & 0.04056 & 0.05186 & 0.08923 \\ 0.06643 & 0.05137 & 0.04801 & 0.05855 & 0.03815 & 0.03913 & 0.03763 & 0.04426 & 0.04157 & 0.05005 \\ 0.07772 & 0.04801 & 0.04375 & 0.02885 & 0.04143 & 0.04081 & 0.03779 & 0.03377 & 0.04611 & 0.04425 \\ 0.06788 & 0.05855 & 0.02885 & 0.01525 & 0.03951 & 0.04228 & 0.03530 & 0.03175 & 0.04105 & 0.04120 \\ 0.04768 & 0.03815 & 0.04143 & 0.03951 & 0.02713 & 0.04368 & 0.03774 & 0.03449 & 0.04590 & 0.04482 \\ 0.04391 & 0.03913 & 0.04081 & 0.04228 & 0.04368 & 0.02850 & 0.03263 & 0.02584 & 0.03972 & 0.04305 \\ 0.04259 & 0.03763 & 0.03779 & 0.03530 & 0.03774 & 0.03263 & 0.01940 & 0.02624 & 0.03506 & 0.08196 \\ 0.04056 & 0.04426 & 0.03377 & 0.03175 & 0.03449 & 0.02584 & 0.02624 & 0.01186 & 0.06248 & 0.06368 \\ 0.05186 & 0.04157 & 0.04611 & 0.04105 & 0.04590 & 0.03972 & 0.03506 & 0.06248 & 0.04806 & 0.06442 \\ 0.08923 & 0.05005 & 0.04425 & 0.04120 & 0.04482 & 0.04305 & 0.08196 & 0.06368 & 0.06442 & 0.05315 \end{pmatrix} \tag{A8}$$

[1] J. Sperling and W. Vogel, Phys. Rev. Lett. **111**, 110503 (2013).
[2] L. Huaixin and Z. Youngde, Int. J. Theor. Phys. **39**, 447 (2000).
[3] R. Simon, S. Chaturvedi, and V. Srinivasan, J. Math. Phys. **40**, 3632 (1999).
[4] R. L. Haupt and S. E. Haupt, *Practical Genetic Algorithms*, 2nd ed. (John Wiley & Sons, Hoboken, New Jersey, 2004).

PHYSICAL REVIEW LETTERS

Multipartite Entanglement of a Two-Separable State

S. Gerke,[1,*] J. Sperling,[1,2] W. Vogel,[1] Y. Cai,[3] J. Roslund,[3] N. Treps,[3] and C. Fabre[3]

[1]*Arbeitsgruppe Theoretische Quantenoptik, Institut für Physik, Universität Rostock, D-18051 Rostock, Germany*
[2]*Clarendon Laboratory, University of Oxford, Parks Road, Oxford OX1 3PU, United Kingdom*
[3]*Laboratoire Kastler Brossel, UPMC-Sorbonne Universités, CNRS, ENS-PSL Research University,
Collège de France; 4 place Jussieu, 75252 Paris, France*

We consider a six-partite, continuous-variable quantum state that we have effectively generated by the parametric down-conversion of a femtosecond frequency comb. We show that, though this state is two-separable, i.e., it does not exhibit "genuine entanglement," it is undoubtedly multipartite entangled. The consideration of not only the entanglement of individual mode decompositions, but also of combinations of those, solves the puzzle and exemplifies the importance of studying different categories of multipartite entanglement.

Introduction.—Entanglement is, nowadays, a major subject of research in quantum physics, long after the pioneering contributions of Einstein, Podolsky, Rosen [1], and Schrödinger [2]. It is the main quantum resource in a vast number of applications in quantum information [3]. Entanglement witnesses uncover such quantum correlations [4,5] in either discrete variables, using measurements with photon counters, or in continuous variables by employing homodyne detection, for characterizing the quantum states of light.

Pure entangled states have been first considered in bipartite systems. The case of mixed correlated states turns out to be more involved. An intermediate situation between factorized and entangled states has been introduced, the separable states, which are statistical mixtures of factorized pure states [6]. A number of entanglement probes for continuous-variable systems have been studied [4,5], partial transpose being one of the most popular inseparability tests. These criteria are in most cases only sufficient to detect the different levels of correlation. The problem simplifies for bipartite Gaussian states, for which the partial transposition of the covariance matrix is a necessary and sufficient entanglement identifier [7–9].

The complexity of the separability problem increases substantially when one studies multipartite systems. In these situations, one has a rapidly increasing number of choices in the bunching of parties on which one searches for a possible factorization. Hence, the inseparability between the individual degrees of freedom exhibits a much richer and complex structure which begins to be studied [10–12]. For example, the difference between bipartite and multipartite systems is highlighted by the existence of multimode Gaussian states whose entanglement cannot be uncovered by the partial transposition [13,14].

As a special case, combinations of bipartitions of the total system are a subject of many studies. A state which is

not a statistical mixture of bipartite factorized density matrices (i.e., not two-separable) is also called "genuinely" multipartite entangled [15]. The detection of genuine entanglement is at the focus of attention [16–24]. This interest can be explained by the fact that genuine entanglement implies multipartite entanglement for every other separation of the modes. However, if a state does not exhibit this specific kind of entanglement (i.e., is two-separable), no conclusions on other forms of multipartite quantum correlations can be drawn. Thus, it is indispensable to study what happens beyond genuine entanglement. This is the subject of the present Letter.

In experiments, continuous-variable quantum correlated states have been produced by mixing, in an appropriate way, different squeezed states on beam splitters [25]. More recently, multimode Gaussian states (either spatial or frequency modes) have been directly generated by a multimode optical nonlinear device [26,27]. In the multifrequency case, the experimental determination of the full covariance matrix of a ten-mode "quantum frequency comb" has allowed us to uncover the complex structure of its quantum properties, in particular, the entanglement of all its possible partitions. [28–30].

In this Letter, we characterize states which are two-separable and yet exhibit a rich multipartite entanglement structure. For achieving this, we formulate different notions of separability and entanglement, then, we provide a method for qualifying them in a general case. Using this technique, we uncover the structure of multimode entanglement in an experimentally produced six-mode Gaussian state, using multimode parametric down-conversion of a femtosecond frequency-comb light source. Even though this state is two-separable, it includes all other forms of higher-order entanglement.

Combinations of modal partitions.—We consider multimode states which are based on an N-fold Hilbert space

$\mathcal{H} = \mathcal{H}_1 \otimes \ldots \otimes \mathcal{H}_N$, where $\mathcal{H}_j$ is the local Hilbert space of the jth mode. A particular K-partition $\mathcal{I}_1:\ldots:\mathcal{I}_K$ decomposes the set of modes, $\{1, \ldots, N\}$, into K nonempty, disjoint subsets $\mathcal{I}_k$ (for $k = 1, \ldots, K$). We will call such a partition an individual K-partition.

The corresponding pure factorized states are product states, $|s_{\mathcal{I}_1:\ldots:\mathcal{I}_K}\rangle = |a_{\mathcal{I}_1}\rangle \otimes \ldots \otimes |a_{\mathcal{I}_K}\rangle$, consisting of states $|a_{\mathcal{I}_1}\rangle \in \bigotimes\limits_{j \in \mathcal{I}_k} \mathcal{H}_j$. Subsequently, a mixed $\mathcal{I}_1:\ldots:\mathcal{I}_K$-separable state is defined as

$$\hat{\sigma}_{\mathcal{I}_1:\ldots:\mathcal{I}_K} = \int dP(s_{\mathcal{I}_1:\ldots:\mathcal{I}_K})|s_{\mathcal{I}_1:\ldots:\mathcal{I}_K}\rangle\langle s_{\mathcal{I}_1:\ldots:\mathcal{I}_K}|, \qquad (1)$$

where P is a classical probability distribution over the set of pure (continuous-variable) separable states.

A state is called K-separable if it can be written as a statistical mixture of separable states with respect to the different K-partitions $\mathcal{I}_1:\ldots:\mathcal{I}_K$,

$$\hat{\sigma}_K = \sum_{\mathcal{I}_1:\ldots:\mathcal{I}_K} p_{\mathcal{I}_1:\ldots:\mathcal{I}_K}\hat{\sigma}_{\mathcal{I}_1:\ldots:\mathcal{I}_K}, \qquad (2)$$

where $p_{\mathcal{I}_1:\ldots:\mathcal{I}_K}$ are probabilities and $\hat{\sigma}_{\mathcal{I}_1:\ldots:\mathcal{I}_K}$ are the corresponding $\mathcal{I}_1:\ldots:\mathcal{I}_K$-separable states in Eq. (1). We will refer to this combination of individual K-partitions as a convex combination of K-partitions. A state is called K-entangled if it cannot be written in the manner specified in Eq. (2). In particular, a state which is not "biseparable" ($K = 2$) is precisely the genuinely multipartite entangled state studied in the literature.

Figure 1 shows the different kinds of separability in the tripartite scenario, $N = 3$, in a schematic Venn diagram. Needless to say, it is impossible to illustrate the full structure of the partitions in infinite dimensional Hilbert spaces. The circles represent pure states that are factorizable with respect to a defined partitioning. These states have to be extremal points of the convex sets, since they are not combinations of any other states. The highlighted areas in between these points represent the considered convex hull of mixed separable states. States lying outside of these sets are entangled in that particular notion for arbitrary, compound Hilbert spaces.

For instance for $K = 3$, we have the statistical mixture of pure, fully separable states $|s_{\{1\}:\{2\}:\{3\}}\rangle$ (red area; left pattern in top row of Fig. 1). In order to get an area, we selected three pure state representatives (D, E, and F) from the equivalence class of all three-separable pure states. Any state that is outside this convex (red) area symbolizes a three-entangled state.

The $K = 2$-separable states (green area; center pattern in top row of Fig. 1) lie in the convex hull of three individual bipartitions, which are depicted in the middle row of Fig. 1. We select the point H to be one pure state representative $|s_{\{1,2\}:\{3\}}\rangle$, which is not of the form $|s_{\{1\}:\{2\}:\{3\}}\rangle$, $|s_{\{1\}:\{2,3\}}\rangle$, or $|s_{\{1,3\}:\{2\}}\rangle$. Similarly, the states represented by point B or points C and G are exclusively separable with
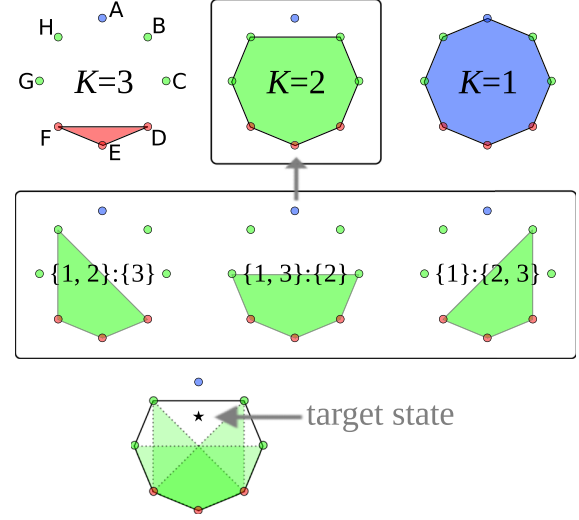

FIG. 1.   Partitioning of a tripartite system. The circles indicate pure state representatives for different notions of separability or entanglement (distinguished by the lightness [color]). The top row depicts the convex sets of K-partitions. The $K = 2$ case is a convex combination of the individual bipartitions $\mathcal{I}_1:\mathcal{I}_2$, which are given in the pattern in the middle row. The bottom shows the overlay of the individual bipartitions (dashed bordered sets) as an inset into the convex set of all bipartitions (solid borders). The target state (filled star) is a convex combination of two-partite separable states. It is, therefore, two-separable, but three-entangled.

respect to the individual partition $\{1\}:\{2,3\}$ or $\{1,3\}:\{2\}$, respectively, forming nonidentical sets of mixed separable states of the individual partitions (middle row). For symmetry reasons, we consider two points (G and C) for the partition $\{1,3\}:\{2\}$. All of them are two-separable in the convex combination of all bipartitions (top row, center pattern).

For $K = 1$, we get all states (blue area, right pattern in top row of Fig. 1). The point A serves as an element of the equivalence class of all pure, two-entangled states. Those are nonfactorizable. As every mixed state is trivially in the full partition $\{1,2,3\}$, this (blue) set includes all quantum states.

In the bottom row of Fig. 1, we also show the three individual bipartitions $\{1,2\}:\{3\}$, $\{1,3\}:\{2\}$, and $\{1\}:\{2,3\}$ (dashed borders) included into the convex combination of biseparable states (solid border). Our target state (indicated by a star) is entangled with respect to all individual bipartitions, but it is separable with respect to the convex combination of bipartitions. These states are particularly interesting as they are not genuinely multipartite entangled (two-separable). We will show explicitly for a six-partite system, $N = 6$, that such states still exhibit rich multipartite entanglement properties.

Entanglement criteria for convex combinations.—A criterion for detecting entanglement of states is based on the entanglement witnesses [31]. It can be formulated as follows: A state is entangled if a Hermitian operator $\hat{L}$

exists, whose expectation value is smaller than the minimal attainable value for all separable states $\hat{\sigma}$ [32],

$$\langle \hat{L} \rangle < \inf_{\hat{\sigma}} \{ \mathrm{tr}(\hat{L}\,\hat{\sigma}) \}. \qquad (3)$$

This criterion is general and covers any kind of inseparability. It applies, therefore, to either individual partitions or convex combinations.

Let us show that the bound in (3) can be achieved by pure state representatives. For this reason, we apply the following property of convex (statistical) mixtures:

$$\inf \left\{ \int dP(x)x \Big| \int dP = 1 \quad \text{and} \quad P \geq 0 \right\} = \inf_{x} \{x\}. \quad (4)$$

This allows us to derive the lower bound in (3) for K-separable states,

$$\inf_{\hat{\sigma}_K} \{ \mathrm{tr}(\hat{L}\hat{\sigma}_K) \} \overset{(2),(4)}{=} \min_{\mathcal{I}_1:\dots:\mathcal{I}_K} \inf_{\hat{\sigma}_{\mathcal{I}_1:\dots:\mathcal{I}_K}} \{ \mathrm{tr}(\hat{L}\hat{\sigma}_{\mathcal{I}_1:\dots:\mathcal{I}_K}) \}$$

$$\overset{(1),(4)}{=} \min_{\mathcal{I}_1:\dots:\mathcal{I}_K} \inf_{|s_{\mathcal{I}_1:\dots:\mathcal{I}_K}\rangle}$$

$$\times \{ \langle s_{\mathcal{I}_1:\dots:\mathcal{I}_K} | \hat{L} | s_{\mathcal{I}_1:\dots:\mathcal{I}_K} \rangle \}.$$

Equation labels over the equal signs indicate that those equations have been used for rewriting. Thus, the minimal expectation value of $\hat{L}$ for separable states in convex combinations of K-partitions is identical to the least expectation value $(\min_{\mathcal{I}_1:\dots:\mathcal{I}_K})$ achievable by pure states of the individual partitions $\mathcal{I}_1:\dots:\mathcal{I}_K$ $(\inf_{|s_{\mathcal{I}_1:\dots:\mathcal{I}_K}\rangle})$.

The minimization of $\langle s_{\mathcal{I}_1:\dots:\mathcal{I}_K} | \hat{L} | s_{\mathcal{I}_1:\dots:\mathcal{I}_K} \rangle$ for pure, $\mathcal{I}_1:\dots:\mathcal{I}_K$-separable states has been treated in Ref. [32]. There, so-called "separability eigenvalue equations" have been derived. The solution of those equations for a given observable $\hat{L}$ yields the minimal separability eigenvalue $g_{\mathcal{I}_1:\dots:\mathcal{I}_K}^{\min}$, which is also the desired infimum for separable states of the individual K-partition $\mathcal{I}_1:\dots:\mathcal{I}_K$. We can conclude: A state is inseparable with respect to the convex combination of all K-partitions (K-entangled), if and only if there exists a Hermitian operator $\hat{L}$, such that

$$\langle \hat{L} \rangle < g_K^{\min} = \min_{\mathcal{I}_1:\dots:\mathcal{I}_K} \{ g_{\mathcal{I}_1:\dots:\mathcal{I}_K}^{\min} \}. \qquad (5)$$

Although this condition clearly differs from the approach for individual partitions [30], it is remarkable that we can use a similar calculus. The method of separability eigenvalues was introduced to uncover entanglement of individual K-partitions $\mathcal{I}_1:\dots:\mathcal{I}_K$, via $\langle \hat{L} \rangle < g_{\mathcal{I}_1:\dots:\mathcal{I}_K}^{\min}$ [32]. Now, it serves for detecting entanglement among convex combinations of all K-partitions [inequality (5)].

Witnessing multimode Gaussian states.—A Gaussian state is fully described by its covariance matrix. In the following, we will use the vector

$$\hat{\boldsymbol{\xi}} = (\hat{x}_1, \dots, \hat{x}_N, \hat{p}_1, \dots, \hat{p}_N)^T, \qquad (6)$$

including the amplitude $(\hat{x}_j)$ and phase $(\hat{p}_j)$ quadratures of all possible modes $(j = 1, \dots, N)$. The covariance matrix C

of a Gaussian state can be written in terms of the symmetrically ordered elements $C^{ij} = \langle \hat{\xi}_i \hat{\xi}_j + \hat{\xi}_j \hat{\xi}_i \rangle / 2 - \langle \hat{\xi}_i \rangle \langle \hat{\xi}_j \rangle$. As local displacements do not affect the entanglement, it is sufficient to analyze the covariance matrix of a Gaussian state, assuming $\langle \hat{\xi}_j \rangle = 0$. Thus, the most general form of a Gaussian test operator $\hat{L}$ is the quadratic combination

$$\hat{L} = \sum_{i,j=1}^{2N} M_{ij} \hat{\xi}_i \hat{\xi}_j, \qquad (7)$$

with a symmetric, positive definite $2N \times 2N$ matrix $M = (M_{ij})_{i,j=1}^{2N}$. Note that Williamson's theorem allows us to diagonalize such a matrix M into a form $\mathrm{diag}(\lambda_1, \dots, \lambda_N, \lambda_1, \dots, \lambda_N)$ in terms of symplectic operations, see, e.g., [33].

The minimal separability eigenvalue of $\hat{L}$ in Eq. (7) for an individual partition $\mathcal{I}_1:\dots:\mathcal{I}_K$ is given by [30]

$$g_{\mathcal{I}_1:\dots:\mathcal{I}_K}^{\min} = \sum_{j=1}^{K} \sum_{k=1}^{|\mathcal{I}_j|} \lambda_k^{\mathcal{I}_j}, \qquad (8)$$

where $|\mathcal{I}_j|$ is the cardinality of $\mathcal{I}_j$, and $\lambda_k^{\mathcal{I}_j}$ are the diagonal values of the Williamson decomposition of the submatrix which solely consists of the rows and columns of M that are in the index set $\mathcal{I}_j$ (see, also, the Supplemental Material of Ref. [30]). Finally, the entanglement condition (5) is given by the bound

$$g_K^{\min} = \min_{\mathcal{I}_1:\dots:\mathcal{I}_K} \{ g_{\mathcal{I}_1:\dots:\mathcal{I}_K}^{\min} \text{ in Eq.(8)} \}. \qquad (9)$$

Hence, we have formulated an infinite number (for any positive, symmetric matrix M) of multipartite K-entanglement probes in an analytical form. This includes, as a subclass, Gaussian tests for two-entanglement, $g_{K=2}^{\min} > \langle \hat{L} \rangle$, which have been recently studied [24]. The analytical minima $g_K^{\min}$ in Eq. (9) are needed in order to correctly apply our entanglement condition (5).

Let us relate our method with other covariance based entanglement probes. For example, in [34,35], entanglement tests are constructed based on the partial transposition. As each mode can be either transposed or not, those criteria are only sensitive to individual bipartitions and, in a convex combination, two-entanglement. As our operator $\hat{L}$ [Eq. (7)] is defined in the most general second-order-moment form, it is well suited for uncovering entanglement in Gaussian states of any partitioning. Even if a test for two-entanglement fails, we can still probe for $K \geq 3$-entanglement. Other methods for inferring multipartite entanglement were introduced, e.g., in [36], based on semi-definite problems. Those approaches are limited to certain states, e.g., Gaussian ones, or they are computationally demanding. Extending the operator in Eq. (7) beyond quadratic terms and solving its separability eigenvalue equations generalizes our method, so it can be

used to verify entanglement, also, in non-Gaussian states by inequality (3).

In order to get the best entanglement signature of all test operators $\hat{L}$ in terms of matrices M [Eq. (7)], we take the analytical solutions in Eqs. (8) and (9) and numerically minimize the signed significances

$$\Sigma_{\mathcal{I}_1:\ldots:\mathcal{I}_K} = \frac{\langle \hat{L} \rangle - g^{\min}_{\mathcal{I}_1:\ldots:\mathcal{I}_K}}{\Delta\langle \hat{L} \rangle} \quad \text{and} \quad \Sigma_K = \frac{\langle \hat{L} \rangle - g^{\min}_K}{\Delta\langle \hat{L} \rangle},$$

$$(10)$$

where $\Delta\langle \hat{L} \rangle$ denotes the experimental error of $\langle \hat{L} \rangle$, by finding the optimal matrix M for each of those significances. The signed significance is negative, $\Sigma_\chi < 0$, if the state is entangled with respect to the given notion of separability, $\chi = K$ or $\chi = \mathcal{I}_1:\ldots:\mathcal{I}_K$, which is certified with a significance of $|\Sigma_\chi|$ standard deviations. The numerical minimization was performed with a genetic algorithm [30] which can, in principle, not only find local minima, but also global ones [37]. Hence, one could claim that a positive value Σ_χ corresponds to a χ-separable covariance matrix. However, we will more carefully state, in such a case, that no χ-entanglement can be detected. As the resulting minima Σ from the genetic algorithm are upper bounds for Σ_χ, $\Sigma_\chi < 0$ is a reliable bound to the full entanglement, and it cannot overestimate the entanglement in our system.

Characterization of the SPOPO multimode quantum state.—The highly multimode light state that we consider in the following is a femtosecond frequency comb of zero mean value spanning over roughly $\sim 10^5$ individual equally spaced frequency components, generated by parametric down-conversion of a pump frequency comb in a synchronously pumped optical parametric oscillator (SPOPO). Details on its experimental generation and characterization can be found in Refs. [28,29] and [38]. The 12×12 covariance matrix C, containing the quadrature noise variances in six different frequency bands covering the whole spectrum of the SPOPO state, as well as the correlations between them, has been experimentally determined. The SPOPO state, being generated by an intense pump laser in a weakly nonlinear medium, is Gaussian to a very good approximation. Thus, the covariance matrix contains the whole information about the generated quantum state, at least within the frequency resolution given by the width of the frequency bands used in the measurements. The generated state is clearly mixed, as its purity, $\text{tr}\hat{\rho}^2 = (\det C)^{-1/2} = 86.4\%$, is below one.

Entanglement structure of a six-mode SPOPO state.—For an $N = 6$-mode state, 203 possible individual partitions exist. That is one trivial partition $\mathcal{I}_1 = \{1,\ldots,6\}$, 31 bipartitions $\mathcal{I}_1:\mathcal{I}_2$, 90 tripartitions, 65 four-partitions, 15 five-partitions, and one six-partition $\{1\}:\ldots:\{6\}$. Hence, we have six convex combinations of K-partitions.

The results of our analysis are shown in Fig. 2 in terms of the minimized signed significances in Eq. (10). The trivial partition $K = 1$ yields $\Sigma_{K=1} > 0$, which means that the measured covariance is a physical one. The value $\Sigma_{K=2} > 0$
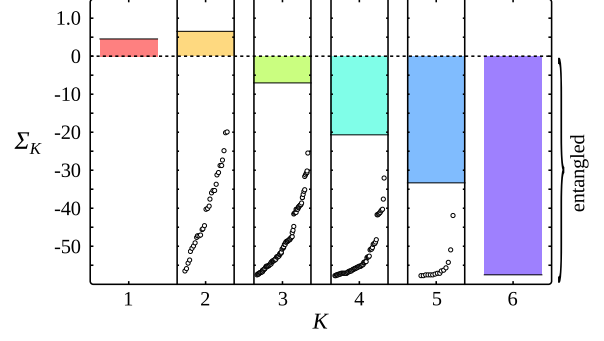

FIG. 2.　Signed significance Σ_K (bars), for $1 \leq K \leq 6$, calculated from the data of the SPOPO state. The insets for $2 \leq K \leq 5$ give the values for the individual partitions, $\Sigma_{\mathcal{I}_1:\ldots:\mathcal{I}_K}$ (circles), sorted in increasing order. For better visibility, the positive part of the ordinate has a different scaling than the negative (entangled) part. Despite no signature of two-entanglement, $\Sigma_2 > 0$, the state shows highly significant other forms of multipartite entanglement.

shows that no detectable two-entanglement exists in the SPOPO quantum frequency comb. Yet, for all $K \geq 3$, K-entanglement is verified with a significance of at least seven standard deviations, $\Sigma_{K>2} < -7$. Such types of multipartite entanglement are not accessible with entanglement probes that are only sensitive to two-entanglement.

Considering the circles in the insets for $1 \leq K \leq 5$ in Fig. 2, it can be seen that the same six-mode state is entangled with respect to all nontrivial, individual partitions—even for $K = 2$. Therefore, the SPOPO state is entangled with respect to any individual bipartition, even though it cannot be identified as a two-entangled state: The subtle structures of multipartite entanglement are invisible for genuine entanglement probes.

Here, we clearly see that entanglement of some or even all individual partitions $\mathcal{I}_1:\ldots:\mathcal{I}_K$ of the length K does not necessarily imply K-entanglement. Rather, it is the convex combination of the individual partitions that is responsible for the separability or inseparability. The inverse, however, is true: K-entanglement implies entanglement with respect to all individual K-partitions. This follows from the condition (5) by taking a proper test operator $\hat{L}$ for the convex combination and the same $\hat{L}$ for every individual K-partition, as $g^{\min}_K \leq g^{\min}_{\mathcal{I}_1:\ldots:\mathcal{I}_K}$. Finally, let us stress that this approach can be extended to study other convex combinations of some individual partitions which are not limited by a fixed K value.

Summary and conclusion.—We have studied different forms of K-party entanglement in multimode states. An analytical approach to construct the corresponding entanglement tests was derived and further elaborated for covariance based entanglement probes. To optimize over the resulting infinite set of all analytical Gaussian witnesses, a numerical optimization was performed. This approach allows us to classify entanglement in Gaussian states with an arbitrary number of modes.

We applied this approach to a parametrically generated multimode frequency comb. It was shown, for a six-mode

example, that our system shows an interesting form of entanglement. That is, the SPOPO state turns out to be a biseparable state which is K-entangled for any $K = 3, \ldots, 6$. Moreover, we detected entanglement with respect to all individual partitions, even all the individual bipartitions. Thus, the absence of so-called genuine entanglement does not give any insight into the entanglement structure.

This work proves of great interest for investigating entanglement beyond two-entanglement in highly multipartite systems. A lot of questions remain to be investigated concerning other possible types of multipartite entanglement and, in particular, their relation to quantum computation and communication protocols between multiple parties. Our construction of general entanglement criteria, likely to access multipartite quantum correlations beyond bipartitions, provides a good starting tool for tackling such problems.

As a comment to the Einstein-Podolsky-Rosen paradox [1], Schrödinger emphasized that a compound quantum system includes more information than provided by the individual subsystems [2]. Considering our scenario at hand, we may extend such a statement. Namely, multipartite entanglement is much richer than the entanglement one can infer from bipartitions only.

---

*stefan.gerke@uni-rostock.de

[1] A. Einstein, B. Podolsky, and N. Rosen, Can quantum-mechanical description of physical reality be considered complete?, Phys. Rev. **47**, 777 (1935).

[2] E. Schrödinger, Die gegenwärtige Situation in der Quantenmechanik, Naturwiss. **23**, 807 (1935); **23**, 823 (1935); **23**, 844 (1935).

[3] S. Braunstein and P. van Loock, Quantum information with continuous variables, Rev. Mod. Phys. **77**, 513 (2005).

[4] R. Horodecki, P. Horodecki, M. Horodecki, and K. Horodecki, Quantum entanglement, Rev. Mod. Phys. **81**, 865 (2009).

[5] O. Gühne and G. Tóth, Entanglement detection, Phys. Rep. **474**, 1 (2009).

[6] R. F. Werner, Quantum states with Einstein-Podolsky-Rosen correlations admitting a hidden-variable model, Phys. Rev. A **40**, 4277 (1989).

[7] A. Peres, Separability Criterion for Density Matrices, Phys. Rev. Lett. **77**, 1413 (1996).

[8] R. Simon, Peres-Horodecki Separability Criterion for Continuous Variable Systems, Phys. Rev. Lett. **84**, 2726 (2000).

[9] L.-M. Duan, G. Giedke, J. I. Cirac, and P. Zoller, Inseparability Criterion for Continuous Variable Systems, Phys. Rev. Lett. **84**, 2722 (2000).

[10] M. Huber and J. I. de Vicente, Structure of Multidimensional Entanglement in Multipartite Systems, Phys. Rev. Lett. **110**, 030501 (2013).

[11] A. A. Valido, F. Levi, and F. Mintert, Hierarchies of multipartite entanglement for continuous-variable states, Phys. Rev. A **90**, 052321 (2014).

[12] F. Shahandeh, J. Sperling, and W. Vogel, Structural Quantification of Entanglement, Phys. Rev. Lett. **113**, 260502 (2014).

[13] R. F. Werner and M. M. Wolf, Bound Entangled Gaussian States, Phys. Rev. Lett. **86**, 3658 (2001).

[14] J. DiGuglielmo, A. Samblowski, B. Hage, C. Pineda, J. Eisert, and R. Schnabel, Experimental Unconditional Preparation and Detection of a Continuous Bound Entangled State of Light, Phys. Rev. Lett. **107**, 240503 (2011).

[15] V. Coffman, J. Kundu, and W. K. Wootters, Distributed entanglement, Phys. Rev. A **61**, 052306 (2000).

[16] M. Horodecki, P. Horodecki, and R. Horodecki, Separability of n-particle mixed states: Necessary and sufficient conditions in terms of linear maps, Phys. Lett. A **283**, 1 (2001).

[17] P. Wocjan and M. Horodecki, Characterization of combinatorially independent permutation separability criteria, Open Syst. Inf. Dyn. **12**, 331 (2005).

[18] C. S. Yu and H. S. Song, Separability criterion of tripartite qubit systems, Phys. Rev. A **72**, 022333 (2005).

[19] A. Hassan and P. Joag, Separability criterion for multipartite quantum states based on the Bloch representation of density matrices, Quantum Inf. Comput. **8**, 773 (2008).

[20] B. C. Hiesmayr, M. Huber, and Ph. Krammer, Two computable sets of multipartite entanglement measures, Phys. Rev. A **79**, 062308 (2009).

[21] M. Huber, F. Mintert, A. Gabriel, and B. C. Hiesmyr, Detection of High-Dimensional Genuine Multipartite Entanglement of Mixed States, Phys. Rev. Lett. **104**, 210501 (2010).

[22] L. K. Shalm, D. R. Hamel, Z. Yan, C. Simon, K. J. Resch, and T. Jennewein, Three-photon energy-time entanglement, Nat. Phys. **9**, 19 (2013).

[23] J. T. Barreiro, J.-D. Bancal, P. Schindler, D. Nigg, M. Hennrich, T. Monz, N. Gisin, and R. Blatt, Demonstration of genuine multipartite entanglement with device-independent witnesses, Nat. Phys. **9**, 559 (2013).

[24] E. Shchukin and P. van Loock, Generalized conditions for genuine multipartite continuous-variable entanglement, Phys. Rev. A **92**, 042328 (2015).

[25] M. Yukawa, R. Ukai, P. van Loock, and A. Furusawa, Experimental generation of four-mode continuous-variable cluster states, Phys. Rev. A **78**, 012301 (2008).

[26] M. Pysher, Y. Miwa, R. Shahrokhshahi, R. Bloomer, and O. Pfister, Parallel Generation of Quadripartite Cluster Entanglement in the Optical Frequency Comb, Phys. Rev. Lett. **107**, 030505 (2011).

[27] M. Chen, N. C. Menicucci, and O. Pfister, Experimental Realization of Multipartite Entanglement of 60 Modes of a Quantum Optical Frequency Comb, Phys. Rev. Lett. **112**, 120505 (2014).

[28] R. Medeiros de Araújo, J. Roslund, Y. Cai, G. Ferrini, C. Fabre, and N. Treps, Full characterization of a highly multimode entangled state embedded in an optical frequency comb using pulse shaping, Phys. Rev. A **89**, 053828 (2014).

[29] J. Roslund, R. Medeiros de Araújo, Shifeng Jiang, C. Fabre, and N. Treps, Wavelength-multiplexed quantum networks

with ultrafast frequency combs, Nat. Photonics **8**, 109 (2014).

[30] S. Gerke, J. Sperling, W. Vogel, Y. Cai, J. Roslund, N. Treps, and C. Fabre, Full Multipartite Entanglement of Frequency-Comb Gaussian States, Phys. Rev. Lett. **114**, 050501 (2015).

[31] M. Horodecki, P. Horodecki, and R. Horodecki, Separability of mixed states: Necessary and sufficient conditions, Phys. Lett. A **223**, 1 (1996).

[32] J. Sperling and W. Vogel, Multipartite Entanglement Witnesses, Phys. Rev. Lett. **111**, 110503 (2013).

[33] R. Simon, S. Chaturvedi, and V. Srinivasan, Congruences and canonical forms for a positive matrix: Application to the Schweinler-Wigner extremum principle, J. Math. Phys. (N.Y.) **40**, 3632 (1999).

[34] P. van Loock and A. Furusawa, Detecting genuine multipartite continuous-variable entanglement, Phys. Rev. A **67**, 052315 (2003).

[35] F. Toscano, A. Saboia, A. T. Avelar, and S. P. Walborn, Systematic construction of genuine-multipartite-entanglement criteria in continuous-variable systems using uncertainty relations, Phys. Rev. A **92**, 052316 (2015).

[36] P. Hyllus and J. Eisert, Optimal entanglement witnesses for continuous-variable systems, New J. Phys. **8**, 51 (2006).

[37] R. L. Haupt and S. E. Haupt, *Practical Genetic Algorithms*, 2nd ed. (John Wiley & Sons, Hoboken, New Jersey, 2004).

[38] G. Patera, G. De Valcárcel, N. Treps, and C. Fabre, Quantum theory of synchronously pumped type I optical parametric oscillators: Characterization of the squeezed supermodes, Eur. Phys. J. D **56**, 123 (2010).

Numerical Construction of Multipartite Entanglement Witnesses

S. Gerke[*] and W. Vogel

Arbeitsgruppe Theoretische Quantenoptik, Institut für Physik, Universität Rostock,
D-18051 Rostock, Germany

J. Sperling

Clarendon Laboratory, University of Oxford, Parks Road, Oxford OX1 3PU, United Kingdom

Entanglement in multipartite systems is a key resource for quantum information and communication protocols, making its verification in complex systems a necessity. Because an exact calculation of arbitrary entanglement probes is impossible, we derive and implement a numerical method to construct multipartite witnesses to uncover entanglement in arbitrary systems. Our technique is based on a substantial generalization of the power iteration—an essential tool for computing eigenvalues—and it is a solver for the separability eigenvalue equations, enabling the general formulation of optimal entanglement witnesses. Beyond our rigorous derivation and direct implementation of this method, we apply our approach to several examples of complexly quantum-correlated states and benchmark its general performance. Consequently, we provide a generally applicable numerical tool for the identification of multipartite entanglement.

I. INTRODUCTION

Quantum entanglement is one of the most fundamental concepts in physics. It was introduced in the pioneering works of Einstein *et al.* [1] and Schrödinger [2]. The pure existence of this quantum phenomenon challenged previously established notions of correlations and paved the way towards a new interpretation of the nature of physics. Eventually, this led to new protocols used in quantum computing and communication, which utilize the resources of entangled quantum states [3]. Examples of such classically infeasible tasks are quantum teleportation [4] and dense coding [5]. Other early protocols concern quantum key distribution, known as BB84 [6] and E91 [7], and significantly improve communication security. Therefore, entanglement plays a key role in fundamental physics and technology-oriented applications.

A primary concern in the research of entanglement is the actual detection of this quantum correlation. Since a lot of protocols for quantum technologies rely on the presence of entanglement, the question of whether or not an experimentally generated state is entangled has become a highly relevant topic. However, determining entanglement of general states—likewise its counterpart, separability—is an NP-hard problem [8,9].

Another challenge specific to multipartite systems is the possibility that classical and quantum correlations can be differently distributed among the parties of an ensemble of systems. This leads to complex structures of multipartite entanglement; see, e.g., Refs. [10–12]. Most notably, there are inequivalent forms of entanglement, which need to be distinguished. These are already present in systems of only three qubits, such as the prominent GHZ and *W* states [13]. Beyond that, current experiments become more and more capable of producing large-scale entanglement [14–16]. However, while entanglement is vital for characterizing such experiments, the tools to uncover highly quantum-correlated systems are rather limited, and the general verification remains an open problem.

Still, several criteria have been developed to successfully determine entanglement in bipartite and multipartite systems; see Refs. [17–19] for thorough lists of these entanglement tests. A prominent example is the partial transposition criterion [20], which has been generalized to general positive, but not completely positive, maps [21]. Furthermore, such maps are equivalent to entanglement witnesses [21–24]. A crucial point of using witness operators is their nature of being observables, which can be directly implemented in experiments. Another main advantage is that

---
[*]stefan.gerke@uni-rostock.de

no full quantum state reconstruction is required to apply such witnesses. Rather, a few measurements of the observable can be sufficient to experimentally uncover entanglement [25–27].

Consequently, witnesses have become a widely applied method for detecting entanglement. Their usefulness for quantum technologies has been shown to be promising by detecting entanglement of multipartite cluster states in theory and experiments; see, e.g., Refs. [28,29]. Also, witnesses are not limited to specific systems; for example, they apply to trapped ions [30] as well as hybrid systems, which correlate vastly different degrees of freedom [31]. In addition, device-independent witnesses have been proposed for a robust verification of entanglement [32]. For instance, such device-independent witnesses can be constructed via so-called matrix-product extensions [33].

An entanglement witness has a non-negative expectation value for separable states as it defines a hyperplane bisecting the set of states—one part containing at least all separable states and another part including exclusively entangled ones. In order to maximize the detectable range of entangled states, optimal witnesses have been introduced [34–38]. A universally applicable approach is the method of separability eigenvalue equations (SEEs), which enables the construction of optimal witnesses in the bipartite and multipartite scenarios [39,40]. The solution of the SEEs renders it possible, in principle, to formulate all entanglement witnesses. However, because of the general complexity of the separability problem, exact solutions are only known for specific scenarios. Still, this has already led to deeper insights into the complex forms of experimentally generated multipartite entanglement [41,42].

Once a witness-construction approach is realized, it can be applied to different physical systems and reveal more insight than the basic indication of entanglement. For example, entanglement in systems of indistinguishable particles can significantly differ from the case of distinguishable particles, but witnessing can be done in a similar manner [43–45]. Furthermore, the quantification of entanglement can be based on witnesses as well [46–49]. This also includes entanglement tests for the so-called Schmidt number in the bipartite systems [50–52], as well as its multipartite extension [12,53].

Since calculating witnesses is a hard problem and exact solutions are rare, a numerical approach is favorable. Numerical methods often use the convexity of the set of separable states. Prime examples are approaches based on semidefinite programming, used for the general, convex optimization of linear problems [54]. The formulation of witnesses has the structure of exactly that kind of problem. Thus, semidefinite programming is a frequently applied method for probing entanglement [55–60]. However, this approach addresses a general class of optimization tasks and is not specifically designed to address the properties of entangled systems. Consequently, such a general approach

cannot present an optimal strategy to construct entanglement witnesses for arbitrary systems. Moreover, numerical standard approaches to solve the eigenvalue equations (EE), such as the well-known power iteration (PI) [61], do not apply to the construction of entanglement witnesses via the nonlinear SEEs.

In this contribution, we devise a numerical approach to construct multipartite entanglement witnesses by finding the maximal separability eigenvalue. Based on the properties of the SEEs, the analytical background is derived for our technique—termed the separability power iteration (SPI). As a special case, our approach includes the PI, which returns the maximal solution of EEs. We implement the SPI algorithm numerically. This is used to demonstrate that the directed design of our numerical approach is an efficient method compared to standard techniques applicable to arbitrary optimization problems. To outline possible applications, we use our algorithm, for example, to verify entanglement of weakly correlated, i.e., bound-entangled, states in the bipartite and multipartite scenarios. Therefore, an accessible algorithm is provided, which renders it possible to construct entanglement probes for certifying multipartite quantum correlations.

We organize the paper as follows. Preliminary statements are made in Sec. II. Here, we introduce the framework used throughout the contribution and recollect information about entanglement. In Sec. III, the SPI algorithm to find the maximal separability eigenvalue of a positive operator is introduced. Proofs for the working behavior and the convergence of the algorithm are given. We analyze the performance of our algorithm in Sec. IV. In Sec. V, entanglement in a selection of bound-entangled states is analyzed. In Sec. VI, we discuss the connection between the SPI and experimental measurements as well as other entanglement criteria and show the broad applicability of our newly devised method to different problems. We conclude in Sec. VII, where we also summarize our results.

II. PRELIMINARIES

In this section, we revisit multipartite entanglement and its verification. In particular, we concentrate on the previously introduced method of SEEs and its relation to standard EEs, which is essential for the following investigations. Eventually, we summarize these methods in the context of the considered problem, which is solved by our numerical approach, the SPI.

A. Multipartite entanglement

Say $\mathcal{S}$ is the set of all pure states that are separable in an N-partite system. This means that the elements of $\mathcal{S}$ take a tensor-product form,

$$|a_1, \ldots, a_N\rangle = \bigotimes_{j=1,\ldots,N} |a_j\rangle, \tag{1}$$

where $|a_j\rangle \in \mathcal{H}_j$ is an arbitrary state in the jth subsystem and $\langle a_j|a_j\rangle = 1$ for $j = 1, ..., N$. Furthermore, a mixed state $\hat{\sigma}$ is separable by definition [62] if it can be written as

$$\hat{\sigma} = \int dP(a_1, ..., a_N)|a_1, ..., a_N\rangle\langle a_1, ..., a_N|, \quad (2)$$

where P is a classical probability distribution over $\mathcal{S}$. Conversely, a state $\hat{\rho}$ is defined to be entangled if it cannot be expressed in this way.

The given form of separability is also called full separability of an N-partite system. To consider instances of partial entanglement, we can assume that each of the N parties is itself a composition of K_j subsystems. This allows us to study arbitrary forms of partial separability—e.g., N-separability—in a system which, in total, consists of $K_1 + \cdots + K_N$ subsystems. It is also worth mentioning that continuous-variable entanglement can always be detected in finite-dimensional subspaces [63]. Hence, we can restrict ourselves to Hilbert spaces with a finite dimensionality, $d_j = \dim \mathcal{H}_j < \infty$.

B. Entanglement witnesses

Based on the convexity of the set of separable states [cf. Eq. (2)], so-called entanglement witnesses $\hat{W}$ have been introduced [21–23]. They fulfill the property that for all separable states $\hat{\sigma}$, the inequality $\mathrm{tr}(\hat{\sigma}\hat{W}) \geq 0$ holds true. Consequently, entanglement is detected if this inequality is violated, $\mathrm{tr}(\hat{\rho}\hat{W}) < 0$. In particular, it has been shown that witness operators can be written in the form [24,39]

$$\hat{W} = g_{\max}\hat{1} - \hat{L}, \quad (3)$$

where $g_{\max}$ is the maximal expectation value of $\hat{L}$ for separable states.

Therefore, the following approach is equivalent to the method of witnessing [39,40]: For any entangled state $\hat{\rho}$, there is a Hermitian operator $\hat{L}$ such that the entanglement of $\hat{\rho}$ is certified by the criterion

$$\mathrm{tr}(\hat{L}\hat{\rho}) > g_{\max}. \quad (4)$$

The other way around, a state $\hat{\sigma}$ is separable if for all $\hat{L}$ the inequality $\mathrm{tr}(\hat{L}\hat{\sigma}) \leq g_{\max}$ holds true. Moreover, it has been shown that it is sufficient to consider (normalized) positive-definite operators only; see, e.g., Ref. [39]. We refer to operators satisfying

$$\hat{L} = \hat{L}^\dagger > 0 \quad (5)$$

as positive operators in this work. To determine the bound $g_{\max}$, applied in the entanglement criterion (4), we introduce the SEEs [39,40] (see also Appendix E).

C. Separability eigenvalue equations

There are two equivalent forms of the SEEs [40]. For this work, the more important representation of the SEE reads

$$\hat{L}|a_1, ..., a_N\rangle = g|a_1, ..., a_N\rangle + |\chi\rangle. \quad (6)$$

Here, the vector $|\chi\rangle$ is N orthogonal to $|a_1, ..., a_N\rangle$ Namely, we have $\langle a_1, ..., a_{j-1}, x, a_{j+1}, ..., a_N|\chi\rangle = 0$ for all $j = 1, ..., N$ and for all $|x\rangle \in \mathcal{H}_j$. The normalized vector $|a_1, ..., a_N\rangle$ is the separability eigenvector. The real value g is the separability eigenvalue, which can also be written as the expectation value of $\hat{L}$ with respect to the separability eigenvector,

$$g = \langle a_1, ..., a_N|\hat{L}|a_1, ..., a_N\rangle. \quad (7)$$

The disturbance to a standard EE, created by the N-orthogonal vector $|\chi\rangle$, couples the individual subsystems represented by the states $|a_j\rangle$. Thereby, it creates a highly nonlinear equation, which, in general, cannot be solved straightforwardly. Furthermore, we can relate the separability eigenvalues to our necessary and sufficient entanglement criterion given in inequality (4). Namely, we have [40]

$$g_{\max} = \max\{g : g \text{ solves Eq. (6)}\}. \quad (8)$$

Let us stress that the maximal separability eigenvalue is the solution to an optimization problem that maximizes the function $\langle a_1, ..., a_N|\hat{L}|a_1, ..., a_N\rangle$ for normalized, pure, and separable states. Moreover, using relation (7), the value of $g_{\max}$ is determined through the corresponding separability eigenvector. Finding this vector $|a_1, ..., a_N\rangle$ is the goal of our algorithm to be introduced. Furthermore, the SEE in Eq. (6) takes the form of a perturbed EE. In fact, for a single party ($N = 1$), the vector $|\xi\rangle$ necessarily vanishes, which means that Eq. (6) corresponds to the EE. This relation between the SEE and the EE is relevant for our algorithm.

Furthermore, let us also recall properties of the SEEs, which are of particular importance for this work. First, the separability eigenvectors of the operator $\mu\hat{L} + \nu\hat{1}$, for real numbers ν and $\mu \neq 0$, are identical to those of the operator $\hat{L}$ [40]. This allows us to restrict ourselves to positive operators, as mentioned above.

The second property to be discussed here addresses the relations between the operators

$$\hat{L} = |\xi\rangle\langle\xi| \quad \text{and} \quad \hat{L}' = \mathrm{tr}_N(\hat{L}), \quad (9)$$

where $|\xi\rangle \neq 0$ is an arbitrary vector in the N-partite system and tr_N denotes the partial trace over the Nth subsystem. This also implies that $\hat{L}'$ is positive semidefinite and acting on an $(N-1)$-partite system. The theorem of cascaded structures [40] states that the nonzero separability

eigenvalues of $\hat{L}$ and $\hat{L}'$ are identical, which also implies that

$$g_{\max} = g'_{\max}. \tag{10}$$

Moreover, the separability eigenvectors of $\hat{L}$ and $\hat{L}'$ read $|a_1, ..., a_N\rangle$ and $|a_1, ..., a_{N-1}\rangle$, respectively, where the Nth component obeys

$$|a_N\rangle \| \langle a_1, ..., a_{N-1}, \cdot | \xi \rangle. \tag{11}$$

This means that $|a_N\rangle$ is parallel to a vector that is obtained from $|\xi\rangle$ by projecting its first $N-1$ components onto $\langle a_j|$. We emphasize that the optimization of the expectation value of the operator $\hat{L}$ over $|a_1, ..., a_N\rangle \in \mathcal{S}$, i.e., $|\langle \xi | a_1, ..., a_N \rangle|^2 \to \max$, corresponds to a maximization using $\hat{L}'$, which is defined in one subsystem less than used for $\hat{L}$. Also recall that the operator $\hat{L}'$ is, in general, not a rank-1 operator anymore, and the cascaded structure is applicable only to rank-1 operators.

D. Preliminary discussion

In Fig. 1, we outline the previously discussed entanglement detection method using three different operators, labeled as $\hat{L}$, $\hat{L}'$, and $\hat{L}''$. The tangent hyperplanes separate the set of separable states from states that are verified to be entangled. The touching points of the tangent represent the separability eigenvectors to the maximal separability eigenvalue. In general, the more operators are used, the better the hyperplanes can approximate the bounds of the set of separable states and the more entangled states can be
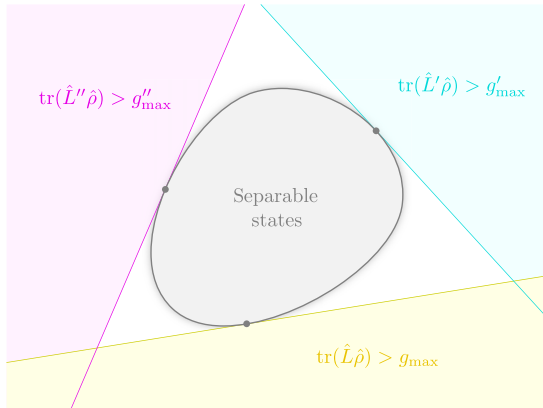

FIG. 1. Visualization of three entanglement criteria. Entanglement is verified in the shaded half-spaces $\mathrm{tr}(\hat{L}\hat{\rho}) > g_{\max}$ (bottom, yellow area), $\mathrm{tr}(\hat{L}'\hat{\rho}) > g'_{\max}$ (right, cyan area), and $\mathrm{tr}(\hat{L}''\hat{\rho}) > g''_{\max}$ (left, magenta area), where the values $g_{\max}$, $g'_{\max}$, and $g''_{\max}$ are the maximal separability eigenvalues of the operators $\hat{L}$, $\hat{L}'$, and $\hat{L}''$ respectively. The boundaries define hyperplanes tangent to the set of separable states (gray area). The bullet points correspond to the separability eigenvector to the maximal separability eigenvalue for each operator.

identified. Note that one can construct a dense set of operators for such an approximation with arbitrarily high precision; see, e.g., Ref. [39].

Both the construction of multipartite entanglement witnesses and the approximation of the set of separable states depend on the solution of the SEEs. Specifically, we need to find the maximal separability eigenvalue, which is determined through its corresponding separability eigenvector. However, the SEEs present a sophisticated mathematical problem, which has at least the complexity of the standard eigenvalue problem [64]. In fact, independently of our specific approach, the separability problem has been shown to be an NP-hard problem [8,9].

Furthermore, the SEE in Eq. (6) shares a number of properties with the EE, $\hat{L}|z\rangle = g|z\rangle$. For the latter EE, there exists an algorithm to compute the eigenvector to the maximal eigenvalue of any positive operator $\hat{L}$, the PI [61]. In this algorithm, a vector $|z\rangle$ is mapped onto a new normalized vector, $|z'\rangle = \hat{L}|z\rangle / \langle z | \hat{L}^2 | z \rangle^{1/2}$. An s-step iteration, $|z\rangle, |z'\rangle, |z''\rangle, ..., |z^{(s)}\rangle$, yields a vector that approaches, for $s \to \infty$, an eigenvector to the maximal eigenvalue of $\hat{L}$ for any initial vector that is not already an eigenvector to $\hat{L}$.

In the following, we aim to generalize the PI to be applicable to the SEE. For this reason, we introduce an algorithm for a numerical implementation, which yields the desired solution of the SEEs—a separability eigenvector to the maximal separability eigenvalue. The resulting SPI algorithm is applicable to all positive operators $\hat{L}$ and enables the construction of witnesses to probe multipartite entanglement.

III. THE SPI ALGORITHM

In this section, we present the SPI algorithm—step by step. The flowchart of this algorithm to construct entanglement criteria is shown in Fig. 2. Our approach yields the separability eigenvector $|a_1, ..., a_N\rangle$ to the desired, maximal separability eigenvalue for a positive operator $\hat{L}$ [Eq. (7)]. Before we study the individual, essential parts of the SPI in a rigorous mathematical framework, let us first get a general overview of how our algorithm operates by applying it to an example.

A. Proof of concept

For demonstrating the function of our algorithm, we consider the bipartite ($N = 2$) and positive operator

$$\hat{L} = 2\hat{1} - \hat{V}, \tag{12}$$

where $\hat{V}$ is the swap operator, $\hat{V}|a_1, a_2\rangle = |a_2, a_1\rangle$. The expectation value $\langle a_1, a_2 | \hat{L} | a_1, a_2 \rangle = 2 - |\langle a_1 | a_2 \rangle|^2$ directly implies that the maximal separability eigenvalue is $g_{\max} = 2$, and it is attained for $|a_1\rangle \perp |a_2\rangle$ [39]. This exact result serves as our reference to assess the success of our
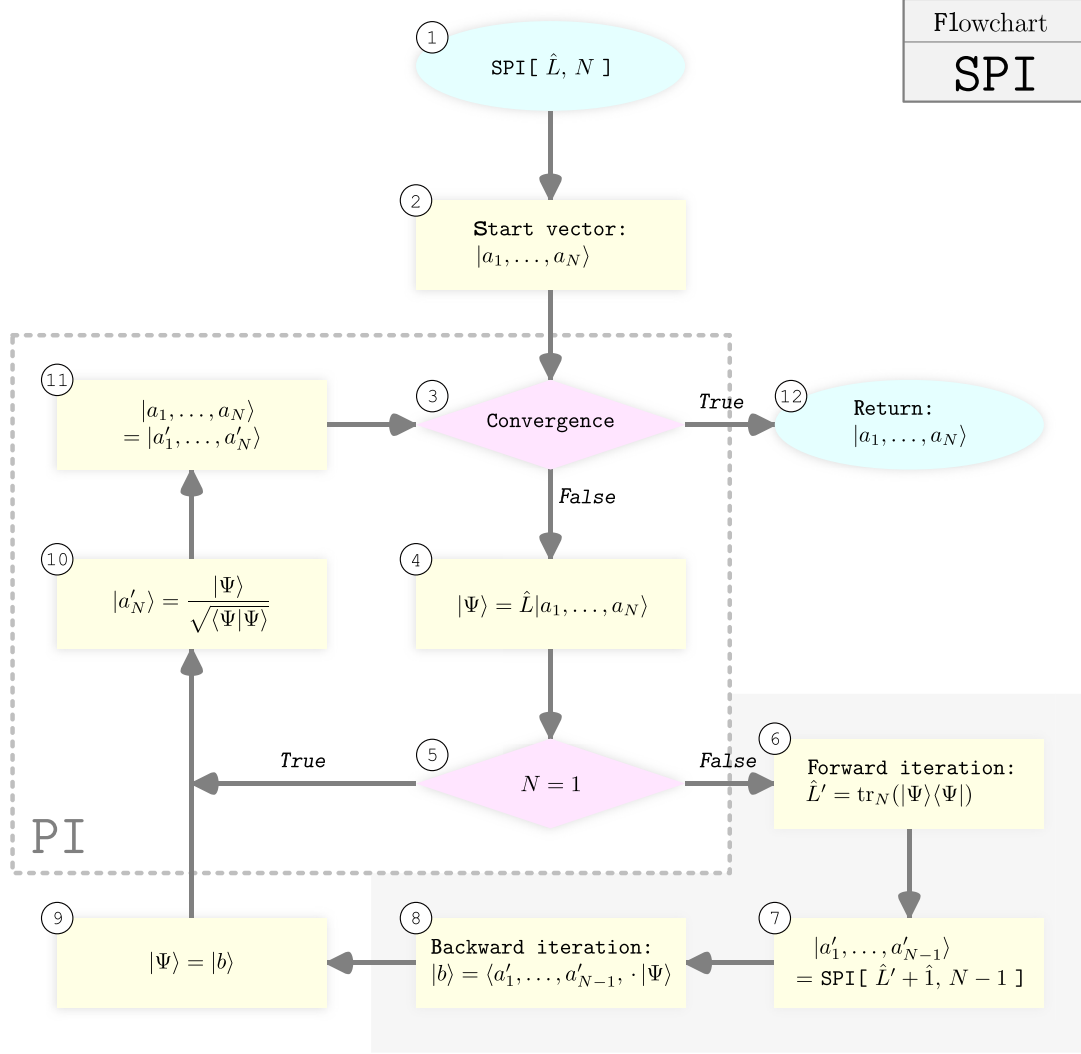
FIG. 2. Flowchart of the SPI algorithm. Branches in the algorithm, either "while" loops or "if" conditions, are represented by magenta diamonds. Yellow rectangles represent assignments and function calls. Entry and exit points of the algorithm are shown as cyan ellipses. Box ① refers to the input, which includes an operator and the number N of parties. A vector is generated in ② to serve as our starting vector. If the convergence criterion ③, studied in Sec. III B 4, is not met, we generate another N-partite vector in ④. For $N = 1$ in ⑤, the algorithm corresponds to the power iteration (PI), which finds the standard eigenvector to the maximal eigenvalue (dashed box). For $N > 1$, our extension consists of three essential parts (gray areas), which are the forward iteration ⑥ and the backward iteration ⑧, as well as a recursion calling the SPI for $N − 1$ parties in ⑦. Eventually, when ③ is satisfied, the desired separability eigenvector is the output of our SPI algorithm and is returned in ⑫.

algorithm for this example. Moreover, since the maximal standard eigenvalue is three, it follows from $g_{max} < 3$ that this operator can be used to detect entanglement [52]. In fact, the swap operator is related to the prominent partial transposition criterion to verify entanglement [20,21,39].

Our algorithm in Fig. 2 is initialized at point ① with the operator (12) and the number of subsystems being $N = 2$. At ②, let us begin with states $|a_1, a_2\rangle$, which are neither parallel nor orthogonal, to exclude the trivial cases. Namely, we have $0 < |\gamma|^2 < 1$, where

$$\gamma = \langle a_1|a_2\rangle. \tag{13}$$

Say that in step ③, we do not have convergence yet; i.e., we follow the branch labeled "false" and compute the vector in step ④,

$$|\Psi\rangle = \hat{L}|a_1, a_2\rangle = 2|a_1, a_2\rangle - |a_2, a_1\rangle. \tag{14}$$

Since $N \neq 1$ (step ⑤), we proceed to ⑥ and compute the operator,

$$\begin{aligned}\hat{L}' &= \mathrm{tr}_2|\Psi\rangle\langle\Psi| \\ &= 4|a_1\rangle\langle a_1| - 2\gamma|a_1\rangle\langle a_2| - 2\gamma^*|a_2\rangle\langle a_1| + |a_2\rangle\langle a_2|, \end{aligned} \tag{15}$$

which is a single-subsystem operator. This step is referred to as forward iteration in Fig. 2. The idea behind this step is a result of the theorem of cascaded structures, which finds the maximal separable projection onto the state $|\Psi\rangle$; see Sec. II C. This also allows us to apply the SPI to $\hat{L}' + \hat{1}$. As $\hat{L}'$ is positive semidefinite by construction, the addition of $\hat{1}$ assures the positivity of $\hat{L}' + \hat{1}$ without modifying the separability eigenvectors.

Calling the SPI with $N \mapsto N - 1 = 1$ in ⑦ and thereby going back to step ① and going through steps ②–⑤, we follow the branch for which $N = 1$ is true. This gives an iteration of steps ⑩, ⑪, ③, ④, and ⑤, indicated through the dashed box in Fig. 2, which describes the PI. The PI is employed for solving the standard EE numerically by returning the eigenvector to the maximal eigenvalue of a positive operator with an arbitrarily high precision. So we can assume that the convergence ③ is true after some iterations of the PI. For the given operator $\hat{L}' + \hat{1}$ (thus, also for $\hat{L}'$), the eigenvector to the maximal eigenvalue reads

$$|a_1'\rangle = \frac{1}{\nu}\left(4|\gamma||a_1\rangle + [\Gamma - 3]\frac{\gamma^*}{|\gamma|}|a_2\rangle\right), \qquad (16)$$

using γ [cf. Eq. (13)], the abbreviation

$$\Gamma = \sqrt{9 - 8|\gamma|^2}, \qquad (17)$$

and the normalization $\nu = [2\Gamma(\Gamma - 3 + 4|\gamma|^2)]^{1/2}$.

Thus, the PI basically returns the vector $|a_1'\rangle$ in step ⑫, which is used to continue with the case $N = 2$, where we exit step ⑦ to perform the backward iteration step ⑧. This gives a vector in the second subsystem. For convenience, this vector is renamed (step ⑨) and normalized (step ⑩); see Fig. 2. Again, the backward iteration is a result of the theorem of cascaded structures, which relates the separability eigenvectors of $\hat{L}'$ for $N - 1$ subsystems with those of the initial operator $\hat{L}$ for N, cf. Sec. II C. This yields the state of the second subsystem,

$$|a_2'\rangle = \frac{1}{\nu}\left(4|\gamma||a_2\rangle + [\Gamma - 3]\frac{\gamma}{|\gamma|}|a_1\rangle\right). \qquad (18)$$

Thus, we obtain a new separable state $|a_1', a_2'\rangle$ in ⑪, where the tensor-product state is formed.

What did we achieve with the construction of this new state? To answer this question, let us recall that the desired separability eigenvector of the operator under study has perpendicular components for the subsystems. Thus, in analogy to Eq. (13), we may compute the scalar product of the states of the subsystems, which yields $\gamma' = \gamma/\Gamma$ and

$$|\gamma'|^2 = |\langle a_1'|a_2'\rangle|^2 = \frac{|\gamma|^2}{9 - 8|\gamma|^2} < |\gamma|^2 = |\langle a_1|a_2\rangle|^2. \qquad (19)$$

This means the states $|a_1'\rangle$ and $|a_2'\rangle$ are closer to orthogonal than the initial states $|a_1\rangle$ and $|a_2\rangle$. Equivalently, we can say that the expectation value of $\hat{L}$ increases, $\langle a_1', a_2'|\hat{L}|a_1', a_2'\rangle = 2 - |\gamma'|^2 > \langle a_1, a_2|\hat{L}|a_1, a_2\rangle = 2 - |\gamma|^2$. Now, we can perform the next cycle, which results in $|\gamma|^2 > |\gamma'|^2 > |\gamma''|^2$. In fact, performing s steps of the SPI, we get vectors $|a_1^{(s)}, a_2^{(s)}\rangle$, for which

$$|\langle a_1^{(s)}|a_2^{(s)}\rangle|^2 < \frac{|\gamma|^2}{(9 - 8|\gamma|^2)^s} \xrightarrow{s\to\infty} 0 \qquad (20)$$

holds. Therefore, we get a convergent sequence of separability eigenvectors, which, in the limit of infinite iterations, yields the desired exact maximal separability eigenvalue, $\langle a_1^{(s)}, a_2^{(s)}|\hat{L}|a_1^{(s)}, a_2^{(s)}\rangle \to 2 - 0 = g_{\max}$ for $s \to \infty$.

In conclusion of this example resulting in an entanglement test based on the swap operator [cf. Eqs. (12) and (4)], our SPI is constructed to deliver the separability eigenvector to the maximal separability eigenvalue. Applying properties of the theorem of the cascaded structure of SEEs, we identify the following essential steps: forward and backward iteration. The forward iteration allows the reduction of the number of subsystems by one in each recursion depth until the recursion depth reaches a maximum when the operator is a single-partite operator. Then, the SEE reduces to the EE, and the PI is used to get the eigenvector to the maximal eigenvalue. The eigenvector is further used in the next step, the backward iteration, to obtain the remaining subsystem components of the separable product vector. After completing multiple instances of such a cycle, we obtain an arbitrarily precise approximation to our sought-after separability eigenvector.

Now, we may consider the general case beyond the specific example, which was used to demonstrate the general operation of our generally applicable algorithm in Fig. 2. This gives the mathematically rigorous formulation of the SPI for arbitrary positive operators $\hat{L}$ and arbitrary numbers N of subsystems, which necessarily requires a rather technical treatment because of the complexity of the underlying separability problem. After this, we perform a benchmarking of our algorithm and apply it to various examples, which provides a more intuitive assessment of our method.

B. Analytic framework

Based on the theorem on cascaded structures for the SEEs, the SPI iterates over the number of parties from N to one. For $N = 1$, the SPI and PI are identical, resembling the underlying fact that the SEE and EE are the same in this case too. Beyond the PI, the SPI algorithm includes two main steps, denoted as forward and backward iteration. Clearly, the major goal of our maximization algorithm for a positive operator $\hat{L}$ is to get a new separable state $|a_1', \ldots, a_N'\rangle$ from the preceding state $|a_1, \ldots, a_N\rangle$, which

increases the expectation value, $\langle a'_1, ..., a'_N | \hat{L} | a'_1, ..., a'_N \rangle >$ $\langle a_1, ..., a_N | \hat{L} | a_1, ..., a_N \rangle$. Here, let us discuss the details; the proofs of some of the required theorems are provided in the corresponding appendixes.

1. Initial considerations

Let us make some more general observations, which we then apply to the separability problem under study. A positive operator $\hat{L}$ induces a scalar product,

$$\langle x | y \rangle_{\hat{L}} = \langle x | \hat{L} | y \rangle, \tag{21}$$

for arbitrary $|x\rangle$ and $|y\rangle$. Therefore, the Cauchy-Schwarz inequality holds true, $|\langle x | y \rangle_{\hat{L}}|^2 \leq \langle x | x \rangle_{\hat{L}} \langle y | y \rangle_{\hat{L}}$, where the equality is equivalent to $|x\rangle \| |y\rangle$. Also, we have $\langle x | x \rangle_{\hat{L}} > 0$ for all $|x\rangle \neq 0$. To apply these features, we have to restrict ourselves to positive operators $\hat{L}$. Note that in our following proofs, we rely on the properties of the scalar product; for example, a positive-semidefinite operator $\hat{L}$ would be insufficient [65].

Say $\mathcal{T}$ is a closed and bounded subset of a finite-dimensional Hilbert space. For a $|z\rangle \in \mathcal{T}$, one can define an iterated state as

$$|z'\rangle = \underset{|y\rangle \in \mathcal{T}}{\mathrm{argmax}} |\langle y | z \rangle_{\hat{L}}|, \tag{22}$$

where we use the function "argmax," which returns the argument for which the maximum is reached. In other words, $|z'\rangle = \mathrm{argmax}_{|t\rangle \in \mathcal{T}} |\langle t | z \rangle_{\hat{L}}|$ if $|z'\rangle \in \mathcal{T}$ satisfies the relation $|\langle z' | z \rangle_{\hat{L}}| = \max_{|t\rangle \in \mathcal{T}} |\langle t | z \rangle_{\hat{L}}|$. Since $|z\rangle$ is also an element of the set $\mathcal{T}$ over which we maximize, we can conclude that $\langle z | z \rangle_{\hat{L}} \leq |\langle z' | z \rangle_{\hat{L}}|$. Applying the Cauchy-Schwarz inequality, we get

$$\langle z | z \rangle_{\hat{L}}^2 \leq |\langle z' | z \rangle_{\hat{L}}|^2 \leq \langle z' | z' \rangle_{\hat{L}} \langle z | z \rangle_{\hat{L}} \leq \langle z' | z' \rangle_{\hat{L}} |\langle z' | z \rangle_{\hat{L}}|. \tag{23}$$

Considering the second and fourth terms, as well as the first and third terms, we find the increasing sequence

$$\langle z | z \rangle_{\hat{L}} \leq |\langle z' | z \rangle_{\hat{L}}| \leq \langle z' | z' \rangle_{\hat{L}}. \tag{24}$$

From the definition of $|z'\rangle$ and the properties of the Cauchy-Schwarz inequality, we can also conclude that the equality holds true if and only if $|z'\rangle \| |z\rangle$.

Therefore, we can state that the iteration $|z\rangle$, $|z'\rangle$, $|z''\rangle$, etc. produces a sequence of increasing expectation values, $\langle z | \hat{L} | z \rangle \leq \langle z' | \hat{L} | z' \rangle \leq \langle z'' | \hat{L} | z'' \rangle \leq \cdots$. However, the elusive arg max function (22) has to be computed for this purpose. In fact, this can be done for separable states, $\mathcal{T} = \mathcal{S}$.

We may use the abbreviation $|\Psi\rangle = \hat{L} | a_1, ..., a_N \rangle$. To maximize the projections of this state onto separable ones, we can apply the theorem of the cascaded structure. This means that the maximal projection of this state onto

separable states is obtained by $|a'_1, ..., a'_N\rangle$ for the maximal separability eigenvalue of $|\Psi\rangle\langle\Psi|$. In Sec. II C and in the flowchart of the SPI in Fig. 2, we describe how this is achieved: We reduce the number of parties N and solve the SEE for $\hat{L}' = \mathrm{tr}_N |\Psi\rangle\langle\Psi|$ (forward iteration, ⑥) to get $|a'_1, ..., a'_{N-1}\rangle$ (step ⑦), which then determines the remaining component $|a'_N\rangle$ from $\langle a'_1, ..., a'_{N-1}, \cdot | \Psi \rangle$ (backward iteration, ⑧).

In summary, the cascaded structure describes how to compute the desired arg max function for separable states. This describes the underlying principle of the SPI, which allows us to compute the bounds $g_{\max}$ for the necessary and sufficient entanglement criteria (4).

2. The SPI

To apply the general relations above, let us begin with the forward iteration step. By the following Theorem 1, it is guaranteed that finding the separability eigenvector corresponds to determining the maximal separability eigenvalue for the $(N-1)$-partite case. More specifically, it enables us to reduce the number of subsystems for the SEE by one.

Theorem 1 (Forward iteration). Let $|a_1, ..., a_N\rangle$ be the separability eigenvector corresponding to the maximal separability eigenvalue of a positive N-partite operator $\hat{L}$. Furthermore, let $|\Psi\rangle = \hat{L} | a_1, ..., a_N \rangle$. For the $(N-1)$-partite operator $\hat{L}' = \mathrm{tr}_N(|\Psi\rangle\langle\Psi|)$, the equality

$$\langle a_1, ..., a_N | \hat{L} | a_1, ..., a_N \rangle$$
$$= \sqrt{\langle a_1, ..., a_{N-1} | \hat{L}' | a_1, ..., a_{N-1} \rangle} \tag{25}$$

holds true. See Appendix A for the proof.

This theorem is a direct consequence of the SEE in Eq. (6) and its properties. In the SPI algorithm, the theorem is applied in the forward iteration step ⑥. To find the full N-partite separability eigenvector, a reverse step has to be taken. Theorem 2 states how the N subsystem separability eigenvector can be generated from the $N-1$ subsystem separability eigenvector.

Theorem 2 (Backward iteration). Consider the same definitions used in Theorem 1. If the $(N-1)$-partite separability eigenvector $|a_1, ..., a_{N-1}\rangle$ maximizes Eq. (25), then the separability eigenvector $|a_1, ..., a_{N-1}\rangle \otimes |a_N\rangle$ maximizes $\langle a_1, ..., a_N | \hat{L} | a_1, ..., a_N \rangle$ if the condition

$$\nu |a_N\rangle = \langle a_1, ..., a_{N-1}, \cdot | \Psi \rangle \tag{26}$$

holds true for $\nu \in \mathbb{C} \backslash \{0\}$.

The proof of this theorem directly follows from the cascaded structure, cf. Eq. (11). It relates the separability eigenvector for N parties to those of a lower number of parties, $N-1$. Thereby, if a solution to the $(N-1)$-partite SEEs for $\hat{L}'$ is known, we directly find the Nth component

of the full solution $|a_1, ..., a_N\rangle$. In the flowchart in Fig. 2, we see the application in the backward iteration step ⑧.

The combination of Theorems 1 and 2 is fundamental for the SPI to work. In fact, one might visualize the working principle of the algorithm as a nested cascading structure. The forward iteration is recursively applied until we reach the case $N = 1$. In that case, the standard PI is performed. After that, the backward iteration finalizes the individual recursion layers of the SPI until we obtain the new N-partite separable vector. Then, we can start a new cycle of forward iterations, the PI, and backward iterations until the convergence is reached. The algorithm will terminate successfully and return the complete separability eigenvector corresponding to the maximal separability eigenvalue g_{max} for detecting entanglement in terms of inequality (4).

To verify the statement that the algorithm converges to the maximal separability eigenvalue, a few observations have to be shown first. Let us take a closer look at the sequence of product vectors created by the SPI. In every step, we find an element of all product states, $|a'_1, ..., a'_N\rangle \in \mathcal{S}$, which projects maximally onto the action of operator $\hat{L}$ onto the previously generated product state $|a_1, ..., a_N\rangle$. This iteration is done until we reach convergence. This generates a monotonously growing sequence of expectation values of $\hat{L}$, which is stated in the following theorem.

Theorem 3 (Monotony). Let $|a_1, ..., a_N\rangle \in \mathcal{S}$ and $|a'_1, ..., a'_N\rangle \in \mathcal{S}$ such that

$$|a'_1, ..., a'_N\rangle = \operatorname*{argmax}_{|b_1, ..., b_N\rangle \in \mathcal{S}} \langle b_1, ..., b_N|\hat{L}|a_1, ..., a_N\rangle. \quad (27)$$

Then, the inequality

$$\langle a_1, ..., a_N|\hat{L}|a_1, ..., a_N\rangle$$
$$\leq \langle a'_1, ..., a'_N|\hat{L}|a_1, ..., a_N\rangle$$
$$\leq \langle a'_1, ..., a'_N|\hat{L}|a'_1, ..., a'_N\rangle \quad (28)$$

holds true. Furthermore, equality in Eq. (28) holds true iff $|a'_1, ..., a'_N\rangle = |a_1, ..., a_N\rangle$. See Appendix B for the proof.

This theorem is a special case of the general considerations made in Sec. III B 1. In addition, the global phase of the separable state $|a'_1, ..., a'_N\rangle$ can be chosen freely, which we conveniently select such that we have positive projections onto $|\Psi\rangle$, i.e., $\langle a'_1, ..., a'_N|\hat{L}|a_1, ..., a_N\rangle = |\langle a'_1, ..., a'_N|\hat{L}|a_1, ..., a_N\rangle|$. Let us stress that the arg max function, i.e., finding the maximal projection onto $|\Psi\rangle = \hat{L}|a_1, ..., a_N\rangle$, is obtained from the cascaded structure; see also Theorems 1 and 2.

Because of Theorem 3, the SPI produces a sequence of increasing expectation values of $\hat{L}$. This observation is an important aspect for the proof of convergence of the SPI, which is shown in two parts. Both theorems rely on the sequence $(g^{(s)})_s$ of expectation values generated by the SPI in each step s, where

$$g^{(s)} = \langle a_1^{(s)}, ..., a_N^{(s)}|\hat{L}|a_1^{(s)}, ..., a_N^{(s)}\rangle. \quad (29)$$

Here, in analogy to the example in Sec. III A, the vector $|a_1^{(s)}, ..., a_N^{(s)}\rangle$ is the approximation to the separability eigenvector for the maximal separability eigenvalue after s iterations of the SPI. First, we consider the local convergence of the algorithm.

Theorem 4 (Local convergence). For any starting vector, the sequence $(g^{(s)})_s$ of expectation values generated by the SPI converges; i.e., the limit

$$\lim_{s \to \infty} g^{(s)} = \bar{g} \quad (30)$$

exists and is bounded as $0 \leq \bar{g} \leq g_{max}$. See Appendix C for the proof.

For an arbitrary starting vector, a sequence of expectation values of $\hat{L}$ for separable states is generated. The generated sequence converges independent of the choice of starting vector. Combining the statements from Theorems 3 and 4, we conclude that there is a monotone growth of expectation values towards a maximum. This maximum does not necessarily need to be the maximal separability eigenvalue g_{max} as shown in Theorem 4. We therefore require an additional observation to prove global convergence of the SPI, which is stated in Theorem 5.

Theorem 5 (Global convergence). Let Σ be a set of separable starting vectors and $(g_\Phi^{(s)})_s$ be sequences of expectation values generated by the SPI for a starting vector $|\Phi\rangle \in \Sigma$. Furthermore, say $\{\bar{g}_\Phi \in \mathbb{R} : |\Phi\rangle \in \Sigma \text{ and } \bar{g}_\Phi = \lim_{s \to \infty} g_\Phi^{(s)}\}$ defines the set of optimal expectation values (limits of the converged sequences) for each starting vector. The maximal separability eigenvalue for the operator $\hat{L}$ is $g_{max} = \max_{\Phi \in \Sigma}\{\bar{g}_\Phi\}$, which is the maximum of the limit to the series of expectation values for each starting vector. See Appendix D for the proof.

The set Σ of different starting vectors $|\Phi\rangle$ that we consider is covered in Sec. III B 3. Even in the worst-case scenario, it is far smaller than the set $\mathcal{S}$ of all separable states.

3. Starting vectors

An important aspect for the implementation of the algorithm is the choice of a starting vector, cf. Theorem 5. Because a proper choice can significantly decrease the runtime of the algorithm, let us provide more details on this aspect.

Assume we start with a separability eigenvector corresponding to any—except for the largest—separability eigenvalue. Then, the algorithm converges immediately, and the resulting separability eigenvalue will not be maximal. It is worth mentioning that such a behavior is already well known for the PI. It is straightforward to check whether an initial vector is a (separability) eigenvector.

Similar results might happen for starting vectors that are too close to any (separability) eigenvector.

To circumvent such problems, the SPI can be run multiple times with different starting vectors, chosen as an operator basis. Namely, the set $\{|a_{1,k}, ..., a_{N,k}\rangle \langle a_{1,k}, ..., a_{N,k}|\}_k$ of starting vectors spans all operators of the underlying Hilbert space. This allows us to cover all parts of the operator space and, of course, also resolves the related problem for the PI.

This choice is valid as the set of separability eigenvectors can be used to find a decomposition of any state, similarly to the spectral decomposition found by regular eigenvectors. In fact, any positive-semidefinite operator can be decomposed in terms of projectors of separability eigenvectors; see Refs. [66,67] for proofs of the bipartite and multipartite cases, respectively. Specifically, the decomposition of at least one vector of the operator basis needs to contain the sought-after separability eigenvector. This warrants the choice of using the operator basis as starting vectors.

Another efficient *ad hoc* ansatz that we used for the implementation of the SPI is described as follows: First, a preliminary run of the SPI is done to find a product vector projecting maximally onto the vector $\hat{L}|v\rangle$, where $|v\rangle$ is the eigenvector to the maximal standard eigenvalue of $\hat{L}$. This choice is inspired by the fact that the wanted vector $|a_1, ..., a_N\rangle$ maximizes the expectation value of $\hat{L}$ with respect to product vectors. The eigenvector $|v\rangle$ maximizes the expectation value of $\hat{L}$ without the restriction to separable states. Second, the product vector that lies maximally parallel to $|v\rangle$ serves as our starting vector. Finding such a maximal projection is in fact exactly what we get when running the SPI for a positive operator $\hat{1} + |v\rangle\langle v|$. Finally, the resulting product vector serves as the initial vector for the SPI algorithm applied to $\hat{L}$.

Our numerical results and comparison with other methods confirm the assumption that the constructed starting vector is sufficient, as the described procedure returns the same values. Still, a rigorous proof of this observation requires further investigations. Until then, the choice of an operator basis of starting vectors is preferable in the general case.

4. Convergence criterion

The flowchart in Fig. 2 requires a check for convergence in step ③. Theorems 4 and 5 guarantee, in theory, the convergence of the SPI. In a practical implementation of the algorithm, however, the computer needs to know when convergence is reached in a numerical sense.

We apply a convergence criterion that is based on the SEE. In the sth cycle of the algorithm, we obtain the vector $|\chi^{(s)}\rangle = (\hat{L} - g^{(s)}\hat{1})|a_1^{(s)}, ..., a_N^{(s)}\rangle$; see Eq. (6). By definition (see Sec. II), $|a_1^{(s)}, ..., a_N^{(s)}\rangle$ is a separability eigenvector if and only if $|\chi^{(s)}\rangle$ is N orthogonal. Likewise, convergence

is reached if and only if $|\chi^{(s)}\rangle$ is N orthogonal. Theorem 4 guarantees that we approach this scenario—meaning that $\lim_{s\to\infty}\langle a_1^{(s)}, ..., a_{j-1}^{(s)}, x, a_{j+1}^{(s)}, ..., a_N^{(s)}|\chi^{(s)}\rangle = 0$ for all $x \in \mathcal{H}_j$ and $j = 1, ..., N$.

In fact, this N-orthogonality requirement can be used to quantify the closeness to the solution. For this purpose, we can evaluate if the following inequality is satisfied:
$$\max_{j=1,...,N}\max_{x\in\mathcal{B}_j}|\langle a_1^{(s)}, ..., a_{j-1}^{(s)}, x, a_{j+1}^{(s)}, ..., a_N^{(s)}|\chi^{(s)}\rangle| < \epsilon,$$
for a sufficiently small ϵ and all $x \in \mathcal{B}_j$, where $\mathcal{B}_j$ is a basis of $\mathcal{H}_j$. The machine precision of the representation of numbers on a computer bounds the value of ϵ. When the inequality is satisfied, the possible numerical convergence is achieved, and the current iteration $|a_1^{(s)}, ..., a_N^{(s)}\rangle$ is the desired approximation to the separability eigenvector.

IV. BENCHMARK

We now want to find out how the SPI performs as opposed to other methods that allow the construction of arbitrary entanglement witnesses. A simple brute-force approach to obtain the entanglement criterion (4) for $\hat{L}$ is to find all separable pure states and calculate the expectation value of $\hat{L}$. Then, g_{max} is the maximum of these values.

As the search space for these vectors is over a continuum, one could use a generally applicable global optimization algorithm, such as genetic algorithms [68]. This presents a state-of-the-art method to solve optimization problems. It is rather fast and inspired by evolutionary processes in biology. Thus, we implemented such a genetic algorithm to evaluate the performance of the SPI. A genetic algorithm requires a fitness function to be minimized, which will be $f(v) = -\langle v|\hat{L}|v\rangle$, the negative of the expectation value of $\hat{L}$. An intermediate step ensures that the argument vector $|v\rangle$ is indeed a product vector. During the runtime, the genetic algorithm will minimize $f(v)$ and converge towards a vector $|v_0\rangle$ with $f(v_0) = \min_v f(v)$. The resulting minimization will give the maximal separability eigenvalue $g_{max} = -f(v_0)$, or at least a close approximation.

To show the advantages of the proposed algorithm, SPI, as opposed to this simple maximization strategy, we compare the two approaches for the following, different scenarios: We consider a bipartite system ($N = 2$) and vary the dimensions, $d_1 = d_2 = d$; we fix the dimensions (here, $d_1 = \cdots = d_N = 2$) and increase the number of parties N. As discussed previously, we choose the convergence criterion in Sec. III B 4. The starting vector is chosen as the maximal separable projection on the (standard) eigenvector corresponding to the maximal eigenvalue of $\hat{L}$.

To exclude any bias, the chosen operators are randomly generated by first defining a random operator $\hat{M}$ acting on the D-dimensional space, where $D = d_1 \cdot ... \cdot d_N$. Then, we construct a positive and normalized operator $\hat{L}$ for which we want to find the maximal separability eigenvalue as

$$\hat{L} = \frac{1}{\mathrm{tr}(\hat{1} + \hat{M}\hat{M}^{\dagger})}(\hat{1} + \hat{M}\hat{M}^{\dagger}). \qquad (31)$$

The SPI and brute-force approaches have been tested for 100 randomly selected operators. To make the runtimes comparable, the same set of random operators was used for both approaches.

Figure 3 shows the average runtime for the SPI compared to the brute-force approach. These results come from running both algorithms on a desktop computer. The runtime of the SPI is, on average, at least 2 orders of magnitude lower for the considered sample size of 100 randomly generated test operators. In bipartite systems (Fig. 3, top panel), we see a smaller scaling behavior of the SPI, whereas the scaling is about the same for an increasing number of qubits (bottom plot). Moreover, focusing on the
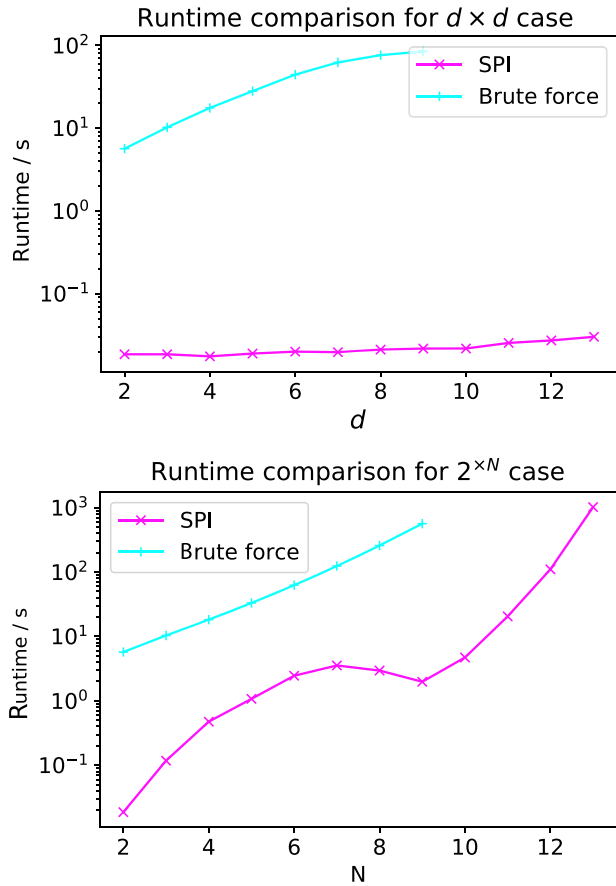

FIG. 3. Benchmark results comparing the SPI (magenta line) to a brute-force approach, which is a genetic algorithm (cyan line). Top panel: The results for the runtime comparison between both approaches are shown when scaling the dimensions of each subsystem for a bipartite state, $N = 2$ and $d_1 = d_2 = d$. Bottom panel: The corresponding results are shown when scaling the number N of parties, which are qubit systems ($d_1 = \cdots = d_N = 2$). It can be seen that the SPI performs better than the competing approach by several orders of magnitude.

numbers of subsystems (Fig. 3, bottom panel), we see that the SPI finds the maximal separability eigenvalue for a state acting on a 13-fold Hilbert space (dimensionality $D = 2^{13} = 8192$) in roughly the same time as the other approach manages to find it in the ninefold case (dimensionality $D = 2^9 = 512$). It is also worth mentioning that all curves of the presented study in Fig. 3 can be roughly approximated by exponential functions of the overall dimensionality [$D = d^2$ (top) and $D = 2^N$ (bottom)], representing the expected exponentially increasing runtime of the separability problem. The dip (in favor of the SPI) at $N = 9$ in the bottom plot cannot be explained at this point and requires further investigations.

Our benchmark indicates the superior potential of the SPI algorithm to numerically construct entanglement tests. Specifically, it outperforms the competing approach for high-dimensional scenarios, which includes the dimensionality of the individual parties as well as the number of parties itself. This enables a comparably efficient tool for the identification of entanglement in complex physical systems. Keep in mind that the runtimes shown in Fig. 3 are from running the SPI on a desktop computer; computation clusters might improve the performance even further by a large margin.

Beyond the genetic algorithm, there exist more specialized algorithms, treating Eq. (7) as a maximization of a multivariate polynomial. Such approaches are also NP-hard problems, meaning they can not be solved in polynomial time by a non-deterministic Turing machine, and only lower bounds of the global maximum can be found in polynomial time [69]. We apply one state-of-the-art realization of such an algorithm to find the maximum of a polynomial [70], using semidefinite programming, instead of the problem of finding the maximal separability eigenvalue of an operator. Semidefinite programming is a frequently applied technique used for entanglement tests, cf., e.g., Refs. [54–60]. Already in a 3×3 case, the algorithm in Ref. [70] failed to be conclusive and, in fact, returned a lower value than our SPI. For use as an optimal witness, the true maximal separability eigenvalue is crucial; thus, the result of the competing algorithm could lead to a false indication of entanglement. In all other tested cases in which the algorithm was conclusive, our SPI was superior in terms of speed and accuracy.

V. EXAMPLES

As a proof of principle, let us apply our algorithm to detect entanglement of states of special relevance. Specifically, we study the two-qutrit Horodecki state [71] and the four-qubit Smolin state [72]. Both states have been classified as bound-entangled states. In the case of the Horodecki state, this arises from the dimensions of the state, which is acting on a 3×3-dimensional Hilbert space. The Smolin state acts on a $2 \times 2 \times 2 \times 2$-dimensional Hilbert space, and the bound-entangled nature arises from

the fact that the state is separable with respect to all bipartitions consisting of two subsystems each, yet still entangled in all other partitions. By applying the SPI algorithm, we aim at confirming the weak entanglement properties of those bound-entangled states for which the well-known partial transposition test [20,73] fails to be conclusive.

The first example, the Horodecki state, is defined as [71]

$$\hat{\rho}_\alpha = \frac{1}{7}(2|\Psi\rangle\langle\Psi| + \alpha\hat{\sigma}_+ + (5-\alpha)\hat{\sigma}_-), \qquad (32)$$

where $\hat{\sigma}_+ = (|0,1\rangle\langle0,1| + |1,2\rangle\langle1,2| + |2,0\rangle\langle2,0|)/3$ and $\hat{\sigma}_- = (|1,0\rangle\langle1,0| + |2,1\rangle\langle2,1| + |0,2\rangle\langle0,2|)/3$ are separable and $|\Psi\rangle = (|0,0\rangle + |1,1\rangle + |2,2\rangle)/\sqrt{3}$ is the entangled contribution. The parameter can be chosen as $0 \leq \alpha \leq 5$; otherwise, the density operator $\hat{\rho}_\alpha$ does not represent a physical state. The Horodecki state was shown to be entangled for $\alpha > 3$ and $\alpha < 2$ [71].

For our entanglement analysis based on the criterion (4), a positive-definite, Hermitian operator $\hat{L}$ is required. For simplicity, the test operator will be chosen as $\hat{L}_\beta = \hat{\rho}_\beta$. We calculate the maximal separability eigenvalues g_β for every $\hat{L}_\beta$, where $0 \leq \beta \leq 5$. In this entanglement test, a state is verified to be entangled if

$$g_\beta - \text{tr}(\hat{\rho}_\alpha \hat{L}_\beta) < 0, \qquad (33)$$

which corresponds to the criterion based on the entanglement witness $\hat{W}_\beta = g_\beta \hat{1} - \hat{L}_\beta$.

The results are shown in Fig. 4. The entanglement criterion (33) is satisfied in the magenta colored areas. The blank area corresponds to parameters $2 \leq \alpha \leq 3$ for which no entanglement could be detected, which agrees with the prediction in Ref. [71]. In all other cases (cyan area), there exists at least one other value β' for which $\hat{L}_{\beta'}$ verifies entanglement. Thus, we correctly and straightforwardly
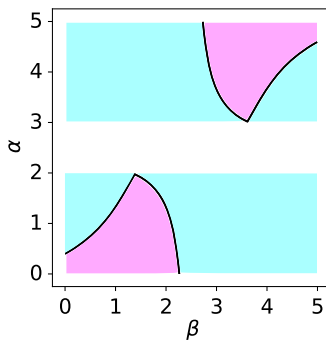

FIG. 4. Results of the entanglement test for the bound-entangled, two-qutrit Horodecki state. No state $\hat{\rho}_\alpha$ with $2 \leq \alpha \leq 3$ (blank area) has been detected as entangled. In the magenta areas, the criterion Eq. (33) certifies entanglement for the given combination of α and β, which does not hold true for the cyan areas.

TABLE I. Separability eigenvalues of the operator $\hat{L} = \hat{S}$ [Eq. (34)]. The maximal separability eigenvalues g_{max} are listed for the corresponding partitions.

Partition	g_{max}
$\{1,2\}:\{3,4\}$	0.250
$\{1\}:\{2,3,4\}$	0.125
$\{1\}:\{2\}:\{3,4\}$	0.125
$\{1\}:\{2\}:\{3\}:\{4\}$	0.125

certify entanglement of all Horodecki states, which are positive under partial transposition, using our SPI approach.

Beyond the bipartite case, let us apply our method to the multipartite scenario for which the partial transposition criterion does not apply in principle. For this reason, we study the four-partite Smolin state [72],

$$\hat{S} = \frac{1}{16}(\hat{1} + \hat{\sigma}_x^{\otimes 4} + \hat{\sigma}_y^{\otimes 4} + \hat{\sigma}_z^{\otimes 4}), \qquad (34)$$

where $\hat{\sigma}_x$, $\hat{\sigma}_y$, and $\hat{\sigma}_z$ denote the Pauli spin matrices. We restrict ourselves to a test operator of the simple form $\hat{L} = \hat{S}$.

In the multipartite case, we can analyze different forms of entanglement, such as bipartitions, tripartitions, and four-partitions for the state under study. In total, we have 14 partitions. However, because of the symmetry, cf. Eq. (34), we can restrict ourselves to the bipartitions $\{1\}:\{2,3,4\}$ and $\{1,2\}:\{3,4\}$, the tripartition $\{1\}:\{2\}:\{3,4\}$, and the four-partition $\{1\}:\{2\}:\{3\}:\{4\}$.

The SPI algorithm was run for all partitions. The results are listed in Table I. For applying entanglement criterion Eq. (4), we additionally compute $\text{tr}(\hat{L}\hat{S}) = 1/4$. Thus, in agreement with the results in Ref. [72], entanglement could be verified for all partitions, except for the bipartition, which consists of two subsystems each, i.e., $\{1,2\}:\{3,4\}$.

In this section, we demonstrated the direct application of our SPI algorithm to construct entanglement probes, for example, to identify bound instances of entanglement. We deliberately chose such weakly entangled states, which have been characterized previously to challenge our method and compare our numerical results with sophisticated exact analysis. In particular, entanglement was verified in bipartite qudit and multipartite qubit states. The entanglement of the states under study is a challenge for other directly applicable methods as the partial transposition criterion gives inconclusive results.

VI. DISCUSSION

We introduced, implemented, and applied a method to numerically construct entanglement tests. In this section, let us discuss how this technique can be used in experiments, how it improves other entanglement probes, and how it can be generalized to detect other forms of entanglement.

Finally, we discuss future research directions that become accessible with our approach and address the interdisciplinary importance of the introduced technique by relating it to a current problem in pure mathematics.

A. Experimental implementation

A major benefit of our approach is the direct applicability in experiments. Suppose that the set of observables $\{\hat{M}_k : k = 1, \ldots, m\}$ describes a measurement scheme. In other words, the data yield the expectation values $\langle \hat{M}_k \rangle = \text{tr}(\hat{M}_k \hat{\rho})$. An example for such operators relates to a displaced photon-number correlation [74]. In general, a family of positive operators $\hat{L}$ can be constructed from the considered measurements,

$$\hat{L} = \nu \hat{1} + \sum_{k=1}^{m} \mu_k \hat{M}_k, \qquad (35)$$

by choosing real-valued coefficients μ_k and adjusting ν to ensure positivity of $\hat{L}$.

The entanglement criterion (4) can be applied. On the one hand, the experimental expectation value is given by $\langle \hat{L} \rangle = \nu + \sum_{k=1}^{m} \mu_k \langle \hat{M}_k \rangle$. On the other hand, we get the maximal expectation value for separable states, $g_{\max}$, from the application of our SPI to the family of operators $\hat{L}$ under study. Note that a variation over the coefficients μ_k also enables an optimal entanglement verification based on the set of measured observables, similarly to the technique applied to Gaussian measurements in Refs. [41,42].

B. Relations to other entanglement criteria

As mentioned earlier, our entanglement criteria are identical to witnesses [Eq. (3)]. Furthermore, based on the Choi-Jamiołkowski isomorphism [75,76], entanglement witnesses enable the formulation of positive, but not completely positive, maps to probe entanglement [21,22]. Thus, our numerical method can be used to construct previously unknown families of such maps. For instance, the test operators that verified the entanglement of the bound-entangled states (Sec. V) necessarily lead to maps that go beyond the partial transposition since the partial transposition cannot detect the entanglement of states considered in those examples.

In addition, in Ref. [33], an elegant approach was formulated that enables the construction of device-independent entanglement witnesses from device-dependent ones. This technique is based on a matrix-product extension that assigns to each subsystem an auxiliary Hilbert space but requires the previous knowledge of a witness. Such desired initial witnesses can be provided by our algorithm and combined with the method from Ref. [33] to construct device-independent entanglement witnesses.

C. Outlook

Beyond the witnessing of multipartite entanglement, the SEE approach has been generalized. Thus, let us briefly discuss some future generalizations of our numerical method for the aim of exploring entanglement in a broader context.

The detection of K-entanglement, and thus of genuine entanglement, is possible by finding the maximum of all maximal separability eigenvalues for an operator with respect to partitions of the length K [42]. It is therefore a straightforward extension to the SPI to find the optimal witness for K-entanglement with the introduced algorithm—the algorithm is run multiple times for different partitions, and the maximum of the results is the required separability eigenvalue.

Furthermore, some physical problems require solutions of a generalized EE, $\hat{L}|\Phi\rangle = \lambda \hat{P}|\Phi\rangle$, where the right-hand side includes a contribution that is different from the identity, $\hat{P} \neq \hat{1}$. Interestingly, the same holds true for the SEE.

One example is the verification of entanglement in systems of indistinguishable particles, which is based on a generalized SEE and where $\hat{P}$ represents the (anti)symmetrization operator for bosons (fermions) [45]. Another example is the quantification of multipartite entanglement via generalized Schmidt-number witnesses [12]. There, $\hat{P}$ takes the form of a spinor projection (details can be found in the supplement to Ref. [12]). A third example is the detection of multipartite entanglement in systems for which the number of subsystems is not fixed. For instance, the underlying generalized SEE applies to the construction of multiparticle-entanglement witnesses for fluctuating particle numbers [77].

Thus, a generalization of the SPI to account for such generalized SEEs, including $\hat{P}$, will further enhance the range of applications. It is worth mentioning that the desired generalization is well known for the PI, which is likely to be applicable to the SPI in a similar manner.

Furthermore, the standard EE applied to the density operator leads to the spectral decomposition of the state. Similarly, the SEE can be used to expand the density operator in terms of separability eigenvectors and a quasiprobability distribution [66,67]. The latter one includes negativities iff the state is entangled; see Ref. [78] for an application to uncover bound entanglement. However, this approach requires the computation of all separability eigenvectors. Therefore, similar to the subspace iteration for the PI, a generalization of the SPI to include all solutions, beyond the one that corresponds to the maximal separability eigenvalue, could lead to a broader applicability of entanglement quasiprobabilities.

As a final example let us consider the dynamics of quantum systems, which is described by the Schrödinger equation. To distinguish the entanglement-generating evolution from the separable dynamics, we recently introduced the separability Schrödinger equations [79], which relate to

the SEE in the static case. Again, the SPI can be the starting point for the numerical implementation of this approach.

Thus, generalizations of the SPI have the potential to uncover multipartite entanglement in a much broader sense. Beyond the already-available construction of positive, but not completely positive, maps and device-independent entanglement witnesses, our numerical approach builds the foundation for the future studies of entanglement.

D. Relations to mathematical problems

The question of positive polynomials is an interesting and, in the most general case, unsolved mathematical problem, which has been studied for a long time [80] and finds many applications [81]. As already indicated in Sec. IV, any entanglement witness can be characterized by the non-negativity of a multivariate polynomial [69]. All entanglement witnesses can be generated through the solution of the SEE. Therefore, the solution of the SEE enables the construction and characterization of positive multivariate polynomials; see also Appendix E. Consequently, the proposed SPI is an alternative approach to numerically solving the positivity problem of polynomials.

Another family of important problems in pure mathematics that could benefit from the SPI are partial differential equations, which are also closely related to many problems in physics. For instance, the applicability of the method of separation of variables corresponds to the question of whether or not solutions are factorizable, i.e., a tensor product. Since a separable eigenfunction is also a separability eigenfunction [39], i.e., eigenvector in the function space, the SPI can be applied to find factorizable solutions of the partial differential equation.

Moreover, nonlinear partial differential equations address questions such as finding the ground state to a nonlinear energy functional. If this functional is polynomial, a problem related to the previously mentioned characterization of multivariate polynomials can be formulated. Namely, the numerical approximation to the ground state can be obtained by the multipartite SPI as the maximum of the negative nonlinear energy functional, resulting in the minimal energy.

VII. CONCLUSION

In this paper, we introduce an algorithm, the SPI, to numerically construct arbitrary multipartite entanglement witnesses. This algorithm enables us to find the maximal separability eigenvalues, which directly results in measurable entanglement tests. Beyond the formulation of our method, we also provide the mathematical background for the SPI, which yields the maximal solution of the nonlinear separability eigenvalue problem addressing the complex entanglement problem in quantum physics. Furthermore, our framework is supplemented by performing a benchmark of our approach, applying it to uncover hard-to-detect forms

of entanglement, and relating it to other methods in the theory of quantum entanglement and their experimental application.

Our algorithm shows two crucial steps—namely, forward and backward iteration—following directly from the cascaded structure of the separability eigenvalue equations. The forward iteration reduces the number of parties until we have a single-party problem, which is then used in the backward iteration to solve the multipartite problem. This property also allows us to prove the convergence of the SPI to reliably produce entanglement tests based on arbitrary observables. Interestingly, our algorithm includes the well-known power iteration, which is able to calculate the maximal (standard) eigenvalue, as a special case.

We show the efficiency of our approach in comparison with another method, which is mainly based on a genetic algorithm. The genetic algorithm presents a state-of-the-art approach to solve arbitrary optimization problems. The SPI is faster by 2 orders of magnitude, which is partly because of its directed design to specifically address the entanglement problem. For example, we analyze the runtime as a function of the dimension of a bipartite quantum system. In addition, we numerically solve the separability eigenvalue equations in a feasible time for operators up to a 13-party qubit Hilbert space, corresponding to 8192 dimensions.

Furthermore, we apply the SPI to bound-entangled states whose entanglement detection is a cumbersome problem. For instance, the frequently applied partial transposition criterion fails to uncover the entanglement of the considered examples. Applying the SPI, we straightforwardly verify this weak form of entanglement, proving the advantage of our method. Moreover, we demonstrate with these examples that our algorithm renders it possible to uncover entanglement of all forms of partial entanglement in multipartite systems. It is also worth mentioning that entanglement of continuous-variable systems can be detected in finite subspaces, allowing us to apply our algorithm to these kinds of states as well.

We outline the versatile nature of our method and its impact on future research by relating it to other open problems in quantum entanglement and beyond. For instance, the construction of entanglement witnesses, which is achieved by our SPI, is the basis for the formulation of positive, but not completely positive, maps for entanglement detection and the construction of device-independent entanglement witnesses. Furthermore, we describe the construction of entanglement criteria based on measured quantities and outline several generalizations, which are—at their core—related to our method.

Thus, we devise a relatively simple, yet versatile approach to numerically construct entanglement tests in multipartite systems. The direct implementation of our method enables us to certify complex forms of quantum correlations based on measurable criteria. In addition, we derive the required mathematical background of our algorithm to ensure its operation and benchmark its performance. To the best of our knowledge, there exists no

alternative method of entanglement verification that is applicable to complex systems that our method can manage. To summarize, we provide a full numerical framework for the detection of multipartite entanglement for theoretical studies and, more importantly, for application in current and future experiments using entanglement in quantum information and communication protocols.

ACKNOWLEDGMENTS

APPENDIX A: PROOF OF THEOREM 1

Theorem 1 (Forward iteration). Let $|a_1, ..., a_N\rangle$ be the separability eigenvector corresponding to the maximal separability eigenvalue of a positive N-partite operator $\hat{L}$. Furthermore, let $|\Psi\rangle = \hat{L}|a_1, ..., a_N\rangle$. For the $(N-1)$-partite operator $\hat{L}' = \mathrm{tr}_N(|\Psi\rangle\langle\Psi|)$, the equality

$$\langle a_1, ..., a_N|\hat{L}|a_1, ..., a_N\rangle$$
$$= \sqrt{\langle a_1, ..., a_{N-1}|\hat{L}'|a_1, ..., a_{N-1}\rangle} \quad (A1)$$

holds true.

Proof.—As a shorthand notation, let $|v_N\rangle = |a_1, ..., a_N\rangle$. Using the cascaded structure (CS) and the abbreviation $\hat{L}' = \mathrm{tr}_N|\Psi\rangle\langle\Psi|$, the statement is derived as follows:

$$\max_{|v_N\rangle\in\mathcal{S}} \langle v_N|\hat{L}|v_N\rangle = \max_{|v_N\rangle,|v_N'\rangle\in\mathcal{S}} \langle v_N'|\hat{L}\underbrace{|v_N\rangle}_{=:|\Psi(v_N)\rangle}$$
$$= \max_{|v_N\rangle\in\mathcal{S}} \max_{|v_N'\rangle\in\mathcal{S}} \langle v_N'|\Psi(v_N)\rangle$$
$$= \max_{|v_N\rangle\in\mathcal{S}} \sqrt{\max_{|v_N'\rangle\in\mathcal{S}}[\langle v_N'|\Psi(v_N)\rangle]^2}$$
$$= \max_{|v_N\rangle\in\mathcal{S}} \sqrt{\max_{|v_N'\rangle\in\mathcal{S}}\langle v_N'|\Psi(v_N)\rangle\langle\Psi(v_N)|v_N'\rangle}$$
$$\overset{\mathrm{CS}}{=} \max_{|v_N\rangle\in\mathcal{S}} \sqrt{\max_{|v_{N-1}'\rangle\in\mathcal{S}}\langle v_{N-1}'|\hat{L}'(v)|v_{N-1}'\rangle},$$

where we chose global phases such that scalar products correspond to non-negative numbers. □

APPENDIX B: PROOF OF THEOREM 3

Theorem 3 (Monotony). Let $|a_1, ..., a_N\rangle \in \mathcal{S}$ and $|a_1', ..., a_N'\rangle \in \mathcal{S}$ such that

$$|a_1', ..., a_N'\rangle = \underset{|b_1,...,b_N\rangle\in\mathcal{S}}{\arg\max} \langle b_1, ..., b_N|\hat{L}|a_1, ..., a_N\rangle. \quad (B1)$$

Then, the inequality

$$\langle a_1, ..., a_N|\hat{L}|a_1, ..., a_N\rangle$$
$$\leq \langle a_1', ..., a_N'|\hat{L}|a_1, ..., a_N\rangle$$
$$\leq \langle a_1', ..., a_N'|\hat{L}|a_1', ..., a_N'\rangle \quad (B2)$$

holds true. Furthermore, the equality in Eq. (B2) holds true iff $|a_1', ..., a_N'\rangle = |a_1, ..., a_N\rangle$.

Proof.—The inequality

$$\langle a_1, ..., a_N|\hat{L}|a_1, ..., a_N\rangle \leq \langle a_1', ..., a_N'|\hat{L}|a_1, ..., a_N\rangle$$

directly follows from the definition of $|a_1', ..., a_N'\rangle$. The second inequality

$$\langle a_1', ..., a_N'|\hat{L}|a_1, ..., a_N\rangle \leq \langle a_1', ..., a_N'|\hat{L}|a_1', ..., a_N'\rangle$$

can be proved using the Cauchy-Schwarz inequality (CSI). As a shorthand, let us define $|v_N\rangle = |a_1, ..., a_N\rangle$ and $|v_N'\rangle = |a_1', ..., a_N'\rangle$ and consider the $\hat{L}$-induced scalar product $\langle v|\rangle v_{\hat{L}} = \langle v|\hat{L}|v\rangle$:

$$\langle v_N|v_N\rangle_{\hat{L}}^2 \leq \langle v_N'|v_N\rangle_{\hat{L}}^2 \overset{\mathrm{CSI}}{\leq} \langle v_N|v_N\rangle_{\hat{L}} \langle v_N'|v_N'\rangle_{\hat{L}}$$
$$\Leftrightarrow \langle v_N|v_N\rangle_{\hat{L}} \leq \langle v_N'|v_N'\rangle_{\hat{L}}$$
$$\Rightarrow \langle v_N'|v_N\rangle_{\hat{L}}^2 \leq \langle v_N'|v_N'\rangle_{\hat{L}} \langle v_N'|v_N'\rangle_{\hat{L}}$$
$$\Rightarrow \langle v_N'|v_N\rangle_{\hat{L}} \leq \langle v_N'|v_N'\rangle_{\hat{L}}.$$

Here, the second row follows from reduction by $\langle v_N|v_N\rangle_{\hat{L}}$; the third row can be found by substituting the inequality in row two into the right side of the inequality in row one. Note that the equality holds if and only if $|v_N\rangle|||v_N'\rangle$. □

APPENDIX C: PROOF OF THEOREM 4

Theorem 4 (Local convergence). For any starting vector, the sequence $(g^{(s)})_s$ of expectation values generated by the SPI converges; i.e., the limit

$$\lim_{s\to\infty} g^{(s)} = \bar{g} \quad (C1)$$

exists and is bounded as $0 \leq \bar{g} \leq g_{\max}$.

Proof.—The state $|v_N\rangle := |a_1^{(s)}, ..., a_N^{(s)}\rangle$ is separable for any s, where s indexes the iteration steps of the SPI. Further, let $|v_N'\rangle := |a_1^{(s+1)}, ..., a_N^{(s+1)}\rangle$ be the next approximation to the separability eigenvector corresponding to an optimal separability eigenvalue. By design, $\langle v_N'|\hat{L}|v_N\rangle \to$ max holds such that Theorem 3 applies. Thus, the sequence $(g^{(s)})_s$ is monotonous. Furthermore, as $\hat{L}$ is a bounded

operator, the sequence is also bounded. By definition of a convergent series, $(g^{(s)})_s$ converges to, at least, a local maximum. □

APPENDIX D: PROOF OF THEOREM 5

Theorem 5 (Global convergence). Let Σ be a set of separable starting vectors and $(g_\Phi^{(s)})_s$ be sequences of expectation values generated by the SPI for a starting vector $|\Phi\rangle \in \Sigma$. Further, say $\{\bar{g}_\Phi \in \mathbb{R} : |\Phi\rangle \in \Sigma$ and $\bar{g}_\Phi = \lim_{s\to\infty} g_\Phi^{(s)}\}$ defines the set of optimal expectation values (limits of the converged sequences) for each starting vector. The maximal separability eigenvalue for the operator $\hat{L}$ is $g_{\max} = \max_{\Phi \in \Sigma}\{\bar{g}_\Phi\}$, which is the maximum of the limit to the series of expectation values for each starting vector.

Proof.—The global convergence of the SPI is shown via proof by induction over the number of subsystems N. The expression $\hat{L}^{(i)}$ denotes an operator acting on a composition of i Hilbert spaces. Further, we use $|v_i\rangle = |a_1, ..., a_i\rangle$ and $\bar{g}_i = \lim_{s_1,...,s_i\to\infty}\langle a_1^{(s_1)}, ..., a_i^{(s_i)}|\hat{L}^{(i)}|a_1^{(s_1)}, ..., a_i^{(s_i)}\rangle$ as the optimal expectation value of the ith subsystem over separable states, with s_i counting the iterations of the SPI in the ith subsystem.

Basis of induction.—For $N = 1$, the SPI is the PI for which the convergence is well known [61]. The optimal expectation value for the one-subsystem operator $\hat{L}^{(1)}$ can be found as

$$\bar{g}_1 = \lim_{s_1\to\infty}\langle a_1^{(s_1)}|\hat{L}^{(1)}|a_1^{(s_1)}\rangle, \tag{D1}$$

where $|a_1^{(s_1)}\rangle = \hat{L}^{(1)}|a_1^{(s_1-1)}\rangle / \||\hat{L}^{(1)}|a_1^{(s_1-1)}\rangle\|$ and $\||\psi\rangle\| = \langle\psi|\psi\rangle^{1/2}$.

Induction hypothesis.—The induction hypothesis reads

$$\bar{g}_N = \lim_{s_N\to\infty}\langle a_N^{(s_N)}|\hat{L}_{a_1,...,a_{N-1}}^{(N)}|a_N^{(s_N)}\rangle, \tag{D2}$$

where $|a_N^{(s_N)}\rangle = \hat{L}_{a_1,...,a_{N-1}}^{(N)}|a_N^{(s_N)}\rangle / \|\hat{L}_{a_1,...,a_{N-1}}^{(N)}|a_N^{(s_N)}\rangle\|$.

Induction step.—Under the assumption of convergence in $N - 1$ subsystems [replacing N by $N - 1$ in the induction hypothesis, Eq. (D2)], we show convergence of the SPI in the Nth subsystem,

$$\bar{g}_N = \max_{a_1,...,a_N}\langle a_1, ..., a_N|\hat{L}^{(N)}|a_1, ..., a_N\rangle$$

$$= \max_{a_1,...,a_{N-1}}\max_{a_N}\langle a_1, ..., a_N|\hat{L}^{(N)}|a_1, ..., a_N\rangle. \tag{D3}$$

In the SPI algorithm, we then define

$$|\Psi\rangle = \hat{L}^{(N)}|a_1, ..., a_N\rangle \tag{D4}$$

and calculate

$$|b_N\rangle = \frac{\langle a_1, ..., a_{N-1}, \cdot|\Psi\rangle}{\|\langle a_1, ..., a_{N-1}, \cdot|\Psi\rangle\|}. \tag{D5}$$

Using these definitions in the calculation of $\bar{g}_N$, we get

$$\bar{g}_N = \max_{a_1,...,a_{N-1}}\max_{a_N}\langle a_1, ..., a_N|\hat{L}^{(N)}|a_1, ..., a_N\rangle$$

$$= \max_{a_1,...,a_{N-1}}\max_{\gamma_N,a_N}\langle \gamma_N|\hat{L}_{a_1,...,a_{N-1}}^{(N)}|a_N\rangle$$

$$= \sqrt{\max_{a_1,...,a_{N-1}}\max_{\gamma_N,a_N}|\langle a_1, ..., a_{N-1}, \gamma_N|\Psi\rangle|^2},$$

where the second line follows from Theorem 3. By construction—following the induction step—convergence has been reached for the subsystems up to and including $N - 1$, which leaves a maximization for $|a_N\rangle$ and $|\gamma_N\rangle$,

$$\bar{g}_N = \sqrt{\max_{\gamma_N,a_N}\langle a_1, ..., a_{N-1}, \gamma_N|\Psi\rangle\langle\Psi|a_1, ..., a_{N-1}, \gamma_N\rangle}.$$

The solution to this maximization problem is found via the cascaded structure and is equal to $|b_N\rangle$ [see Eq. (D5)],

$$\bar{g}_N = \langle a_1, ..., a_{N-1}, b_N|\hat{L}^{(N)}|a_1, ..., a_{N-1}, b_N\rangle.$$

We use the induction hypothesis, Eq. (D2), to solve the problem of finding the states $|a_1\rangle, ..., |a_{N-1}\rangle$. Then, we need to maximize $\hat{L}_{a_1,...,a_{N-1}}^{(N)}$. Since this is an operator in one subsystem, the PI can be applied to maximize the expectation value. This is shown in the induction hypothesis. As the PI is guaranteed to converge, Eq. (D2) will indeed return a separable vector, which optimizes the expectation value of $\hat{L}^{(N)}$. Thus, for a single starting vector, the SPI finds a separability eigenvector, which might correspond to the maximal separability eigenvalue.

Convergence towards the separability eigenvector corresponding to the globally maximal separability eigenvalue is guaranteed by the choice of starting vectors. The operator basis is chosen as a set of starting vectors after every forward iteration. The PI converges towards the dominant eigenvalue of a matrix for a given starting vector, if the decomposition of the starting vector into the eigenbasis of the matrix has a nonzero contribution of the eigenvector corresponding to the maximal eigenvalue. As the operator basis spans the considered operator space, the separability eigenvector will have a nonzero contribution to the decomposition of at least one of the starting vectors. □

APPENDIX E: BRIEF DERIVATION OF THE SEEs

For a self-consistent reading of the present contribution, we review the derivation of the multipartite separability eigenvalue equations (see Ref. [40]). Here, the derivation is based on an equivalent approach (see Ref. [45]), which

relies on the Rayleigh quotient and is also the main idea behind the PI.

The (multipartite) Rayleigh quotient reads

$$R_{\hat{L}}(a_1, \dots, a_N) := \frac{\langle a_1, \dots, a_N | \hat{L} | a_1, \dots, a_N \rangle}{\langle a_1, \dots, a_N | a_1, \dots, a_N \rangle}, \quad \text{(E1)}$$

which is the expectation value of operator $\hat{L}$ for a possibly unnormalized vector $|a_1, \dots, a_N\rangle$. To relate R to multivariate polynomials, we can think of $|a_j\rangle$ in terms of wave functions being Taylor expanded in terms of polynomials of the order $d_j - 1$. Thus, we can conclude that the desired task of maximizing the Rayleigh quotient is equal to both maximizing a multivariate polynomial and finding the maximal expectation value of $\hat{L}$ with respect to separable states, i.e., finding its maximal separability eigenvalue.

The optimal values of the Rayleigh quotient in Eq. (E1) are found for

$$0 = \frac{\partial R_{\hat{L}}(a_1, \dots, a_N)}{\partial \langle a_j |}$$
$$= \frac{\hat{L}_{a_1, \dots, a_{j-1}, a_{j+1}, \dots, a_N} | a_j \rangle}{\langle a_1, \dots, a_N | a_1, \dots, a_N \rangle} - g \frac{|a_j\rangle}{\langle a_j | a_j \rangle} \quad \text{(E2)}$$

for $j = 1, \dots, N$, where we use the notation $g = R_{\hat{L}}(a_1, \dots, a_N)$ and the so-called reduced operator $\hat{L}_{a_1, \dots, a_{j-1}, a_{j+1}, \dots, a_N} = \langle a_1, \dots, a_{j-1}, \cdot, a_{j+1}, \dots, a_N | \hat{L} | a_1, \dots, a_{j-1}, \cdot, a_{j+1}, \dots, a_N \rangle$, acting solely on the jth subsystem (cf. Refs. [40,45]).

As the Rayleigh quotient is invariant under the norm of the vector, we may assume $\langle a_j | a_j \rangle = 1$. Consequently, the optimization of the Rayleigh quotient [cf. Eq. (E2)] yields the SEE in the first form as

$$\hat{L}_{a_1, \dots, a_{j-1}, a_{j+1}, \dots, a_N} | a_j \rangle = g | a_j \rangle \quad \text{(E3)}$$

for $j = 1, \dots, N$. The SPI does not evaluate this first form; rather, it solves Eq. (6), the second form of the SEE, which has been shown to be equivalent to Eq. (E3) (a comprehensive proof can be found in the Supplement Material to Ref. [40]).

---

[1] A. Einstein, B. Podolsky, and N. Rosen, *Can Quantum-Mechanical Description of Physical Reality Be Considered Complete?*, Phys. Rev. **47**, 777 (1935).

[2] E. Schrödinger, *Die gegenwärtige Situation in der Quantenmechanik*, Naturwissenschaften **23**, 807 (1935); **23**, 823 (1935); **23**, 844 (1935) [J. D. Trimmer, *The Present Situation in Quantum Mechanics: A Translation of Schrödinger's " Cat Paradox" Paper*, Proc. Am. Philos. Soc. **124**, 323 (1980)].

[3] M. A. Nielsen and I. L. Chuang, *Quantum Computation and Quantum Information* (Cambridge University Press, Cambridge, England, 2000).

[4] C. H. Bennett, G. Brassard, C. Crépeau, R. Jozsa, A. Peres, and W. K. Wootters, *Teleporting an Unknown Quantum State via Dual Classical and Einstein-Podolsky-Rosen Channels*, Phys. Rev. Lett. **70**, 1895 (1993).

[5] C. H. Bennett and S. J. Wiesner, *Communication via One- and Two-Particle Operators on Einstein-Podolsky-Rosen States*, Phys. Rev. Lett. **69**, 2881 (1992).

[6] C. H. Bennett and G. Brassard, *Quantum Cryptography: Public Key Distribution and Coin Tossing*, Proc. IEEE Int. Conf. Comput. Signal Proc. **1**, 175 (1984); Theor. Comput. Sci. **560**, 7 (2014).

[7] A. K. Ekert, *Quantum Cryptography Based on Bell's Theorem*, Phys. Rev. Lett. **67**, 661 (1991).

[8] L. Gurvits, *Classical Deterministic Complexity of Edmonds' Problem and Quantum Entanglement*, in *Proceedings of the Thirty-Fifth ACM Symposium on Theory of Computing* (ACM, New York, 2003), pp. 10–19.

[9] L. M. Ioannou, *Computational Complexity of the Quantum Separability Problem*, Quantum Inf. Comput. **7**, 4 (2007).

[10] M. Huber and J. I. de Vicente, *Structure of Multidimensional Entanglement in Multipartite Systems*, Phys. Rev. Lett. **110**, 030501 (2013).

[11] F. Levi and F. Mintert, *Hierarchies of Multipartite Entanglement*, Phys. Rev. Lett. **110**, 150402 (2013).

[12] F. Shahandeh, J. Sperling, and W. Vogel, *Structural Quantification of Entanglement*, Phys. Rev. Lett. **113**, 260502 (2014).

[13] W. Dür, G. Vidal, and J. I. Cirac, *Three Qubits Can Be Entangled in Two Inequivalent Ways*, Phys. Rev. A **62**, 062314 (2000).

[14] S. Yokoyama, R. Ukai, S. C. Armstrong, C. Sornphiphatphong, T. Kaji, S. Suzuki, J.-i. Yoshikawa, H. Yonezawa, N. C. Menicucci, and A. Furusawa, *Ultra-Large-Scale Continuous-Variable Cluster States Multiplexed in the Time Domain*, Nat. Photonics **7**, 982 (2013).

[15] M. Chen, N. C. Menicucci, and O. Pfister, *Experimental Realization of Multipartite Entanglement of 60 Modes of a Quantum Optical Frequency Comb*, Phys. Rev. Lett. **112**, 120505 (2014).

[16] Y. Cai, J. Roslund, G. Ferrini, F. Arzani, X. Xu, C. Fabre, and N. Treps, *Multimode Entanglement in Reconfigurable Graph States Using Optical Frequency Combs*, Nat. Commun. **8**, 15645 (2017).

[17] B. M. Terhal, *Detecting Quantum Entanglement*, Theor. Comput. Sci. **287**, 313 (2002).

[18] R. Horodecki, P. Horodecki, M. Horodecki, and K. Horodecki, *Quantum Entanglement*, Rev. Mod. Phys. **81**, 865 (2009).

[19] O. Gühne and G. Tóth, *Entanglement Detection*, Phys. Rep. **474**, 1 (2009).

[20] A. Peres, *Separability Criterion for Density Matrices*, Phys. Rev. Lett. **77**, 1413 (1996).

[21] M. Horodecki, P. Horodecki, and R. Horodecki, *Separability of Mixed States: Necessary and Sufficient Conditions*, Phys. Lett. A **223**, 1 (1996).

[22] M. Horodecki, P. Horodecki, and R. Horodecki, *Separability of n-Particle Mixed States: Necessary and Sufficient*

Conditions in Terms of Linear Maps, Phys. Lett. A **283**, 1 (2001).

[23] B. M. Terhal, *Bell Inequalities and the Separability Criterion*, Phys. Lett. A **271**, 319 (2000).

[24] G. Tóth, *Entanglement Witnesses in Spin Models*, Phys. Rev. A **71**, 010301(R) (2005).

[25] M. Bourennane, M. Eibl, C. Kurtsiefer, S. Gaertner, H. Weinfurter, O. Gühne, P. Hyllus, D. Bruss, M. Lewenstein, and A. Sanpera, *Experimental Detection of Multipartite Entanglement Using Witness Operators*, Phys. Rev. Lett. **92**, 087902 (2004).

[26] G. Tóth and O. Gühne, *Detecting Genuine Multipartite Entanglement with Two Local Measurements*, Phys. Rev. Lett. **94**, 060501 (2005).

[27] O. Gühne, P. Hyllus, D. Bruss, A. Ekert, M. Lewenstein, C. Macchiavello, and A. Sanpera, *Experimental Detection of Entanglement via Witness Operators and Local Measurements*, J. Mod. Phys. **50**, 1079 (2003).

[28] B. Jungnitsch, T. Moroder, and O. Gühne, *Entanglement Witnesses for Graph States: General Theory and Examples*, Phys. Rev. A **84**, 032310 (2011).

[29] N. Kiesel, C. Schmid, U. Weber, G. Toth, O. Gühne, R. Ursin, and H. Weinfurter, *Experimental Analysis of a Four-Qubit Photon Cluster State*, Phys. Rev. Lett. **95**, 210502 (2005).

[30] H. Häffner, W. Hänsel, C. F. Roos, J. Benhelm, D. Chek-al-kar, M. Chwalla, T. Körber, U. D. Rapol, M. Riebe, P. O. Schmidt, C. Becher, O. Gühne, W. Dür, and R. Blatt, *Scalable Multiparticle Entanglement of Trapped Ions*, Nature (London) **438**, 643 (2005).

[31] M. Borrelli, M. Rossi, C. Macchiavello, and S. Maniscalco, *Witnessing Entanglement in Hybrid Systems*, Phys. Rev. A **90**, 020301(R) (2014).

[32] C. Branciard, D. Rosset, Y.-C. Liang, and N. Gisin, *Measurement-Device-Independent Entanglement Witnesses for All Entangled Quantum States*, Phys. Rev. Lett. **110**, 060405 (2013).

[33] A. Rutkowski and P. Horodecki, *Tensor Product Extension of Entanglement Witnesses and Their Connection with Measurement-Device-Independent Entanglement Witnesses*, Phys. Lett. A **378**, 2043 (2014).

[34] M. Lewenstein, B. Kraus, J. I. Cirac, and P. Horodecki, *Optimization of Entanglement Witnesses*, Phys. Rev. A **62**, 052310 (2000).

[35] D. Bruß, J. I. Cirac, P. Horodecki, F. Hulpke, B. Kraus, M. Lewenstein, and A. Sanpera, *Reflections upon Separability and Distillability*, J. Mod. Opt. **49**, 1399 (2002).

[36] L. O. Hansen, A. Hauge, J. Myrheim, and P. Ø. Sollid, *Extremal Entanglement Witnesses*, Int. J. Quantum. Inform. **13**, 1550060 (2015).

[37] B.-H. Wang, H.-R. Xu, S. Campbell, and S. Severini, *Characterization and Properties of Weakly Optimal Entanglement Witnesses*, Quantum Inf. Comput. **15**, 1109 (2015).

[38] F. Shahandeh, M. Ringbauer, J. C. Loredo, and T. C. Ralph, *Ultrafine Entanglement Witnessing*, Phys. Rev. Lett. **118**, 110502 (2017).

[39] J. Sperling and W. Vogel, *Necessary and Sufficient Conditions for Bipartite Entanglement*, Phys. Rev. A **79**, 022318 (2009).

[40] J. Sperling and W. Vogel, *Multipartite Entanglement Witnesses*, Phys. Rev. Lett. **111**, 110503 (2013).

[41] S. Gerke, J. Sperling, W. Vogel, Y. Cai, J. Roslund, N. Treps, and C. Fabre, *Full Multipartite Entanglement of Frequency-Comb Gaussian States*, Phys. Rev. Lett. **114**, 050501 (2015).

[42] S. Gerke, J. Sperling, W. Vogel, Y. Cai, J. Roslund, N. Treps, and C. Fabre, *Multipartite Entanglement of a Two-Separable State*, Phys. Rev. Lett. **117**, 110502 (2016).

[43] K. Eckert, J. Schliemann, D. Bruß, and M. Lewenstein, *Quantum Correlations in Systems of Indistinguishable Particles*, Ann. Phys. (Amsterdam) **299**, 88 (2002).

[44] M. Oszmaniec and M. Kuś, *Universal Framework for Entanglement Detection*, Phys. Rev. A **88**, 052328 (2013).

[45] A. Reusch, J. Sperling, and W. Vogel, *Entanglement Witnesses for Indistinguishable Particles*, Phys. Rev. A **91**, 042324 (2015).

[46] F. G. S. L. Brandão, *Quantifying Entanglement with Witness Operators*, Phys. Rev. A **72**, 022310 (2005).

[47] F. G. S. L. Brandão and R. O. Vianna, *Witnessed Entanglement*, Int. J. Quantum. Inform. **04**, 331 (2006).

[48] K. M. R. Audenaert and M. B. Plenio, *When are Correlations Quantum?—Verification and Quantification of Entanglement by Simple Measurements*, New J. Phys. **8**, 266 (2006).

[49] J. Eisert, F. G. S. L. Brandão, and K. M. R. Audenaert, *Quantitative Entanglement Witnesses*, New J. Phys. **9**, 46 (2007).

[50] B. M. Terhal and P. Horodecki, *Schmidt Number for Density Matrices*, Phys. Rev. A **61**, 040301(R) (2000).

[51] A. Sanpera, D. Bruß, and M. Lewenstein, *Schmidt-Number Witnesses and Bound Entanglement*, Phys. Rev. A **63**, 050301(R) (2001).

[52] J. Sperling and W. Vogel, *Determination of the Schmidt Number*, Phys. Rev. A **83**, 042315 (2011).

[53] J. Eisert and H. J. Briegel, *Schmidt Measure as a Tool for Quantifying Multiparticle Entanglement*, Phys. Rev. A **64**, 022306 (2001).

[54] L. Vanderberghe and S. Boyd, *Semidefinite Programming*, SIAM Rev. **38**, 49 (1996).

[55] E. M. Rains, *A Semidefinite Program for Distillable Entanglement*, IEEE Trans. Inf. Theory **47**, 2921 (2001).

[56] K. Audenaert and B. De Moor, *Optimizing Completely Positive Maps Using Semidefinite Programming*, Phys. Rev. A **65**, 030302(R) (2002).

[57] A. C. Doherty, P. A. Parrilo, and F. M. Spedalieri, *Distinguishing Separable and Entangled States*, Phys. Rev. Lett. **88**, 187904 (2002).

[58] Y. C. Eldar, *A Semidefinite Programming Approach to Optimal Unambiguous Discrimination of Quantum States*, IEEE Trans. Inf. Theory **49**, 446 (2003).

[59] F. G. S. L. Brandão and R. O. Vianna, *Robust Semidefinite Programming Approach to the Separability Problem*, Phys. Rev. A **70**, 062309 (2004).

[60] A. C. Doherty, P. A. Parrilo, and F. M. Spedalieri, *Detecting Multipartite Entanglement*, Phys. Rev. A **71**, 032333 (2005).

[61] G. H. Golub and C. F. van Loan, *Matrix Computations*, 4th ed. (The Johns Hopkins University Press, Baltimore, 2013).

[62] R. F. Werner, *Quantum States with Einstein-Podolsky-Rosen Correlations Admitting a Hidden-Variable Model*, Phys. Rev. A **40**, 4277 (1989).

[63] J. Sperling and W. Vogel, *Verifying Continuous-Variable Entanglement in Finite Spaces*, Phys. Rev. A **79**, 052313 (2009).

[64] This can be seen from the observation that the SEEs for an operator of the form $\hat{L} = \hat{L}^{(1)} \otimes \cdots \otimes \hat{L}^{(N)}$ are identical to the EE for each $\hat{L}^{(j)}$ [39,40].

[65] A counterexample is to replace the positive operator in Eq. (12) with a positive-semidefinite one, $\hat{L} = \hat{1} - \hat{V}$. This gives a nonconverging (alternating) sequence of iterated vectors.

[66] J. Sperling and W. Vogel, *Representation of Entanglement by Negative Quasiprobabilities*, Phys. Rev. A **79**, 042337 (2009).

[67] J. Sperling and I. A. Walmsley, *Quasiprobability Representation of Quantum Coherence*, Phys. Rev. A **97**, 062327 (2018).

[68] R. L. Haupt and S. E. Haupt, *Practical Genetic Algorithms*, 2nd ed. (John Wiley & Sons, Hoboken, New Jersey, 2004).

[69] G. Blekherman, P. A. Parrilo, and R. R. Thomas, *Semidefinite Optimization and Convex Algebraic Geometry* (MOS-SIAM Series on Optimization, Philadelphia, 2013).

[70] D. Henrion, J.-B. Lasserre, and J. Lofberg, *GloptiPoly 3: Moments, Optimization and Semidefinite Programming*, arXiv:0709.2559.

[71] P. Horodecki, M. Horodecki, and R. Horodecki, *Bound Entanglement Can be Activated*, Phys. Rev. Lett. **82**, 1056 (1999).

[72] J. A. Smolin, *Four-Party Unlockable Bound Entangled State*, Phys. Rev. A **63**, 032306 (2001).

[73] P. Horodecki, *Separability Criterion and Inseparable Mixed States with Positive Partial Transposition*, Phys. Lett. A **232**, 333 (1997).

[74] B. Kühn, W. Vogel, and J. Sperling, *Displaced Photon-Number Entanglement Tests*, Phys. Rev. A **96**, 032306 (2017).

[75] M.-D. Choi, *Completely Positive Linear Maps on Complex Matrices*, Linear Algebra Appl. **10**, 285 (1975).

[76] A. Jamiołkowski, *Linear Transformations which Preserve Trace and Positive Semidefiniteness of Operators*, Rep. Math. Phys. **3**, 275 (1972).

[77] J. Sperling and I. A. Walmsley, *Entanglement in Macroscopic Systems*, Phys. Rev. A **95**, 062116 (2017).

[78] P. Thomas, M. Bohmann, and W. Vogel, *Verifying Bound Entanglement of Dephased Werner States*, Phys. Rev. A **96**, 042321 (2017).

[79] J. Sperling and I. A. Walmsley, *Separable and Inseparable Quantum Trajectories*, Phys. Rev. Lett. **119**, 170401 (2017).

[80] N. K. Bose, *Multivariate Polynomial Positivity Test Efficiency Improvement*, Proc. IEEE **67**, 1443 (1979).

[81] J. B. Lasserre, *Moments, Positive Polynomials and Their Applications*, Imperial College Press Optimization Series (Imperial College Press, London, England, 2009), Vol. 1.

Stefan Gerke

Schützenstraße 25
29379 Wittingen
Mobile: (+49) 173 2562161
Email: stefangerke@gmail.com

CURRICULUM VITAE

Date of birth: January 9, 1989
Citizenship: German

Education

Since April 2014	**PhD Student**: University of Rostock, *Theoretical Quantum Optics*
	▶ Emphasis on Entanglement Verification, Entanglement Quantification, Optimization, and Numerical Physics
	▶ Advisor: Prof. Dr. Werner Vogel
April 2012 – March 2014	**Master of Science (Physics):** University of Rostock
	▶ Emphasis on Photonics and Quantum Optics
	▶ Masters Thesis: *Iterative Method for the Separability Eigenvalue Equations* Advisor: Prof. Dr. Werner Vogel
October 2008 – September 2012	**Bachelor of Science (Mathematics):** University of Rostock
	▶ Emphasis on Numerical Mathematics
	▶ Bachelors Thesis: *Eigenwertberechnungen für den Laplace-Operator auf einem Rechteckgebiet* Advisor: Prof. Dr. Klaus Neymeyr
October 2008 – September 2011	**Bachelor of Science (Physics):** University of Rostock
	▶ Emphasis on Theoretical Physics
	▶ Masters Thesis: *Nonclassicality and Entanglement in a Two-Mode Squeezed Vacuum State* Advisor: Prof. Dr. Werner Vogel
October 2007 – July 2008	**General Studies**: Northern Virginia Community College, Alexandria, VA, USA
June 2007	**German High School Degree** (*Abitur*): German School of Washington, D.C.

Teaching

Since April 2014	**Lecture**: Various classes on electrodynamics, quantum mechanics, and quantum optics
October 2017 – March 2018	**Seminar**: Theoretical Quantum Mechanics for Teachers
April 2017 – July 2017	**Lab course**: Classical Mechanics and Thermodynamics
April 2016 – July 2016	**Lab course**: Introductory Lab Courses for Electrical Engineering Students
October 2015 – March 2016	**Seminar**: Theoretical Electrodynamics
October 2014 – March 2015	**Lab course**: Advanced Experimental Physics

Publications

▶ S. Gerke, W. Vogel, and J. Sperling,
Numerical Construction of Multipartite Entanglement Witnesses, Phys. Rev. X **8**, 031047 (2018).

▶ S. Gerke, J. Sperling, W. Vogel, Y. Cai, J. Roslund, N. Treps, and C. Fabre,
Multipartite Entanglement of a Two-Separable State, Phys. Rev. Lett. **117**, 110502 (2016).

▶ S. Gerke, J. Sperling, W. Vogel, Y. Cai, J. Roslund, N. Treps, and C. Fabre,
Full Multipartite Entanglement of Frequency Comb Gaussian States, Phys. Rev. Lett. **114**, 050501 (2015).

Conference Contributions

QCUMbER Conference, Oxford, England (2018)	**Contributed Talk**: Entanglement detection via numerical approaches
International Forum for Young Scientists & The Third International Symposium for Young Researchers on Atomic, Molecular, and Optical Physics (ISYRAMO-III), Shanghai, China (2018)	**Invited Talk**: Numerical Verification of Entanglement by Witnessing Approaches
Quantum and Nonlinear Optics 2018, Kuala Lumpur, Malaysia	**Poster**: Definition and Detection of Multimode Entanglement
6th Quantum Information School and Workshop 2017, Paraty, Brazil	**Poster**: Multimode Entanglement: Definition and Detection
4th Quantum Information and Measurement 2017, Paris, France	**Contributed Talk**: Versatile Forms of Multimode Entanglement
3rd International Conference on ''Correlation Effects in Radiation Fields'' 2016, Rostock, Germany	**Poster**: Detecting Entanglement in Multipartite Frequency Entangled Gaussian States
CLEO/Europe-EQEC 2015, Munich, Germany	**Poster**: Detecting Entanglement in Multipartite Frequency Entangled Gaussian States

Skills

Programming Languages	C, C++, Python, Matlab
Software	Linux, Windows, LaTeX, Mathematica, Word, Excel, Powerpoint
Data Science	Optimization Algorithms (Genetic Algorithms), Currently learning Neural Networks, Deep Learning
Languages	German (Mothertongue), English (Fluent), French (Beginner), Spanish (Beginner)
Communication Skills	Open Minded, Visualization, Team Work, Logical Thinking

Scientific Achievements

- ▶ h-index: 2

- ▶ 100 citations (Source: Google scholar; June 2, 2019)

- ▶ 3 peer reviewed publications

    – 2 Physical Review Letters (1 Editor's Suggestion and Viewpoint in Physics)
    – 1 Physical Review X

- ▶ 7 conference contributions

Interests

- ▶ Quantum Optics

- ▶ Quantum Entanglement

- ▶ Quantum Information

- ▶ Mathematical Physics

- ▶ Numerical Mathematics

- ▶ Algebra

S. Gerke

Wittingen, June 2, 2019

List of Publications and Conference Contributions

Publications

- S. Gerke, W. Vogel, and J. Sperling,
  Numerical Construction of Multipartite Entanglement Witnesses, Phys. Rev. X **8**, 031047 (2018).

- S. Gerke, J. Sperling, W. Vogel, Y. Cai, J. Roslund, N. Treps, and C. Fabre,
  Multipartite Entanglement of a Two-Separable State, Phys. Rev. Lett. **117**, 110502 (2016).

- S. Gerke, J. Sperling, W. Vogel, Y. Cai, J. Roslund, N. Treps, and C. Fabre,
  Full Multipartite Entanglement of Frequency Comb Gaussian States, Phys. Rev. Lett. **114**, 050501 (2015).

Talks

QCUMbER Conference, Oxford, England (2018)	**Contributed Talk**: Entanglement detection via numerical approaches
International Forum for Young Scientists & The Third International Symposium for Young Researchers on Atomic, Molecular, and Optical Physics (ISYRAMO-III), Shanghai, China (2018)	**Invited Talk**: Numerical Verification of Entanglement by Witnessing Approaches
4th Quantum Information and Measurement 2017, Paris, France	**Contributed Talk**: Versatile Forms of Multimode Entanglement

Poster

Quantum and Nonlinear Optics 2018, Kuala Lumpur, Malaysia	**Poster**: Definition and Detection of Multimode Entanglement
6th Quantum Information School and Workshop 2017, Paraty, Brazil	**Poster**: Multimode Entanglement: Definition and Detection
3rd International Conference on "Correlation Effects in Radiation Fields" 2016, Rostock, Germany	**Poster**: Detecting Entanglement in Multipartite Frequency Entangled Gaussian States
CLEO/Europe-EQEC 2015, Munich, Germany	**Poster**: Detecting Entanglement in Multipartite Frequency Entangled Gaussian States